A SIMULATION-BASED FRAMEWORK FOR INFORMING DESIGN OF PROSTHETIC FEET

By

MICHAEL A. MCGEEHAN

A DISSERTATION

Presented to the Department of Human Physiology
and the Graduate School of the University of Oregon
in partial fulfillment of the requirements
for the degree of
Doctor of Philosophy

December 2020

DISSERTATION APPROVAL PAGE

Student: Michael A. McGeehan

Title: A Simulation-Based Framework for Informing Design of Prosthetic Feet

This dissertation has been accepted and approved in partial fulfillment of the requirements for the Doctor of Philosophy degree in the Department of Human Physiology by:

Michael Hahn, PhD	Chairperson
Andy Karduna, PhD	Core Member
Damien Callahan, PhD	Core Member
Keat Ghee Ong, PhD	Institutional Representative

and

Kate Mondloch Interim Vice Provost and Dean of the Graduate School

Original approval signatures are on file with the University of Oregon Graduate School.

Degree awarded December 2020

DISSERTATION ABSTRACT

Michael A. McGeehan

Doctor of Philosophy

Department of Human Physiology

December 2020

Title: A Simulation-Based Framework for Informing Design of Prosthetic Feet

Individuals with lower limb amputation face a variety of conditions associated with decreased quality of life, including elevated metabolic cost during ambulation, gait asymmetry, and a variety of psychological disorders. Sustained prosthesis use may also induce overloading of joints, leading to orthopedic injuries. These issues may be attenuated by improving user specificity in the design characteristics of foot prostheses. However, the effects of varied design parameters (e.g. stiffness) are not well characterized, and thus achieving meaningful improvements in gait mechanics has proven elusive. In order to achieve improvements, a robust understanding of the relationship between anthropometry, gait mechanics, and prosthesis design is necessary.

Simulations based on computational gait models are powerful tools for evaluating potential biomechanical interventions, such as implementing a novel prosthesis. However, the utility of simulations to evaluate the effects of varied prosthesis design parameters on gait mechanics has not been fully realized due to lack of a readily-available limb loss-specific gait model and methods for efficiently simulating the mechanics of passive foot prostheses. The purpose of this dissertation was to develop computational models of a semi-active variable-stiffness foot prosthesis (VSF) and a limb loss-specific gait model to

elucidate the relationships between anthropometry, gait mechanics, and variable prosthesis stiffness.

This dissertation was divided into three distinct, yet related projects. Project 1 consisted of developing and validating a computational model of a VSF, a model of VSF-ground contact dynamics, and an optimization algorithm for programmatically deriving model parameters. In Project 2, a limb loss-specific gait model was developed and validated. Project 3 entailed developing a spatial contact model for the interface between the prosthetic socket and residual limb, and using that model for a simulation-based analysis of the effects of variable prosthesis stiffness on residual limb-socket dynamics. Projects 1 and 2 resulted in models and code for simulating gait with a VSF. Project 3 resulted in a reduced order spatial contact model of residual limb-socket interface dynamics. Simulated interfacial pressure and shear stress, as well as residual limb kinematics were similar to values previously reported in the literature. The effects of variable prosthesis stiffness on these outcomes were subject-dependent.

CURRICULUM VITAE

NAME OF AUTHOR: Michael A. McGeehan

GRADUATE AND UNDERGRADUATE SCHOOLS ATTENDED

University of Oregon, Eugene, OR
Willamette University, Salem, OR

DEGREES AWARDED

Doctor of Philosophy, Human Physiology, 2020, University of Oregon
Master of Science, Human Physiology, 2016, University of Oregon
Bachelor of Arts, Exercise Science, 2008, Willamette University

AREAS OF SPECIAL INTEREST

Computational modeling
Model-based design of lower limb prostheses
Biomechanical gait simulations

PROFESSIONAL EXPERIENCE:

Graduate Research Assistant, University of Oregon Dept. Human Physiology (Neuromechanics Laboratory), 2016-present

Graduate Employee, University of Oregon Dept. Human Physiology, 2014-present

Graduate Research Assistant, University of Oregon Human Dept. Human Physiology (Sensorimotor Physiology Laboratory), 2014-2016

Sr. Research Technologist, Washington State University Dept. Mechanical and Materials Engineering (Sports Science Laboratory), 2013-2014

GRANTS, AWARDS, AND HONORS

ASME PhD Student Paper Competition Finalist, American Society of Mechanical Engineers Summer Biomechanics, Bioengineering, and Biotransport Conference, 2020

Jan Broekhoff Fellowship, Department of Human Physiology, University of Oregon, 2020

Graduate Teaching Excellence Award (First alternate), University of Oregon, 2020

Graduate Teaching Award, Department of Human Physiology, University of Oregon, 2020

Graduate Student Presentation Award, Oregon Bioengineering Symposium, 2019

David Winter Young Investigator Award Finalist, International Society of Biomechanics, 2019

Lokey Doctoral Science Fellowship, University of Oregon, 2019

Joseph K. Starr Scholarship, University of Oregon, 2019

Shapiro Family Scholarship, Department of Human Physiology, University of Oregon, 2019

Jan Broekhoff Fellowship, Department of Human Physiology, University of Oregon, 2019

Shapiro Family Scholarship, Department of Human Physiology, University of Oregon, 2018

PUBLICATIONS

Day, E., Alacantara, R., McGeehan, M., Grabowski, A., & Hahn, M. (2020). Low-pass filter cutoff frequency affects sacral-mounted accelerometer estimations of peak vertical ground reaction force during treadmill running. *Journal of Biomechanics*. UNDER REVIEW

McGeehan, M., Adamczyk, P., Nichols, K., and Hahn, M. (2020). A Reduced Order Computational Model of a Semi-Active Variable-Stiffness Foot Prosthesis. *Journal of Biomechanical Engineering*. UNDER REVIEW

McGeehan, M., Woollacott, M., & Dalton, B. (2017). Vestibular control of standing balance is enhanced with increased cognitive load. *Experimental Brain Research*. 235, 1031-1040.

Kessler, N., Kim, S., McGeehan, M., & Hong, J. (2012). Applications of whole body vibration therapy in the clinical setting: a brief review. *International Journal of Therapy and Rehabilitation*. 19, 405- 413.

ACKNOWLEDGEMENTS

Thank you to my advisor, Dr. Mike Hahn. I am sincerely grateful for your guidance throughout my graduate school experience. Through your dedication as a mentor, you continually position your students to succeed in both their professional and personal lives. You have been a constant source of encouragement and an excellent role model. Thank you for providing such a wonderful environment for me to learn and grow as a scientist. I will forever be grateful for all that I have learned from you and the fun that I have had throughout the process. You are an outstanding advisor, mentor, colleague, and friend.

I would also like to graciously thank each member of my dissertation committee. To Dr. Andy Karduna: You have been an exceptional mentor to me from the outset of my graduate studies. Thank you for challenging me both as a student and as a researcher. Your lighthearted but thorough approach to science is the model of what I strive for in my own career. To Dr. Damien Callahan: Your response when I asked you to join my dissertation committee ("Sounds like a cool project – I'm in!") is representative of your unabated enthusiasm as a researcher and mentor. Thank you for the encouragement. Your ability to approach science with an "outside the box" perspective improved my own outlook on this project, since I always had to consider what your viewpoint might be. To Dr. Keat Ghee Ong: Thank you for your eagerness to participate in a committee outside of your department and for your insightful contributions to this project. The sincerity with which your mentor and the enthusiasm with which you approach science and engineering are benchmarks that most can only hope to achieve. Beyond this project, I am grateful for all that you have invested towards cultivating my future as a scientist. As committee members, each of you provided exceptional mentorship and have played an integral role in shaping

this research. Thank you for dedicating your time, effort, and enthusiasm.

Thank you to our research collaborators at the University of Wisconsin-Madison, Dr. Peter Adamczyk and Mr. Kieran Nichols, who provided a protype variable-stiffness foot prosthesis, access to a database of experimental data for individuals walking on the prosthesis, and countless intellectual contributions. This work would not have been possible without your collaboration and support.

Thank you to the current and former members of the Neuromechanics Laboratory: Seth Donahue, Katie Farina, Emily Karolidis, Ola Adeniji, Dr. Evan Day, Dr. Li Jin, Marissa Burnsed-Torres, Dr. Jake Hinkel-Lipsker, and Dr. Bryson Nakamura. You made this lab a wonderful place to study (and an even better place to not study). I am truly grateful to have been surrounded by such outstanding scientists and friends during my time in the lab.

Lastly and most importantly, thank you to my wonderful partner Kate. You have provided so much support, big and small. I cannot express my gratitude for all that you do. Thank you for the love, support, guidance, brainstorming, peer review, copy editing, scientific debates, tech support, dog wrangling, and fun throughout our time in graduate school. You are a wonderful partner and a brilliant scientist. I am elated to have shared this adventure with you.

Thank you to the University of Oregon Graduate School, Department of Human Physiology, and generous benefactors who helped fund my graduate education and research.

This dissertation is dedicated to my family for their unconditional love and support. To my mom: your enthusiasm for translating science to improve the lives of others inspires me to aim high and pursue impactful research. Thank you also for teaching me the value and vitality of a strong cup of coffee. To my dad: your ability to approach hard work with kindness, compassion, and a smile on your face motivates me to persevere through challenges. Thank you also for teaching me the importance of taking a day off and going on an adventure. To my sister: I aspire to reach your level of thoughtfulness, empathy, and fun-loving attitude in both academics and daily life. Thank you also for teaching me to enjoy the world around me, no matter where I am. To my partner, Kate: I learn so much from you on a daily basis. Thank you for your patience, never-ending encouragement, and ability to make me laugh even in stressful times. The kindness that you show the world is nothing short of exemplary. This dissertation would not have been possible without you.

TABLE OF CONTENTS

Chapter Page

Chapter Page

Chapter Page

LIST OF FIGURES

Figure Page

LIST OF TABLES

Table Page

CHAPTER I

INTRODUCTION

Background and Significance

Introduction

Individuals with lower limb amputation (LLA) exhibit distinct gait characteristics, which may limit mobility and decrease quality of life. Those using lower limb prostheses may display gait asymmetry (Sanderson and Martin, 1997; Schaarschmidt et al., 2012), elevated metabolic cost during locomotion (van Schaik et al., 2019), and a variety of psychological disorders including anxiety and depression (Mckechnie and John, 2014). Sustained prosthesis use may also induce overloading of intact joints and ultimately, orthopedic injuries (Gailey et al., 2008). Each of these issues may be attenuated by improving user specificity in the design characteristics of foot prostheses. However, the effects of varied prosthesis design parameters (e.g. stiffness) are not well characterized, and thus achieving meaningful improvements in gait mechanics has proven elusive (Casillas et al., 1995; Postema et al., 1997). In order to achieve improvements, a robust understanding of the relationship between the anatomical morphologies associated with LLA, gait mechanics, and prosthesis design is necessary.

Rehabilitation following a LLA often includes prescription of a prosthesis designed to replace the coordinated energy absorption and generation properties of the removed limb. Use of a lower limb prosthesis can improve mobility, health, and quality of life. Passive energy storage and return (ESR) foot prostheses are the current standard technology for replacing this functionality. However, the fixed stiffness behavior of these

devices contrasts that of the healthy foot-ankle complex, which modulates stiffness in response to varied gait conditions (e.g. velocity and terrain). Glanzer and Adamczyk (2018) recently developed a variable-stiffness foot (VSF) prosthesis designed with an actuated keel support fulcrum to semi-actively control sagittal forefoot stiffness and thereby adapt to different gait conditions with low power. The VSF is an ideal device for studying the relationships between prosthesis stiffness and gait mechanics for several reasons: a) It can readily exhibit a range of stiffness values, thereby eliminating the need to purchase or manufacture multiple prostheses as in Fey et al. (2011), Jin et al. (2016) and Zelik et al. (2011), b) in doing so, this also eliminates confounding variables that accompany this experimental design, and c) The VSF can modulate stiffness along a continuous scale, which provides improved resolution compared the typical discrete stiffness options available for fully passive designs.

Simulations based on computational gait models are useful for evaluating potential biomechanical interventions such as implementing a novel ESR prosthesis. Inverse simulations provide the ability to estimate values that cannot be measured *in vivo* (e.g. socket-residual limb interface dynamics), whereas predictive simulations provide insights regarding how humans may interact with and adapt to new prosthetic devices. Computational gait models have been employed previously to investigate the effects of prosthesis alignment (Laprè et al., 2014) and a biarticular clutched spring mechanism (Willson et al., 2020) on gait mechanics among persons with LLA. However, these models do not account for the ESR properties of the prosthetic foot, thus limiting their ecological validity. Due to these limitations, the use of simulations to inform the design and prescription of ESR prostheses remains largely unexplored.

Limb Loss Population

Lower limb amputation is an expanding problem in the United States, particularly among combat veterans and patients with diabetes and/or dysvascular diseases (Johansson et al., 1988; Robbins et al., 2009). Two million Americans currently have an amputation, and this population expected to surpass 3.6 million by 2050 (Ziegler-Graham et al., 2008). Among these individuals, nearly 40 percent have a major LLA, classified as amputation of a lower limb excluding toes (Ziegler-Graham et al., 2008). Individuals with LLA vary widely by etiology, age, sex, and ethnicity. Recent data suggest that LLA arising from dysvascular complications comprise the majority (80%) of LLA cases in the United States, with more than 66% of these cases attributed to diabetes mellitus. An additional 17% of LLA was attributed to trauma and 3% to cancer. These instance rates vary by age, but are relatively similar across sex. The variation by age may stem from increased incidence of dysvascular diseases and/or diabetes with age, as these conditions contribute substantially to rates of LLA. Across all etiologies, 42% of individuals with limb loss are over the age of 65, 25% are female, and 42% are non-white (Ziegler-Graham et al., 2008).

Lower limb amputation adversely affects quality of life through increased biomechanical, physiological, and psychological stress (Gailey et al., 2008; Sagawa et al., 2011). Impaired mobility is a major factor in reduced quality of life, with individuals with LLA often reporting seemingly simple tasks of daily living as major challenges (Legro et al., 1998; Sagawa et al., 2011). Unilateral below-knee amputation (BKA), the most common form of major LLA, is associated with a 20% increase in metabolic energy expenditure during walking, a 20% decrease in preferred walking velocity, asymmetric

gait, and increased incidence of falls (Linde et al., 2004; Major et al., 2014; Russel Esposito and Miller, 2018; Sagawa et al., 2011). Fey et al. (2009) also found that walking with a lower limb prosthesis requires greater activation of muscles responsible for moving the lower limbs compared to individuals with healthy intact limbs. In addition to increased biomechanical and physiological stress during walking, individuals with LLA exhibit increased prevalence of psychological depression and anxiety compared to non-amputees (Mckechnie and John, 2014). These mobility limitations and secondary conditions may be attributed to functional inadequacies of prosthetic feet. However, it is believed that improving mobility and reducing incidence of secondary ailments can be accomplished through innovative prosthetic foot designs and improved methodology for matching individuals with LLA with the appropriate prosthetic devices.

Design and Prescription of Passive Foot Prostheses

Rehabilitation following a BKA often includes prescription of a lower limb prosthesis system, consisting of a prosthetic socket, which interfaces with the residual limb, a rigid pylon, and a foot prosthesis. One of the primary design goals of a lower limb prosthesis is to replace the coordinated energy absorption and generation properties of a lost limb. Passive energy storage and return (ESR) prostheses are the current standard technology for mimicking this functionality. These devices are designed to store and return energy to the user through deformation of compliant materials (e.g. carbon fiber or fiberglass composite) and/or structures (e.g. leaf springs or bumpers). By storing energy when the prosthesis impacts the ground and releasing it later in the gait cycle, ESR prostheses help stabilize and propel the user during gait, thereby mimicking the behavior

of the intact foot-ankle complex and associated musculature. Stiffness of the elastic structure(s) is a key design characteristic of passive prostheses, due to its role in determining the magnitude and rate of energy storage and return during load bearing movements (e.g. gait) (Lin et al., 2004; Peterson, 2012; Webber and Kaufman, 2017). However the user-specific effects of prosthesis stiffness on gait mechanics remain unclear, and thus selecting the appropriate prosthetic foot for a prosthesis user is not well-defined.

Prosthetic foot stiffness affects the gait characteristics of the wearer (Fey et al., 2013, 2012; Major et al., 2014; Ventura et al., 2011; Zelik et al., 2011). However, previous efforts to elucidate the relationships between prosthesis stiffness and gait outcomes have often yielded small and/or variable changes. Major et al. (2014) showed reduced stiffness to decrease net metabolic cost of gait, whereas Zelik et al. (2011) showed energy expenditure to be least with an intermediate stiffness. Fey et al. (2013) associated reduced stiffness with decreased mechanical efficiency. Varied results have also been reported for lower limb kinematics, kinetics, and muscle activation (Fey et al., 2013, 2012; Major et al., 2014; Ventura et al., 2011). Previous attempts to optimize gait through prosthesis stiffness parameterization have also proven arduous (Casillas et al., 1995; Postema et al., 1997).

Despite the opaque relationship between prosthesis stiffness and gait mechanics, stiffness remains one of the key variables considered in the design and prescription of ESR prostheses (Linde et al., 2004; Webber and Kaufman, 2017). There are currently dozens of commercially-available ESR prostheses, often with multiple models of varying stiffnesses (Webber and Kaufman, 2017). However, there remains no clinical consensus

regarding the prescription of prosthetic feet, and there is currently a dearth of quantitative data to inform such a consensus. Moreover, commercially available feet designed for the same user may exhibit vastly different stiffness and hysteresis characteristics (Figure 1.1) (Webber and Kaufman, 2017). The linear stiffness values for seven popular models of prosthetic feet were summarized by Webber and Kaufman (2017) (Figure 1.1).

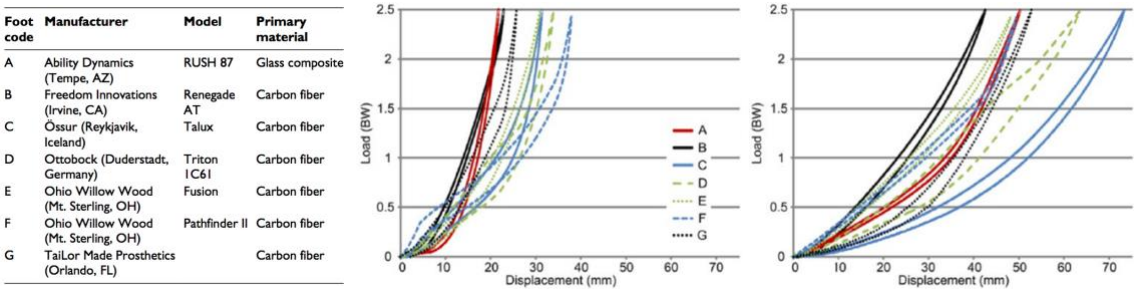

Foot code	Manufacturer	Model	Primary material
A	Ability Dynamics (Tempe, AZ)	RUSH 87	Glass composite
B	Freedom Innovations (Irvine, CA)	Renegade AT	Carbon fiber
C	Össur (Reykjavik, Iceland)	Talux	Carbon fiber
D	Ottobock (Duderstadt, Germany)	Triton 1C61	Carbon fiber
E	Ohio Willow Wood (Mt. Sterling, OH)	Fusion	Carbon fiber
F	Ohio Willow Wood (Mt. Sterling, OH)	Pathfinder II	Carbon fiber
G	TaiLor Made Prosthetics (Orlando, FL)		Carbon fiber

Figure 1.1: Summary of material composition (left) and linear heel (center) and forefoot (right) stiffness characteristics for a 90 kg subject on seven popular models of prosthetic feet (size 27). Figure reproduced from Webber and Kaufman (2017).

The current process for prescribing a foot prosthesis typically involves assessing one or more of the following patient characteristics: age, height, weight, activity level, mobility abilities (i.e. K level), and amputation level (Hofstad et al., 2004; Menard et al., 1992; Versluys et al., 2008). Prosthetists rely on these metrics, along with their qualitative experience to match the user with the best available prosthesis. Manufacturers often assign prosthetic feet a specific category, which were summarized by Peterson et al. (2012) (Tables 1.1 and 1.2). Manufacturers offer limited and discrete options, and thus prosthetists may be forced to choose between a prosthesis that is too stiff for a patient and one that is too compliant. Given the aforementioned ailments and mobility limitations faced by amputees, it is clear that the current standard of care is insufficient and that there

is a need to establish a quantitative framework to inform the design and prescription of passive prosthetic feet.

Table 1.1: Subject classification for prosthetic foot stiffness prescription based on height (cm) and weight (kg). These data are from Peterson et al. (2012).

		Height (cm)					
		< 160	**160-168**	**168-175**	**175-183**	**183-190**	**>190**
Weight (kg)	**<77.3**	1A	2A	3A	4A	5A	6A
	77.3 – 90.9	1B	2B	3B	4B	5B	6B
	> 91.0	1C	2C	3C	4C	5C	6C

Table 1.2: Subject classifications (see Table 1.1) and their corresponding linear forefoot stiffness values (N/mm). Classifications are for a compliant foot (C), for daily use or less active individuals, and a stiff foot (S), for active individuals. These data are from Peterson et al. (2012).

	1a	**1b**	**1c**	**2a**	**2b**	**2c**	**3a**	**3b**	**3c**	**4a**	**4b**	**4c**	**5a**	**5b**	**5c**	**6a**	**6b**	**6c**
C	14	36	52	14	36	52	27	37	46	27	37	46	27	37	46	27	37	46
S	52	69	79	52	69	79	46	62	89	46	62	89	46	89	89	46	62	89

Design of the Semi-Active Variable-Stiffness Foot Prosthesis

Passive ESR prostheses remain the standard performance foot prosthesis for individuals with LLA. However, the fixed stiffness behavior of these devices contrasts that of the intact human foot-ankle complex, which modulates performance to match a

variety of gait conditions (e.g. push off power, velocity, and terrain) (Farris and Sawicki, 2012; Winter, 1991). Powered devices offer increased performance and adaptability, but characteristics such as cost, build height, and power consumption remain substantial design challenges, severely limiting the ability of a broad population to access and use these devices.

Glanzer and Adamczyk (2018) recently developed a semi-active variable-stiffness foot (VSF) prosthesis that balances the simplicity of a passive ESR design with the adaptability of a powered design. The keel of the VSF (Figure 1.2) is a G10/FR4 composite leaf spring designed as an overhung cantilever beam. The supported beam length (l) is modulated via an actuated keel support fulcrum (B). The total beam length (L) is 229 mm, whereas the supported length (l) is variable between 66–151 mm. By

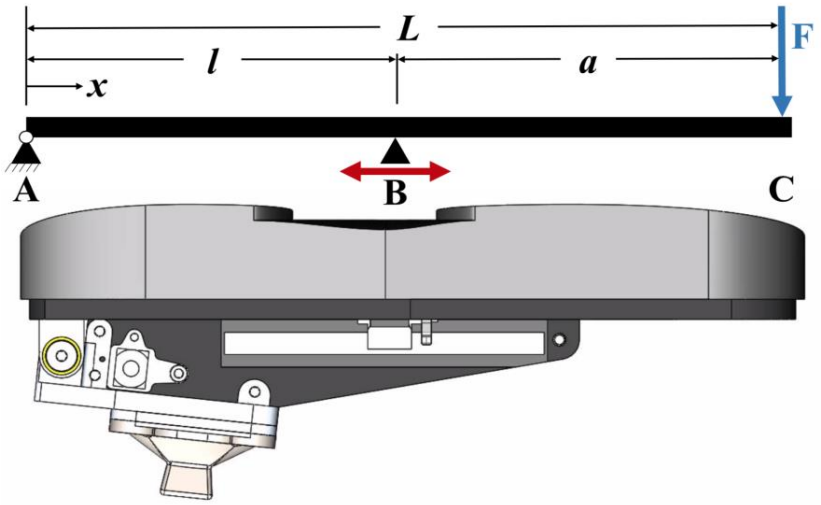

Figure 1.2: Euler-Bernoulli overhung beam model of the VSF. The schematic illustrates keel length (L) pinned at A and simply supported at B. Overhung length (a) = $L - l$ (supported length).

modulating the overhung length, the VSF's forefoot stiffness can be semi-actively controlled and thereby adapt to different gait conditions with low power. The heel component of the VSF has a consistent linear stiffness of 65 N/mm. The forefoot is capable of exhibiting a continuous range of stiffness values between 10–32 N/mm, corresponding to fulcrum positions ranging 66–151 mm (Figure 1.3). Importantly, this

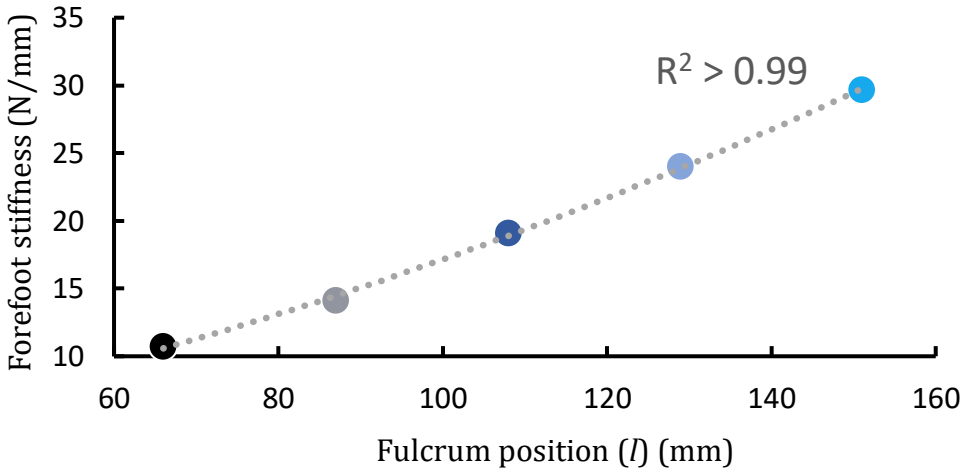

Figure 1.3: Forefoot stiffness values for the VSF under five fulcrum configurations. Data were derived from static compression tests at 50 mm/min (Glanzer and Adamczyk, 2018). A second-order polynomial fit is depicted (grey dashed line).

encompasses the discrete stiffness values of a range of commercially-available ESR prostheses (Webber and Kaufman, 2017). Forefoot stiffness (k) of the VSF can be calculated as a function of keel deflection (y_c), force (F), flexural elastic modulus (E), and fulcrum position (eq. 1.1, eq. 1.2, Table 1.3).

eq. 1.1: $y_c = -\frac{FLa^2}{3EI}$

eq. 1.2: $k = \frac{F}{y_c} = \frac{3El}{La^2}$

Table 1.3: Nominal properties of the VSF keel (Glanzer and Adamczyk, 2018).

L	Beam length	229 mm
a	Overhung length (variable)	163 – 78 mm
l	Supported length (*l = L – a*)	66 – 151 mm
I	Moment of inertia ($bh^3/12$)	992 mm^4
b	Cross section width	46.5 mm
h	Cross section height	6.35 mm
E	Flexural elastic modulus	18.6 GPa (Poisson's ratio: 0.136)

The VSF is designed to balance the simplicity of passive ESR feet with the adaptability of powered foot-ankles in order to maximize functionality for the user while minimizing weight, build height, and power consumption. The operating principle of the semi-active design is to drive the fulcrum carriage only during swing phase. As such, the VSF behaves principally as a passive ESR device during stance phase, with the ability to adjust passive stiffness between stance phases (Glanzer and Adamczyk, 2018). The VSF has an onboard potentiometer, which conveys feedback about fulcrum position, and an inertial measurement unit (IMU), which conveys information regarding the VSF's linear acceleration, angular velocity, and heading. Data from these sensors are transmitted to an onboard microcontroller and streamed wirelessly to a nearby computer via radio transceiver. Based on this configuration, VSF stiffness can be adjusted using closed-loop control laws (e.g. adjusting stiffness based on IMU-derived gait velocity) or manually adjusted based on user input (i.e. open-loop).

Simulating Gait for Lower Limb Prosthesis Users

Computational simulations based on musculoskeletal gait models are promising tools to explore the relationships between human anatomy, gait mechanics, and prosthesis design (Russell-Esposito and Miller, 2018; Fey et al., 2013; Seth et al., 2011; Willson et al., 2020). These models are mathematical representations of human biomechanics, which use laws of Newtonian physics and knowledge of the mechanical, anatomical, and physiological properties of the human body to derive equations of motion related to movement. These equations can then be used to mathematically simulate human movement. Inverse simulations provide the ability to estimate values that cannot be measured *in vivo* (e.g. dynamics between the residual limb and prosthetic socket), whereas predictive simulations suggest hypotheses regarding how humans may interact with and adapt to new prosthetic devices. Typically, human gait simulations are computed within a forward kinematics framework (joint kinetics and end effector positions are calculated using joint angles as inputs) or a forward dynamics framework (joint kinematics and end effector positions are calculated using joint torques as inputs).

Computational musculoskeletal models have been used to evaluate human movement under a variety of conditions, including walking (Rajagopal et al., 2016), running (Seth et al., 2011), and jumping (Porsa et al., 2015). However, the models used in these studies are not suitable for simulating gait among individuals with BKA, as the mass, inertial, and mechanical properties of prosthetic limb systems are dissimilar compared to those of the biological human shank. LaPré et al. (2014) and Willson et al. (2020) both developed limb loss-specific models in OpenSim, a popular musculoskeletal modeling and simulation platform. These studies used simulations to investigate the

effects of prosthesis alignment and a biarticular clutched spring mechanism on gait mechanics, respectively. However, the models used in these studies do not account for the ESR properties of the prosthetic foot, thus limiting their ecological validity. Other studies, which did incorporate the force and torque contributions of ESR feet into gait models focused on characterizing biomechanical and muscle activation responses with prosthesis use, rather than validation of the prosthesis model (Fey et al., 2012; Russel Esposito and Miller, 2018). While these studies made important progress toward investigating the relationship between anthropometry, gait mechanics, and prosthetic foot design, they had limited ability to verify simulation results in the context of experimental values. Due to these limitations, the use of simulations to inform the design of ESR foot prostheses has not been fully realized.

General and Specific Aims

The objective of this dissertation was to use computational modeling and simulations to discover the distinctive effects of foot prosthesis stiffness on gait mechanics. This knowledge can be applied better understand the relationships between human anthropometry, gait mechanics and prosthesis design and also to improve the design and prescription of user-specific prosthetic feet. Towards this overarching objective, four specific aims were addressed.

Specific Aim 1. Model the geometry and dynamics of a semi-active variable-stiffness foot prosthesis. The focus of this aim was to develop a forward simulation-capable model of a

semi-active variable-stiffness ESR foot prosthesis. This model was designed to be used in subsequent aims to simulate gait with variable prosthesis stiffness.

Specific Aim 2. Design and optimize contact models to predict ground reaction forces from kinematics during gait simulations. Forward simulations require an accurate model of the contact dynamics between the human and their environment (i.e. walking surface). The focus of this aim was to model the geometry and mechanical properties of the VSF's foam base to predict ground reaction forces from gait kinematics.

Specific Aim 3. Develop a gait model specific to individuals with lower limb loss. The focus of Aim 3 was to develop and validate a scalable forward simulation-capable gait model with the anatomical morphologies associated with a below-knee amputation. The models from *Specific Aims 1 and 2* were integrated with the gait model in order to simulate gait with varied prosthesis stiffness.

Specific Aim 4. Simulate gait to estimate the effects of variable prosthesis stiffness on dynamics between the residual limb and prosthetic socket. A spatial contact model of the residual limb-prosthetic socket interface was developed and integrated into the gait model from *Specific Aim 3*. Gait simulations were computed for subjects walking with a foot prosthesis set to 32, 19, and 10 N/mm stiffness values. The effects of varied prosthesis stiffness on socket-residual limb interface dynamics were estimated from the model.

By completing these aims, the current understanding of the relationship between prosthetic foot stiffness and user-specific gait outcomes is improved. This knowledge may be applied to develop a quantitative biomechanical simulation-based framework to inform prosthetic foot selection and design. Such a framework could augment or supplant a largely qualitative and unreliable process with a quantitative and systematic one. In doing so, the goal is to make considerable improvements on the current standard of care for lower limb prosthesis users, attenuate biomechanical and physiological stressors associated with limb loss, and establish a quantitative basis for user-specific prosthetic foot designs.

Organization of Dissertation

This dissertation is written in a journal style format, where chapters III-V have been or will be submitted for publication to peer-reviewed journals. The following explains how these chapters fit together into a coherent body of work. A bridge statement explaining the flow of studies is included at the conclusion of Chapters III-V.

The current chapter (Chapter I) provides relevant background information regarding the prevalence of LLA, distinctive mobility characteristics among individuals with BKA, prosthesis design, and use of computational simulations to explore each of the relationships between each of these factors. This chapter establishes the basis and need for the research presented in this dissertation. Chapter II will detail the methodology used for model development and simulations. Chapter III describes methods, model development, and validation procedures related to Specific Aims 1 and 2. Chapters IV and V correspond to the model development and methods used to complete Specific

Aims 3 and 4, respectively. Finally, Chapter VI summarizes the notable results of the overall body of work, recapitulating the key findings while acknowledging limitations and outlining future directions for work in this area of research.

This dissertation includes co-authored work, some which has already been submitted for publication in peer-reviewed journals. Chapter III has been submitted to *Journal of Biomechanical Engineering*. Chapter IV is currently in preparation for submission to *Journal of Biomechanical Engineering* via an invited submission. Chapter V will be submitted for publication to an appropriate journal. For all work in this dissertation, Michael McGeehan was the primary investigator, responsible for model design, study design, simulation methodology, data analysis, interpretation, and dissemination. Dr. Michael E. Hahn, Dr. Peter G. Adamczyk, and Kieran M. Nichols are co-authors of all studies. Dr. Hahn advised on all aspects of this dissertation. Dr. Adamczyk and Mr. Nichols are collaborators on these studies, providing access to their database of individuals with BKA walking on the VSF, and input regarding data processing, analysis, interpretation, and manuscript preparation.

CHAPTER II

OVERVIEW OF METHODOLOGY

Chapters III and IV of this dissertation describe the development and validation of a computational prosthesis model and a gait model for forward gait simulations. Chapter V describes the development of a residual limb-prosthetic socket spatial contact model and an analysis of the effects of prosthesis stiffness on socket dynamics using the aforementioned models. Experimental data from benchtop testing of the variable-stiffness foot (VSF) and motion capture data of human subjects walking with the VSF were used in the model development and validation processes. This chapter provides a summary of the methodologies used to develop the models and the experimental data used to drive them. A brief overview of the statistical methods employed to characterize the models' response compared to experimental benchmarks is also provided. All models and code associated with this work are freely available at: https://github.com/m-mcgeehan.

General Modeling and Simulation Methodology

The models presented in this dissertation were developed in Simscape Multibody, which is a 3D multi-body dynamics modeling and simulation platform built into the MATLAB computational suite (Mathworks Inc. Natick, MA). Simscape models are designed as articulated mechatronic systems, consisting of bodies interconnected through joints and constraints. Bodies may be rigid or flexible and compose the mass and inertial properties of the modeled system. Joints are typically constrained between zero (i.e. weld joint) and six degrees-of-freedom with the option to define more complex motions such

as gearing or cam motions. Bodies and joints are connected through interface frames. Model assembly occurs in two phases. First, the assembly algorithm computes the initial position states of the model (p and q), so that the resulting assembly satisfies all kinematic constraints. This process is then repeated for the initial velocity states ($\dot{p}$ and $\dot{q}$).

The MATLAB *KinematicsSolver* function is used to formulate and numerically solve kinematics problems for the model. Six steps are executed to initialize and simulate a typical model: 1) **Model validation**: The Simscape solver validates the model configuration by checking for violation of model construction rules. For example, each component must be connected directly or indirectly to one or more physical networks (analogous to a world frame) and units must match between source blocks and their connection. 2) **Network construction**: The Simscape solver then constructs the physical network based on principles of energy conservation. Two directly connected ports share the same value for their "across" variables (e.g. angular velocity), whereas "through" variables (e.g. torque) may be divided among multiple connected components such that the sum of all values flowing through a branch point equals the sum of all values flowing out. **3) Equation construction**: The Simscape solver constructs the system of equations for the model. These equations may contain both dynamic and algebraic variables. Dynamic variables appear in the system of equations along with their time derivatives. They add dynamics to the system and require numerical integration to compute their values. Algebraic variables appear in the system of equations independent of their time derivates, but the state of these variables is dependent upon one or more dynamic variables. For example, the algebraic variable mass is constant due to the law of

conservation of mass, but the state of this variable may be dependent upon a dynamic variable, such as angular velocity. **4) Initial conditions computation**: The Simscape solver computes the model's initial condition only once at the beginning of the simulation ($t = 0$). For all simulations in this dissertation, the model conditions are assumed to start from steady state (i.e. zero derivative). The solver computes the initial conditions by finding initial values for all system variables that exactly satisfy the model's system of equations. **5) Transient initialization**: After computing the model's initial conditions, or after a discontinuity (see Step 6: Transient solve), the solver fixes all dynamic variables and solves for algebraic variables and the time derivatives of dynamic variables. The goal of transient initialization is to provide a consistent set of initial conditions for the transient solve phase. **6) Transient solve**: In this step, continuous differential equations are integrated with respect to time in order to compute all model variables as a function of time. The solver performs the simulation according to the results of the transient solve until a discontinuity occurs, at which point the solver returns to the transient initialization step. A discontinuity may be anything that alters the continuous state of the model. For example, onset of an external force. The solver cycles through the transient solve and initialization steps until the simulation is complete ("Simscape Multibody Documentation," 2020).

A variety of MATLAB-based approaches can be used to solve the model. These include both continuous and discrete options, an extensive set of ordinary differential equation (ODE) solvers, and a variety of numerical integration settings (e.g. fixed or variable time steps, step size constraints, and tolerance values). Each of these parameters may be strategically selected based on their suitability for a given simulation scenario,

such as system dynamics, solution stability, computation speed, and solver robustness. The *ode*15s solver was used for all simulations, per the recommendations of the Simscape documentation ("Simscape Multibody Documentation," 2020).

Chapter III

VSF Model Stiffness

A computational model of the VSF was developed in Simscape Multibody using the lumped parameter approach for approximating the dynamics of flexible bodies. A model of a materials testing system was also developed and used to simulate static compression tests on the VSF model. Experimental data from static compression testing of the physical VSF configured to five discrete fulcrum configurations were used as benchmark values to validate the model's stiffness response. Forefoot stiffness was calculated for each setting based on the load-displacement response of the forefoot. These data were used to validate the stiffness response of the VSF model outlined in Chapter III (Specific Aim 1). Simulated and experimental data were compared using root-mean-squared-error (RMSE) and coefficient of determination (R^2).

VSF Ground Contact Model

An overall model of the VSF's contact dynamics with the ground was developed using 24 sphere-to-plane contact models distributed on the plantar surface of the VSF model. Experimental ground reaction force (GRF) and center of pressure (COP) data from a male subject with a transtibial amputation (Table 2.1, Subject 1) walking with the VSF configured to "high", "medium", and "low" stiffness settings were used as

comparator values to develop and validate the ground contact model. A Latin Hypercube-based optimization algorithm was developed to programmatically derive stiffness, damping, and friction terms for each contact sphere. Simulated and experimental data were compared using root-mean-squared-error (RMSE) and coefficient of determination (R^2).

Chapter IV

Human Musculoskeletal Gait Model

A scalable, 28 degree-of-freedom (DOF) musculoskeletal gait model was developed in Simscape Multibody. Open-source cadaveric skeletal 3D surface geometry data were first used to develop a generic model and then custom MATLAB scripts were developed to programmatically scale and assemble subject-specific models based on marker coordinates from optical motion capture data. The tibia and fibula were transected and encapsulated within a prosthetic socket to represent a transtibial amputation. The VSF model developed in *Specific Aims 1* and *2* was then integrated.

Motion capture data from four individuals with a transtibial amputation (Table 2.1) walking with the VSF were used to develop and evaluate the gait model (*Specific*

Table 2.1: Participant characteristics

Subject	Sex	Age (y)	Height (cm)	Mass (kg)	Amputation side	Years post-amputation
1	Male	34	181	77.3	Right	15
2	Male	51	175	111	Right	8
3	Male	70	180	83.8	Left	14
4	Female	61	163	63.8	Right	8
Mean ± SD	–	54 ± 15	175 ± 19.9	84.0 ± 19.9	–	11 ± 3.8

Aim 3). To be included, participants were required to be at least 2 years post-amputation and be able to safely complete nine gait trials walking at 1.2 ± 1 m/s. Motion capture data consist of 38 lower body retroreflective marker trajectories collected through optical motion capture and GRF data measured through in-ground force plates. Subjects completed three trials with the VSF configured to "high", "medium", and "low" stiffness settings (Table 2.2); however Subject 2 did not complete one "medium" stiffness trial, and Subject 4 did not complete one "high" stiffness trial. Simulated lower limb joint

Table 2.2: Summary of experimental trials.

Number of trials	VSF condition	Gait condition
3	"High" stiffness (32 N/mm)	1.2 ± 0.1 m/s , over ground walking
3	"Medium" stiffness (19 N/mm)	1.2 ± 0.1 m/s, over ground walking
3	"Low" stiffness (10 N/mm)	1.2 ± 0.1 m/s, over ground walking

kinematics, center of mass trajectory, GRF, and COP data were compared to experimental data using root-mean-squared-error (RMSE) and coefficient of determination (R^2).

Chapter 5

A spatial contact model of the interface between the residual limb and prosthetic socket was developed and integrated into the larger gait model. The spatial contact model was parameterized using previously reported experimental data for material properties of human skin and socket liner materials, socket interface kinematics, and values for pressure and shear stress occurring at the socket interface during gait. Forward

kinematics simulations were computed for four subjects with a below-knee amputation (Table 2.1) for nine trials each (Table 2.2). Vertical translational motion (i.e. socket pistoning) and axial angular motion of the residual with respect to the socket were evaluated across the conditions. Estimates for normal pressure and shear stress were derived from the spatial contact model and compared across stiffness conditions using repeated measures ANOVA analyses. As it was hypothesized that these effects would be subject-specific, the outcomes were also analyzed on an individualized basis.

CHAPTER III

A REDUCED ORDER COMPUTATIONAL MODEL OF A SEMI-ACTIVE VARIABLE-STIFFNESS FOOT PROSTHESIS

This work is currently under review in the *Journal of Biomechanical Engineering* (Submission date: May 22, 2020). Dr. Michael E. Hahn, Dr. Peter G. Adamczyk, and Mr. Kieran M. Nichols provided mentorship including assistance with study design, data interpretation, and editing and finalizing the final manuscript.

Introduction

Individuals with lower limb loss exhibit distinct gait characteristics, which may limit mobility and decrease quality of life. Those using lower limb prostheses may display gait asymmetry (Sanderson and Martin, 1997; Schaarschmidt et al., 2012), elevated metabolic cost during locomotion (van Schaik et al., 2019), and a variety of psychological disorders including anxiety and depression (Mckechnie and John, 2014). Sustained prosthesis use may also induce overloading of intact joints and ultimately, musculoskeletal ailments (Gailey et al., 2008). Each of these issues may be attenuated by improving user specificity in the design characteristics of foot prostheses. However, the effects of foot prosthesis design parameters (e.g. stiffness) are not well characterized, and thus achieving meaningful improvements in gait has proven arduous (Casillas et al., 1995; Postema et al., 1997). In order to achieve improvements, a robust understanding of

the relationships between anthropometry, gait mechanics, and prosthesis design are necessary.

One of the primary design goals of a lower limb prosthesis is to replace the coordinated energy absorption and generation properties of a lost limb. Passive energy storage and return (ESR) foot prostheses are the current standard for mimicking this functionality. However, the fixed stiffness behavior of these devices contrasts that of the healthy foot-ankle complex, which modulates its behavior in response to varied gait conditions (e.g. velocity and terrain) (Farris and Sawicki, 2012; Winter, 1983). Glanzer and Adamczyk (2018) recently developed a variable-stiffness foot (VSF) prosthesis designed with an actuated keel support fulcrum to semi-actively control sagittal forefoot stiffness and thereby adapt to different gait conditions with low power (Figure 3.1). The

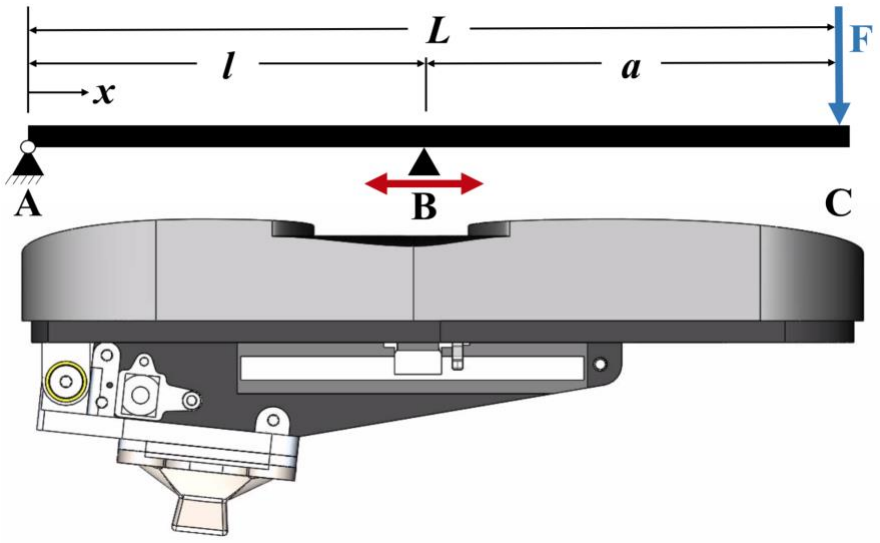

Figure 3.1: Overhung cantilever beam model of the VSF. The schematic illustrates keel length (L) pinned at A and simply supported at B, with a force applied at C. Overhung length (a) = $L - l$ (supported length). Image reproduced with permission from Glanzer and Adamczyk (2018).

ESR keel of the VSF is a composite leaf spring designed as an overhung beam, which modulates the supported length (l) via an actuated keel support fulcrum (B). The total beam length (L) is 229 mm, whereas the supported length (l) is variable between 66–151 mm. By modulating overhung length, the VSF's forefoot is capable of exhibiting roughly a three-fold range of forefoot stiffness values (10–32 N/mm). The heel component of the VSF has a consistent linear stiffness of 65 N/mm. The VSF's fulcrum position is designed to be adjusted during swing phase, thus minimizing the power necessary for actuation. As such, the VSF behaves principally as a passive ESR prosthesis, which can adapt stiffness in response to variable gait conditions.

Simulations based on computational models can be powerful tools for evaluating potential biomechanical interventions, such as the implementation of a novel ESR prosthesis. Recently, simulations have been used to aid in the iterative design process and improve user-specificity (Fey et al., 2013; Strbac and Popović, 2012; Tryggvason et al., 2020). Inverse simulations provide the ability to estimate values that cannot be measured *in vivo* (e.g. socket-residual limb interface dynamics), whereas predictive simulations suggest hypotheses regarding how humans may interact with and adapt to new prosthetic devices.

Computational modeling has been used to investigate the effects of prosthesis alignment (Laprè et al., 2014) and a biarticular clutched spring mechanism (Willson et al., 2020) on gait mechanics among persons with lower limb loss. However, these models do not account for the ESR properties of the prosthetic foot, thus limiting their ecological validity. Other studies, which did incorporate the force and torque contributions of ESR feet into gait models focused on characterizing biomechanical and muscle activation

responses with prosthesis use, rather than validation of the prosthesis model (Fey et al., 2012; Russel Esposito and Miller, 2018). While these studies made important progress toward investigating the relationship between anthropometry, gait mechanics, and prosthetic foot design, they had limited ability to verify simulation results in the context of experimental values. Due to these limitations, the utility of simulations to inform the design of ESR foot prostheses has not been fully realized. The purpose of this study was to further couple experimental and simulation prosthesis data by modeling and validating the mechanical stiffness properties and resulting ground reaction forces of a semi-active VSF.

Methods

Model design

A computational model of the VSF was developed in Simscape Multibody (Mathworks, Inc., Natick, MA). The assembly, geometry, mass, and inertial properties were derived from SolidWorks (Dassault Systemes Inc., Waltham, MA). A reduced order model of the VSF's variable-stiffness elastic keel was designed using the lumped parameter approach for approximating flexible body dynamics. This approach involved discretizing the continuous geometry of the keel into finite rigid segments coupled via revolute joints, springs, and dampers (Figure 3.2). This simplification of the original state space of the continuous elastic keel system to finite dimensions allows the partial differential equations of the infinite-dimensional time-space states of the physical VSF to be represented by ordinary differential equations with a finite number of parameters.

The keel of the VSF model was discretized into 16 segments (eight DoF). The most posterior segment is 66 mm in length, which matches the minimum possible fulcrum position. The rest of the keel consists of 11.64-mm segments for a total beam length of 229 mm (Figure 3.2). These dimensions were selected to allow the VSF model to be configured to stiffness settings previously reported for the physical VSF (Glanzer and Adamczyk, 2018). The stiffness and damping values for the revolute joints were

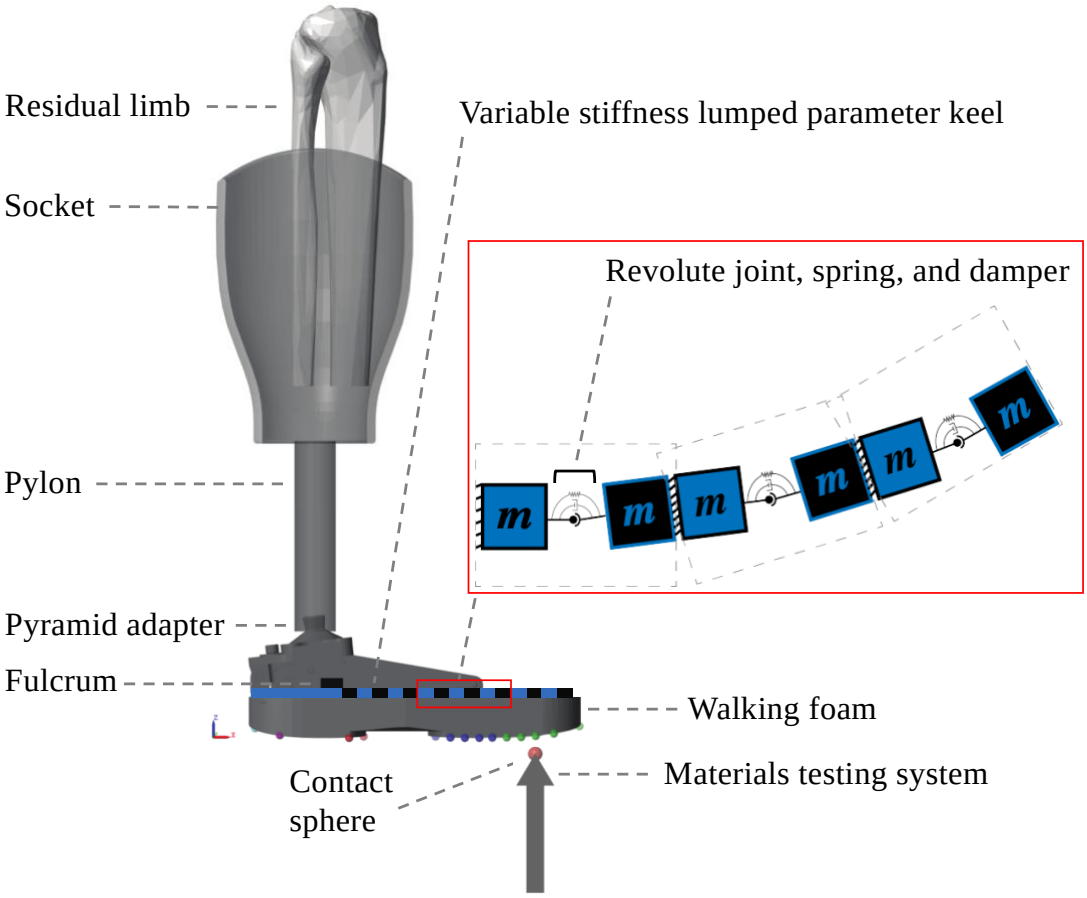

Figure 3.2: Modeled VSF, pylon, socket, and materials testing system (MTS). The MTS translates vertically, contacting the VSF 30 mm proximal to the end of the keel (Glanzer and Adamczyk, 2018). A fulcrum position of 66 mm is depicted.

parameterized to represent the material properties of the VSF's G10/FR4 Garolite keel (flexural elastic modulus: 18.6 GPa, Poisson's ratio: 0.136). A MATLAB script controls continuous fulcrum position (i.e. variable stiffness). The VSF model was rigidly attached to a prosthetic pylon and socket via a pyramid adapter, as the device would be used *in vivo*. These connections were modeled as weld joints. Each segment is independently scalable, allowing the model to be integrated into an anatomically scaled computational gait model.

Foot-ground contact consists of 24 sphere-to-plane contact models (Miller, 2020) parameterized to represent the geometry and dynamics of the VSF's foam base. Each of these models estimates normal (F_n) and frictional (F_f) forces associated with the collision of a viscoelastic sphere (a massless spring and damper system) and a rigid plane (Figure 3.3). The overall foot contact model was divided into five zones; the sphere-to-plane models were parameterized by zone (Figure 3.3, Table 3.1). The heel of the VSF model is comprised of three zones; this choice was motivated by the sensitivity of contact parameters when few spheres are in contact with the walking plane (e.g. the heel of the foot early in stance phase). Contact parameters are less sensitive when many spheres are in contact with the walking plane (e.g. the midfoot and forefoot late in stance phase). The foam base of the physical VSF undergoes compression throughout stance phase. To

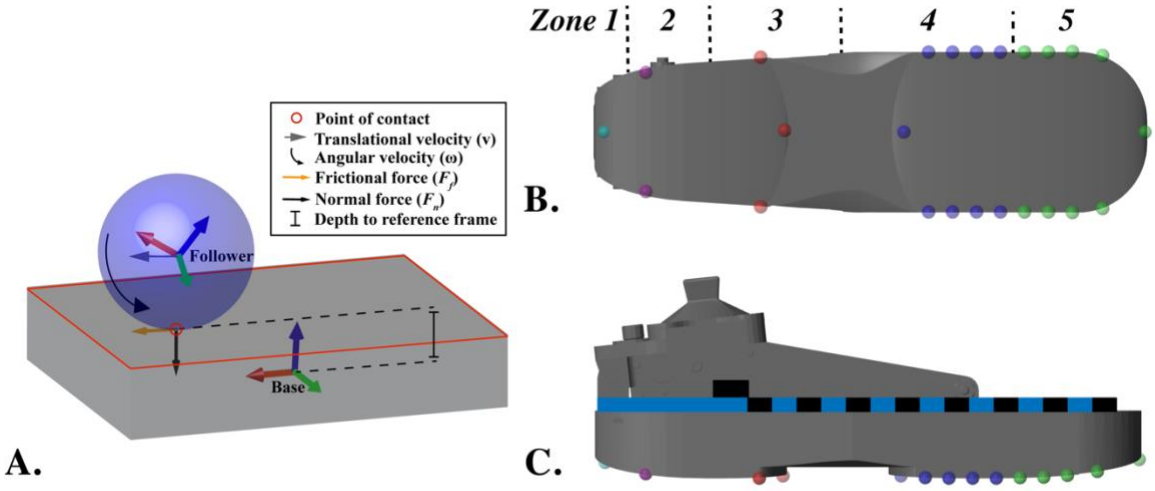

Figure 3.3: Schematic of a single sphere-to-plane contact model (A) and plantar (B) and lateral (C) perspectives of the VSF sphere-to-plane contact models. Heel contact spheres vary in color by zone.

Table 3.1: Summary of sphere-to-plane contact model parameters for the VSF.

Location	*k* (N/mm)	b (N·s/mm)	Penetration for full damping (mm)	Penetration exponent
Zone 1	90.16	3.525	7.474	297.7
Zone 2	91.11	390.9	2.000	458.4
Zone 3	18.01	292.9	2.900	3.152
Zone 4	1003	252.1	0.765	0.977
Zone 5	123.8	476.7	1.700	0.754

k: stiffness, **b**: damping

account for these effects, a modified Kelvin-Voigt nonlinear spring and damper force law (eq. 3.1) was implemented to represent contact between the VSF and walking plane. The spring force increases exponentially as the sphere penetrates the contact plane. The damping force is multiplied by a scaling factor (*y*), which increases from zero to one as a

eq. 3.1: $F_n = \begin{cases} (k \times \delta^n) + y(b \times \dot{\delta}) & \delta > 0, \dot{\delta} > 0 \\ k \times \delta & \delta > 0, \dot{\delta} < 0 \\ 0 & \delta < 0 \end{cases}$

$\boldsymbol{F_n}$: normal force

$\boldsymbol{k}$: contact stiffness

$\boldsymbol{\delta}$: penetration depth

$\boldsymbol{n}$: penetration exponent

$\boldsymbol{y}$: damping force scaling factor

$\boldsymbol{b}$: contact damping coefficient

polynomial as it approaches a user-defined value for full damping. Frictional force (eq. 3.2) is the product of the normal force and coefficient of friction (μ). A stick-slip friction law defines the transition between static (μ_{static}) and kinetic ($\mu_{kinetic}$) coefficients of friction based on a velocity threshold (v_{thresh}):

eq. 3.2: $F_f = \begin{cases} F_n \times \mu_{static} & v_{poc} < v_{threshold} \\ F_n \times \mu_{kinetic} & v_{poc} > v_{threshold} \end{cases}$

$\boldsymbol{F_f}$: frictional force

$\boldsymbol{\mu}$: coefficient of friction

$\boldsymbol{v_{poc}}$: velocity at point of contact

$\boldsymbol{v_{threshold}}$: velocity threshold

Static and kinetic coefficients of friction were set to 0.5 and 0.3 with a velocity threshold of 0.1 m/s. Resultant ground reaction force (GRF_R) was derived by summing and low-pass filtering (4th order Butterworth, f_c: 40 Hz) the normal and frictional forces arising from each contact sphere.

In order to improve GRF_R predictions, contact model parameterization was formulated as a least-squares optimization problem with the objective of minimizing the sum of squared errors between model-predicted and experimentally measured GRF_R (see "Model Validation"). Initial parameter settings at the outset of the optimization were derived by increasing stiffness until the contact spheres were able to support the weight of the model. Initial damping coefficients (N·s/mm) were set to half the numerical value of stiffness (N/mm). Penetration exponents and penetration for full damping values were initialized at 1 and 1 mm, respectively. These initial values were used as inputs to the optimization problem. Latin hypercube sampling (LHS) was applied to generate simulation scenarios with pseudo-random sets of parameters. The LHS approach is a method of stratified sampling, which divides parameter values into equal strata based on an assumed normal distribution and constrained by user-defined bounds. Random parameter values are sampled from within these strata to generate a simulation scenario with a pseudo-random set of parameters. The LHS technique effectively samples the search space, while providing the randomness required to explore the efficacy of a range of variable values to minimize the objective function. The objective function value of each iteration is compared to the previous iteration; the parameter scenario which best minimizes the objective function is passed to the next iteration of the algorithm. The optimization algorithm proceeds for 100 iterations or until an objective function tolerance

of 0.1 N is reached (i.e. convergence). If the optimization algorithm did not meet any of the termination criteria, the initial parameter values were updated using the results of the first run, and an additional run was initiated. Parameter tolerances were set to 0.001 (varying units) in order to avoid false minima.

Model validation

Static compression testing

The operational stiffness range of the physical VSF was determined through static compression testing (TestResources, Shakopee, MN) (Glanzer and Adamczyk 2018). Load was applied at a constant speed of 50 mm/min to a point 30 mm proximal to the anterior tip of the VSF (i.e. supported beam length = 199 mm). To validate the ESR properties of the VSF model, a simulated materials testing system (MTS) was developed in Simscape Multibody. The MTS simulator consists of a massless body, which translates vertically according to a user-defined time-position vector (Figure 3.2). Simulated static compression tests were performed as in Glanzer and Adamczyk (2018). Contact was maintained throughout VSF deflection. Contact dynamics between the VSF and MTS were estimated using a sphere-to-sphere contact model. Stiffness (k) (eq. 3.3) was computed as the average slope of the load-displacement data for loads above 200 N.

eq. 3.3: $k = \frac{\bar{\Delta}_{\text{Load}}}{\bar{\Delta}_{\text{Displacement}}}$ for loads 200 N to F_{max}

Deformation for loads under 200 N was considered to arise primarily from foam compression, rather than keel displacement. Mid-range keel displacement was also

calculated for the VSF model as the displacement of the keel at 50 percent of the maximal load applied during the static compression test.

Static compression tests were simulated at five discrete fulcrum positions (66, 87, 108, 129, and 151 mm), which span the full continuous range of possible positions. These ascending fulcrum positions represent decreases in overhung length (a), depicted in Figure 3.1, and therefore yield increases in endpoint stiffness. Simulation-derived values were compared to those from static compression tests of the physical VSF via coefficient of determination and root mean squared error (RMSE). Due to limitations of the compression testing machine used to test the physical VSF, simulated loads were limited to 700 N. This was further limited for the softest settings of the physical VSF due to the large displacements. Simulations were computed in Simscape Multibody using the *ode15s* solver profile with variable step size.

Gait conditions

Model-predicted GRF_R was validated under two scenarios: static and dynamic gait conditions. For both validations, the VSF model was integrated into a seven-segment, 28-DoF anatomically-scaled gait model of a subject with a unilateral below-knee amputation. Three-dimensional optical motion capture data (Optitrack, Natural Point, Inc. Corvallis, OR) of a male subject (181 cm, 77.3 kg) with a right side transtibial amputation walking with the physical VSF were used as inputs to the model. Retroreflective marker coordinates from a static motion capture trial were used to estimate and scale limb dimensions for the pelvis, leg, intact shank, residual shank, and intact foot. Within the gait model, the residual shank was encapsulated in a prosthetic

socket and welded to the pyramid adapter of the VSF model (Figure 3.2). The interface between the prosthetic socket and residual limb was modeled as a high-stiffness 6-DoF bushing joint, similar to previous work by LaPrè et al. (2018). The rotational and translational stiffness as well as displacement and velocity constraints were designed according to previous gait experiments (LaPrè et al., 2018) and finite element analysis (Jia et al., 2004). The mass and inertial properties of the lower limbs and pelvis were modeled as conical frusta and an ellipsoid, respectively. Segment masses were estimated according to De Leva (1996).

For the static condition, the model was simulated with anatomically neutral joint angles for ten seconds. Model-predicted GRF_R was averaged over the course of the trial and compared to the mass of the subject. Dynamic gait simulations were calculated based on experimental motion capture trials of the subject walking over ground at 1.2 ± 0.1 m/s with the VSF under low, medium and high stiffness configurations (fulcrum positions: 66, 108, and 151 mm). Three trials were collected for each stiffness configuration for a total of nine trials. Three-axis pelvis, hip, knee, and ankle angles were calculated from three-dimensional marker coordinate data (Grood and Suntay, 1983; Wu et al., 2002) and used as inputs to drive the corresponding joints of the model. Motion at the socket-limb interface was considered to be passive based on the aforementioned velocity and displacement constraints. The pyramid adapter-pylon interface was assumed to be rigid.

Contact model-derived GRF_R prediction was optimized for a single trial at the 66-mm fulcrum position. The GRF_R error resulting from this trial represents the theoretical optimal performance of the comprehensive VSF-ground contact model. The transferability of the optimized parameter values was determined by simulating the two

remaining low stiffness trials and the three remaining trials each for the medium and high stiffness configurations.

Joint kinematics and GRF_R data were low-pass filtered (4th order Butterworth: f_c: 6 Hz and 40 Hz, respectively). Simulation and experimental GRF_R were time locked and indexed to 0.25 s before and 0.25 s after stance phase. Including the brief period before and after stance phase provides insights regarding how the contact model behaves outside of stance phase and whether or not key gait events (e.g. heel strike and toe off) occur at similar time points in the simulated and experimental data. Resultant ground reaction force time series were re-sampled to 101 data points via cubic spline interpolation to allow for comparison between stance phases of differing lengths. Ensemble curves (mean ± SD) were generated for each condition. The impulse of GRF_R was calculated to assess the simulation's ability to predict GRF_R trajectory.

Anterior-posterior center of pressure (CoP_{AP}) position was calculated as the weighted sum of each contact sphere's predicted force multiplied by its anterior-posterior position (x). Raw normal forces arising from each sphere during stance phase were low-pass filtered (4th order Butterworth: f_c: 40 Hz) and summed. Anterior-posterior CoP position was calculated across stance phase (eq. 3.4). The CoP_{AP} time series data were

eq. 3.4: $\mathrm{CoP_{AP}} = \frac{\sum_{i=1}^{N} x_i F_{n_i}}{\sum F_n}$

CoP_{AP}: Anterior-posterior center of pressure position

x_i: Anterior posterior coordinate of contact sphere

low-pass filtered (4th order Butterworth: f_c: 6 Hz) and re-sampled to 101 data points via cubic spline interpolation to allow for comparison between stance phases of differing lengths. Joint kinematics, GRF_R, and CoP_{AP} data measured during experimental gait trials were compared to those derived from the simulations using coefficient of determination and RMSE.

Results

Static compression tests

Simulated VSF stiffness effectively reproduced experimental stiffness across the five fulcrum configurations ($R^2 > 0.98$, RMSE = 1.37 N/mm) (Figure 3.4, Table 3.2). Simulated mid-range displacement also matched well ($R^2 > 0.99$) with small offset from experimental displacement in each condition (RMSE = 0.45 mm). Experimental load-displacement relationships were most linear in the 66 and 87 mm fulcrum configurations, as indicated by variance in the slope of the relationship. The stiffest three conditions exhibited curvilinear relationships. Simulated load-displacement data were linear in all conditions due to the linear spring and damper force parameters for the revolute joints in the lumped parameter keel model.

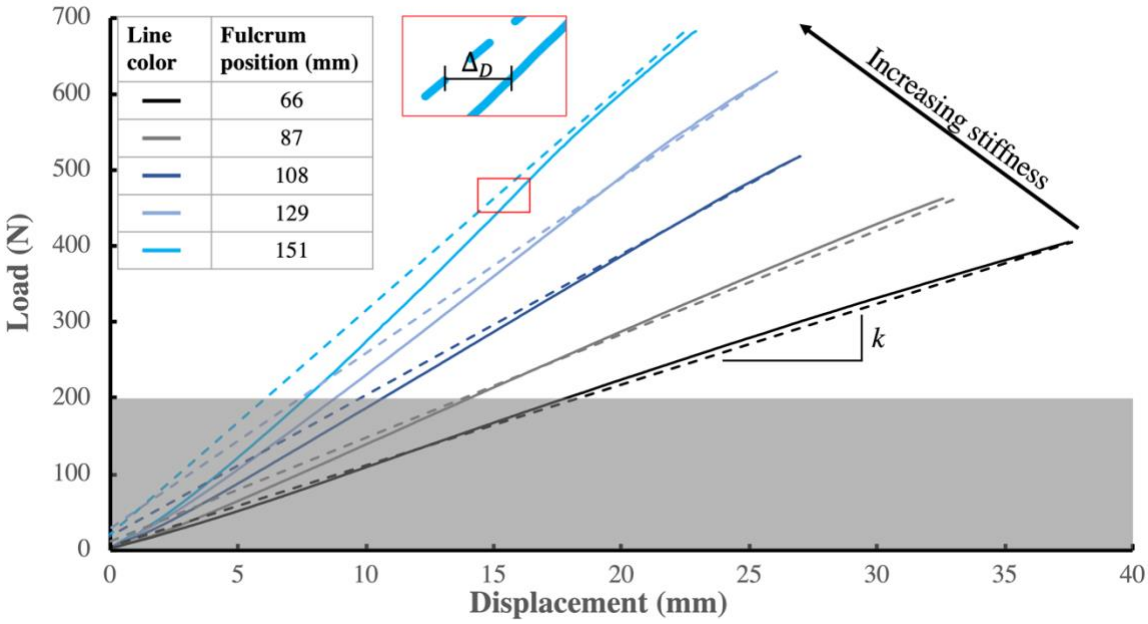

Figure 3.4: Load-displacement relationships for simulation (dashed) and experimental data (solid). Data are best fit ± 95% confidence interval. Displacement offset (Δ_D), example depicted with a bracket (|–|), is the difference between simulated and experimental mid-range displacement (eq. 3.3). Fulcrum position is equivalent to supported length.

Table 3.2: Comparative summary of experimental and simulated stiffness and mid-range displacement. Data are mean ± SD. Fulcrum position is equivalent to supported length.

Fulcrum position (mm)	k_{exp} (N/mm)	k_{sim} (N/mm)	Displacement offset (mm)
66	10.43 ± 0.07	10.94 ± 0.00	0.02
87	14.17 ± 0.08	13.62 ± 0.00	-0.46
108	19.45 ± 0.10	18.52 ± 0.00	0.23
129	24.83 ± 0.16	23.04 ± 0.00	0.32
151	31.59 ± 0.24	29.41 ± 0.00	0.79

Displacement (D) offset: $D_{sim} - D_{exp}$.

Resultant ground reaction force predictions

In the static condition, model-predicted subject mass was 2.6 ± 0.0% less than measured mass. In the dynamic conditions, simulated joint angles matched experimental

joint angles well, but exhibited a small phase lag (mean RMSE: 1.9 ± 1.0 deg, mean R^2: 0.98 ± 0.02). Simulated and experimental GRF_R data agreed well in the time domain (Figure 3.6). Amplitude discrepancies, quantified via RMSE, were least in low stiffness configuration and greatest in the high stiffness configuration. Coefficient of determination values were similar for the low and medium stiffness conditions and lower for the high stiffness condition. Impulse was similar in the low and high stiffness conditions and lower for the medium stiffness condition (Table 3.3).

Optimization of the single low stiffness trial resulted in a GRF_R RMSE of 5.3% body weight (BW) and R^2 of 0.98 across stance phase. Impulse also matched well (RMSE: 0.01 BW·s, $R^2 > 0.99$) (Figure 3.5). In the time domain, model-predicted heel

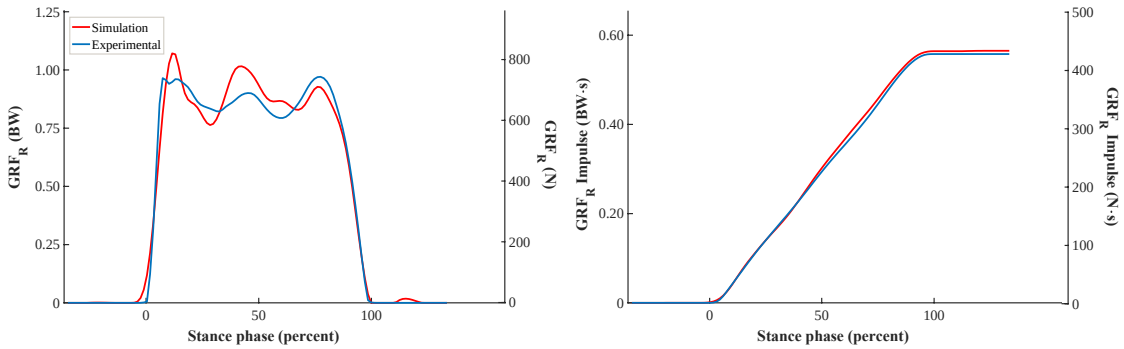

Figure 3.5: Optimized GRF_R and GRF_R impulse for a single trial at 66 mm fulcrum position.

contact preceded experimental heel contact by 0.02 s, resulting in a 0.02-s longer stance phase. Simulating the two additional low stiffness trials with the optimized contact parameters resulted in average RMSE and R^2 values of 0.10 ± 0.05 BW and 0.93 ± 0.05 for GRF_R and 0.02 ± 0.01 BW·s and > 0.99 ± 0.01 for GRF_R impulse (Figure 3.6, Table 3.3).

Experimental GRF_R and GRF_R impulse responses were similar in the time and amplitude domains across the three stiffness conditions (Figure 3.6). On average, stance phase time was 0.05 ± 0.03 s longer in the simulations across the stiffness conditions. Time errors were least in the low stiffness condition and greatest in the high stiffness. Variability for GRF_R was greatest during the first 25% of stance phase for all conditions. Variability for GRF_R impulse was greatest near the end of stance phase. The ability of the contact parameters optimized for the low stiffness condition transferred well across the other two conditions, which is evident by the similar RMSE values for GRF_R (Table 3). Resultant ground reaction force RMSE and R^2 values were better in the medium stiffness configuration, whereas RMSE and R^2 were better in the high stiffness condition for GRF_R

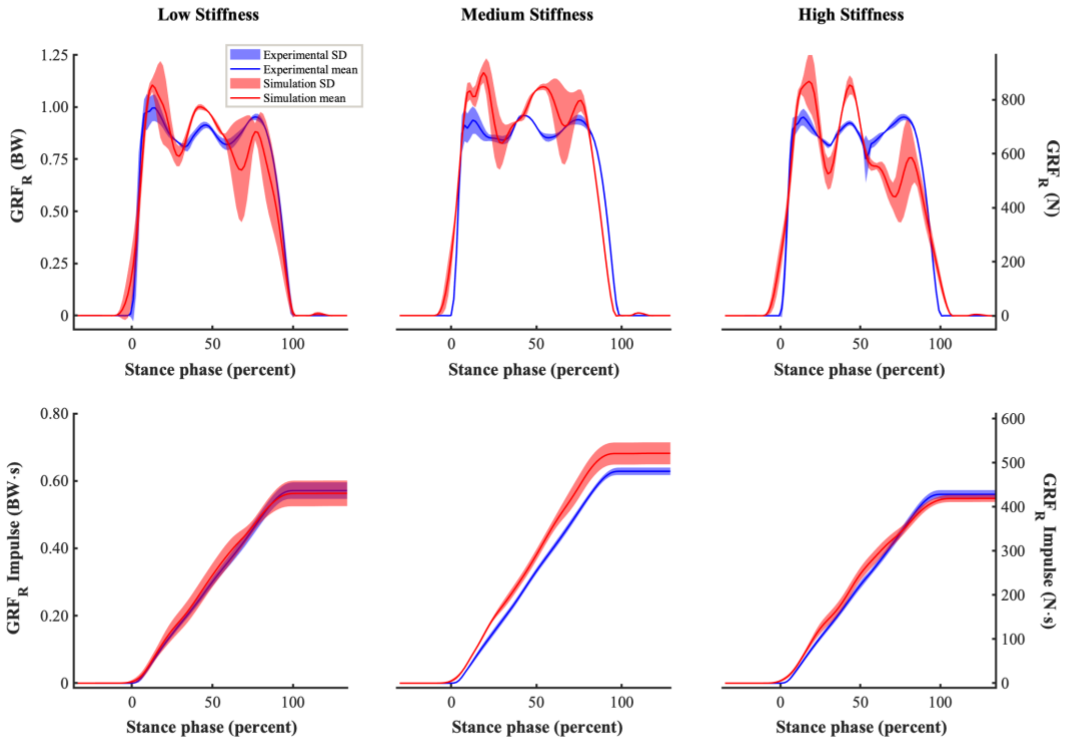

Figure 3.6: Ensemble curves for GRF_R (top) and GRF_R Impulse (bottom) for the low, medium, and high stiffness conditions (left, middle, and right).

impulse. The medium stiffness condition demonstrated the least variability for the GRF_R response, whereas the low and high stiffness conditions showed similarly low variability for GRF_R impulse (Table 3.3).

Anterior-posterior CoP trajectory during stance phase was similar between simulated and experimental data (Figure 3.7). Root mean squared errors were 8.9 ± 1.0,

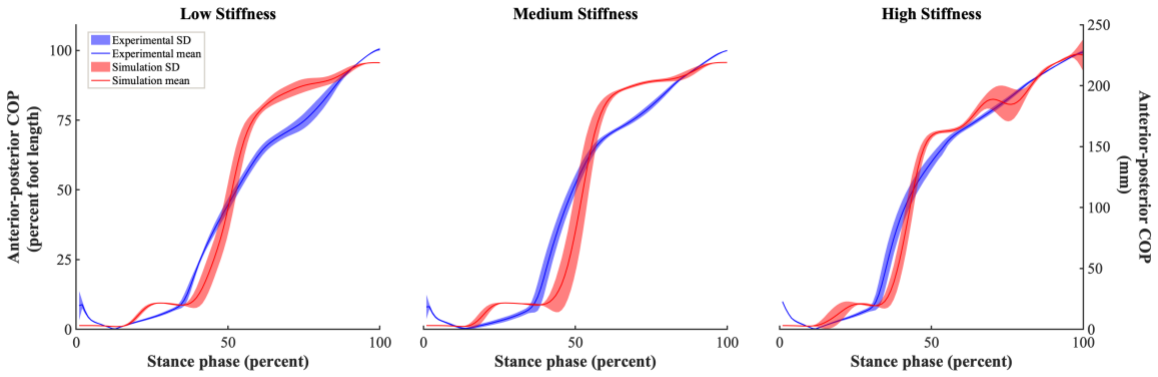

Figure 3.7: Ensemble curves for COP_{AP} position for the low, medium, and high stiffness conditions (left, middle, and right).

Table 3.3: Summary of GRF_R, GRF_E impulse, and COP_{AP} comparison between simulated and experimental data.

Stiffness Configuration	GRF_R		GRF_R Impulse		COP_{AP}	
	R^2	RMSE (BW)	R^2	RMSE (BW·s)	R^2	RMSE (% FL)
Low	0.93 ± 0.05	0.10 ± 0.04	> 0.99 ± 0.01	0.02 ± 0.01	0.95 ± 0.01	8.93 ± 0.99
Medium	0.92 ± 0.01	0.13 ± 0.02	0.96 ± 0.02	0.05 ± 0.01	0.94 ± 0.01	9.45 ± 0.92
High	0.87 ± 0.07	0.14 ± 0.07	> 0.99 ± 0.01	0.02 ± 0.01	0.97 ± 0.01	5.68 ± 1.39

BW: Body weight, **COP_{AP}**: Anterior-posterior center of pressure, **FL**: Foot length, Data are mean ± SD

9.5 ± 0.9, and 5.7 ± 1.4 percent foot length for the low, medium, and high stiffness conditions, respectively (Table 3.3). Simulated data correlated well with experimental

data across all conditions. Coefficient of determination values were 0.95 ± 0.01, 0.94 ± 0.01, and 0.97 ± 0.01 for the low, medium, and high stiffness conditions.

Discussion

The goal of this study was to develop a reduced-order computational model of a semi-active variable-stiffness foot prosthesis. Results from simulated static compression tests showed good agreement with experimental data. These outcomes suggest that the variable-stiffness ESR properties of the VSF were modeled with high fidelity using a reduced order lumped parameter approach for approximating flexible body dynamics. One of the goals of reduced order modeling is to capture a structure's dynamic behavior in a computationally inexpensive way. A common benchmark for reduced-order models is the ability to simulate at or near real-time (Kikuchi et al., 2016; Thakallapelli et al., 2016), which contrasts with more computationally expensive methods such as mesh-based finite element modeling. Including initialization time, static compression simulations computed 3.3 ± 0.8 times faster than real-time (i.e. the length of time required to complete the experimental static compression test) on computer with a four core 4.0 GHz processor. Initialization time, which includes model compiling and building, can be minimized using "Accelerator" and "Fast Restart" modes in Simscape Multibody. Using these tools, simulations computed 39 ± 16 times faster than real time. This computational efficiency is useful if the model is to be simulated iteratively, for example in parameter optimization or machine learning frameworks.

The VSF is an ideal device for studying the effects of prosthesis stiffness on gait mechanics because it can readily exhibit a range of forefoot stiffness values, thereby

eliminating the need to purchase or manufacture multiple prostheses, as in Fey et al. (2011), Jin et al. (2016), and Zelik et al. (2011). In doing so, this also eliminates confounding variables that accompany a foot-switching experimental design, such as mismatched or out-of-order stiffness from foot prostheses of different categories. The VSF can also modulate stiffness along a continuous scale, which provides improved resolution compared to the typical discrete stiffness options available for fully passive designs. The range of forefoot stiffness values exhibited by the physical VSF and captured by the VSF model represent a range of stiffness values available in many commercially-available prosthetic feet (Webber and Kaufman, 2017; Womac et al., 2019). Accurate characterization of this range is important, should this model be used to inform the design and/or prescription of prosthetic feet. Further, this model can be easily re-parameterized to exhibit a different range of stiffness values, which could aid in the selection of keel dimensions or material properties to meet design goals. Two primary limitations are present for the static compression testing simulations. Experimental load-displacement data were only available for positive loading conditions, and thus a comparison of the model's hysteresis behavior was not possible. Similarly, experimental data were only available for the 50 mm/min loading rate. A robust characterization of the VSF's stiffness behavior under a range of higher loading rates would likely improve the model's behavior under dynamic conditions. Experimental load-displacement data could also be influenced by imperfections in maintaining a constant contact point with the prosthesis. Results of the present study are difficult to compare to previous work, as there is a paucity of prior research that evaluated simulated prosthesis dynamics compared to mechanical testing data of a physical prosthesis under multiple conditions. However,

errors exhibited by this model are similar to those reported in Tryggvason et al. (2020), who compared the angular stiffness response of a finite element foot prosthesis model to data from mechanical tests.

Under dynamic gait conditions, simulated joint angles agreed well with experimental values, indicating that the model is numerically stable when actuated by joint kinematics measured during gait with the VSF. Joint angles were strongly correlated, but exhibited a small phase lag, possibly due to ODE solver settings and numerical integration. This phase lag may be also be present in the kinetic data, but masked by the larger inherent variability of the simulated GRF_R. Total simulation times were 8.95 ± 3.92, 12.7 ± 0.67, and 46.2 ± 1.19 times slower than real time for the low, medium, and high stiffness configurations respectively. Execution times were 3.12 ± 0.10, 3.40 ± 0.67, and 38.4 ± 1.19 times slower than real time. Increased execution times for the stiff conditions may reflect the need for small time-steps in solving a rapidly-evolving, stiff differential equation.

Optimization of the GRF_R for the low stiffness configuration achieved a RMSE of 5.3% BW and R^2 of 0.98. These values are similar to those reported in previous biomechanical contact modeling work (Brown and McPhee, 2018; Lopes et al., 2015; Van Hulle et al., 2020). However, those studies focused on quantification of foot-ground contact during gait for individuals with intact limbs. Direct comparison of these data was limited to work in intact limb biomechanical modeling due to a lack of studies reporting validation data for prosthesis-ground contact modeling in gait biomechanics. The strong correlation and low error for GRF_R impulse indicates that the contact model is able to predict the shape and trajectory of the GRF_R arising from gait kinematics. Accurate

predictions of GRF_R impulse is important for capturing whole-body energetics throughout gait. The concomitant agreement for both kinematics and kinetics further suggests that these methods are viable for simulating whole-body energetics during gait.

The transferability of the optimized contact model parameters from the low stiffness condition was assessed by simulating two additional low stiffness trials and three trials each with medium and high stiffness configurations. Compared to the optimized trial, simulation-derived GRF_R predictions did not perform as well in the unoptimized trials. Mean GRF_R RMSE and R^2 were 12.7 ± 1.44% BW and 0.91 ± 0.02 for the remaining low stiffness trials. These values were similar for the medium and low stiffness trials (Table 3.3). The impulse of these data matched well across the unoptimized trials (RMSE: 0.03 ± 0.02 BW·s, R^2: 0.98 ± 0.01). Variability of the model's performance was similar across the unoptimized conditions for all outcome measures. It is possible that the contact model parameters were over-fitted to the specific conditions of a single trial, resulting in decreased generalizability. Future work should assess the balance between optimization specificity and generalizability.

The amplitude and shape of experimental GRF_R waveforms were similar across the three stiffness conditions. However, stance phase times did vary by condition for the subject tested. The medium stiffness condition resulted in the longest stance phase time (0.79 ± 0.01 s), high stiffness resulted in the shortest (0.71 ± 0.02 s), and low stiffness (0.73 ± 0.02 s) was in the middle. The same pattern was present in the simulated data, although stance phase times were 0.05 ± 0.03 s longer on average compared to the experimental data. Stance phase times derived from simulations were correlated with

experimental times ($R^2 = 0.65$). More data are necessary to discern the strength, repeatability, and significance of these relationships.

Simulated CoP_{AP} values agreed well with experimental values. The RMSE values achieved using this model were similar to those reported in previous work involving subject-specific biomechanical contact modeling for individuals with intact limbs (Jackson et al., 2016). Accurate mapping of CoP_{AP} throughout stance phase is vital for simulating the effects of variable prosthesis stiffness on joint forces and moments during gait. Errors in model-predicted CoP_{AP} may be reduced by increasing the density of contact spheres distributed on the plantar surface of the foot, which would improve the resolution of CoP_{AP} predictions. However, this would likely result in increased execution time for simulations and also increase complexity of the contact parameter optimization problem.

The present data show promise for predicting GRF_R arising from a semi-active VSF prosthesis. These methods may be applied to the design and prescription of lower limb prostheses and forward dynamics simulations in robotics and biomechanics. Within biomechanics, future work could integrate the VSF model into a gait model of an individual with lower limb loss. Gait simulations could be formulated as an optimal control problem in which prosthesis stiffness is tuned to minimize a biomechanical cost function such as joint loading or metabolic cost. Evaluating these effects within a simulation-based framework rather than traditional *in vivo* experimentation minimizes risk and time spent by the user. Further, a broad spectrum of prosthesis design parameters could be modeled and simulated without the need to manufacture multiple devices or the costs associated with doing so. Further optimization of the VSF-ground contact model

may be necessary for simulation scenarios with error tolerances less than 12% BW. Similar improvements may be required if the mean difference between simulation conditions is less than the error of the model. Reducing error in model-predicted GRF_R may be accomplished by evaluating the objective function under a variety of conditions and choosing the parameter set that achieves the best minimization across several conditions. A deformable contact model, such as presented in Jackson, Hass, and Fregly (2016), may also be a viable means of representing foam deformation throughout stance phase and thus reducing error.

These methods assume accurate estimation of segment length, joint centers, and joint angles which were derived from marker-based motion capture data. Each of these metrics likely suffers from small errors due to marker placement, localization, and coordinate system design. Such errors would contribute to decrements in contact model performance. The components and joints of the prosthetic limb were also modeled as rigid, which may not be completely accurate to represent the physical limb. This discrepancy would manifest as small differences in kinematics and energy transfer between the components of the prosthetic limb. Nevertheless, simulated motions were consistent with experimental data of subjects walking with the VSF and other previously reported data of spatiotemporal gait patterns among persons with lower limb loss (Su et al., 2008; Winter and Sienko, 1988). Another limitation is inherent to the reduced order design of the lumped parameter VSF keel, which constrains keel motion to the sagittal plane. While this design is computationally efficient compared to more robust finite element models, it fails to account for small torsional keel motions that would be possible under ecological gait conditions with the physical VSF.

Conclusions

The present study demonstrates that the ESR properties of a semi-active VSF can be modeled with high fidelity. Foot-ground contact models were used to estimate GRF_R with 5.3% BW error in an optimized gait trial, which translated to mean errors of 13% for unoptimized trials. The contact models also predicted COP_{AP} with mean error of 9.3% foot length. This model performance may be sufficient for gait simulations among persons with lower limb loss. Such simulations may be used to aid in the prosthesis design and prescription process in order to improve user mobility. These methods may also be helpful to identify other important prosthesis design parameters, which can be modified to optimize gait. Further contact model optimization and error reduction may be required for simulation-based comparisons of varied prosthesis stiffness, where differences in GRF_R magnitude may be nuanced.

Statement of acknowledgements: The authors would like to thank Evan Glanzer for his work in developing and testing the variable-stiffness foot and Terry Denery for his intellectual contributions in optimizing the contact model.

Funding sources: This work was funded in part by the Lokey Doctoral Science Fellowship (MAM) and NIH grant HD074424 (PGA).

Acronyms widely used in text

BW	Body weight; M*g
CoP	Center of pressure
DoF	Degrees of Freedom
ESR	Energy storage and return
GRF_R	Resultant Ground Reaction Force, N; $\sqrt{GRF_X{}^2 + GRF_y{}^2 + GRF_z{}^2}$
LHS	Latin Hypercube Sampling
MTS	Material Testing System
ode15s	Ordinary differential equation 15 solver
SD	Standard Deviation
RMSE	Root Mean Square Error; $\sqrt{\frac{\sum_{i=1}^{N}(Experimental_i - Simulation_i)^2}{N}}$
VSF	Variable Stiffness Foot

Abbreviations

a	Overhung length, mm
b	Damping coefficient, N·s/mm
B	Support fulcrum position, mm
D	Displacement, mm
F	Force, N
k	Linear stiffness, N/mm
L	Total beam length, mm
l	Supported length, mm
n	Penetration exponent
R^2	Coefficient of determination
μ	Coefficient of friction
v	Linear velocity
y	Scaling factor
δ	Penetration depth, mm
$\dot{\delta}$	Penetration velocity, mm/s
ω	Angular velocity, rad/s

Superscripts and subscripts

CoP_{AP}	Anterior-posterior (Center of Pressure)
D_{sim}	Simulation (Displacement)
D_{exp}	Experimental (Displacement)
F_f	Frictional force, N
F_n	Normal force, N
GRF_R	Resultant ground reaction force, N
k_{sim}	Simulation (stiffness), N/mm
k_{exp}	Experimental (stiffness), N/mm
v_{poc}	Linear velocity at point of contact, mm/s
$v_{threshold}$	Linear velocity threshold, m/s
$\mu_{kinetic}$	Coefficient of kinetic friction
μ_{static}	Coefficient of static friction

Bridge

This study demonstrates the ability to capture the ESR properties of a semi-active VSF in a computationally economical model. Results of controlled static compression tests show agreement between the simulated and experimental data. Under dynamic gait conditions where there is increased variation in the load distribution and rate of loading, the model exhibited greater error compared to static compression tests, but similar predictive capacity compared to previous work in this area.

There remains a need to assess the ability of these methods to predict ground reaction forces among multiple subjects with varying anthropometric characteristics and gait patterns. The VSF model and algorithm for programmatically deriving ground contact parameters are integral components in subsequent chapters of this dissertation. The VSF and ground contact models are tested across multiple subjects in Chapters IV and V. They are integrated into the limb loss-specific gait model discussed in Chapter IV (Specific Aim 3) and are used in the simulation-based analysis of the effects of VSF stiffness on residual limb-socket interface dynamics (Chapter V, Specific Aim 4).

CHAPTER IV

A COMPUTATIONAL GAIT MODEL WITH A BELOW-KNEE AMPUTATION AND A SEMI-ACTIVE VARIABLE-STIFFNESS FOOT PROSTHESIS

This work is currently in preparation for submission through an invited for submission in the *Journal of Biomechanical Engineering.* Dr. Michael E. Hahn, Dr. Peter G. Adamczyk, and Mr. Kieran M. Nichols provided mentorship including assistance with study design, data interpretation, and editing and finalizing the final manuscript.

Introduction

Individuals with lower limb loss exhibit distinct gait characteristics, which may limit mobility and decrease quality of life. Those using lower limb prostheses may display gait asymmetry (Sanderson and Martin, 1997; Schaarschmidt et al., 2012), elevated metabolic cost during locomotion (van Schaik et al., 2019), increased muscle activity (Fey et al., 2013), and a variety of psychological disorders including anxiety and depression (Mckechnie and John, 2014). Sustained prosthesis use may also lead to musculoskeletal injury through overloading of intact joints (Gailey et al., 2008) and residual limb tissue damage due to pressure and shear forces at the prosthetic socket interface (Al-Fakih et al., 2016; Courtney et al., 2016; Sanders and Daly, 1993). Each of these issues may be attenuated by improving user specificity in the design characteristics of foot prostheses. However, the effects of foot prosthesis design parameters (e.g. stiffness) are not well characterized, and thus achieving meaningful improvements in gait has proven elusive (Casillas et al., 1995; Postema et al., 1997). In order to achieve

improvements, a robust understanding of the relationships between the anatomical morphologies associated with lower limb amputation (LLA), gait mechanics, and prosthesis design is necessary.

Gait simulations based on computational musculoskeletal models can be powerful tools to investigate human movement. Simulations have been used previously to evaluate musculoskeletal dynamics under a variety of conditions, including walking (Rajagopal et al., 2016), running (Seth et al., 2011), and jumping (Porsa et al., 2015). However, the models used in these studies are not suitable for simulating gait among individuals with LLA, due to the altered lower limb mass, inertial properties, and mechanical properties associated with a prosthetic foot and socket. LaPrè et al. (2018) and Willson et al. (2020) developed limb loss-specific models in OpenSim (Rajagopal et al., 2016), a popular musculoskeletal modeling and simulation platform. These studies used simulations to investigate the effects of prosthesis alignment and a biarticular clutched spring mechanism on gait mechanics, respectively. However, the models used in these studies do not account for the ESR properties of the prosthetic foot, thus limiting their ecological validity. Other studies, which did incorporate the force and torque contributions of ESR feet into gait models focused on characterizing biomechanical and muscle activation responses with prosthesis use, rather than validation of the gait and prosthesis models (Fey et al., 2012; Russel Esposito and Miller, 2018). While these studies made important progress toward investigating the relationship between anthropometry, gait mechanics, and prosthetic foot design, they had limited ability to verify simulation results in the context of experimental values. Due to these limitations, the use of simulations to inform the design of ESR foot prostheses has not been fully realized.

Previously, a reduced order computational model of a semi-active variable-stiffness foot (VSF) prosthesis was developed (Glanzer and Adamczyk, 2018) and validated in McGeehan et al., (2020). However, there remains a need to integrate this model into a scalable forward kinematics and forward dynamics simulation capable gait model. Such a model would be useful for simulating gait and elucidating the relationships between ESR prosthesis design and gait mechanics on an individualized basis. The purpose of this study was to develop and validate a forward simulation-capable gait model with lower limb loss and a semi-active VSF.

Methods

Gait model design

A seven-segment, 28 degree-of-freedom (DoF) gait model (Figure 4.1) was developed in Simscape Multibody (Mathworks, Inc., Natick, MA). Simscape was chosen for its application to model-based design, customizability in simulation computing (e.g. differential equation solver profiles, numerical integration settings, and tolerance controls), and rich libraries of contact models, mechatronic components, and signal processing modules. Further, its integration with the rest of the Mathworks computational suite provides a link by which complex algorithms and data processing tools can be easily incorporated into the model.

The anatomical structures for the generic model were derived from open-source cadaveric skeletal 3D surface geometry data from Mitsuhashi et al. (2009). A massless head and torso (HAT) segment is included in the model for future uses; however, the present study utilized only kinematics of the pelvis and lower limbs. The pelvis interacts

with the world frame via a 6-DoF bushing joint, which is the model's parent joint. For this study, pelvis translational movement in the frontal plane was prescribed using the experimental gait data described below in order to account for subjects that walked diagonally or performed minor turning during the gait trial. Other translational movements were unconstrained. Pelvis rotations in three planes with respect to the world frame were prescribed using experimental gait data. Each joint of the lower limb is modeled as a 3-DoF gimbal joint, with the coronal and axial rotations of the knee constrained to have no movement. Rotational movements in each plane may be constrained through user-defined inputs. To represent a below-knee amputation (BKA), the tibia and fibula were transected via a planar cut and encapsulated within a prosthetic socket. The residual limb and prosthetic socket were connected via a high-stiffness bushing joint to assess 6 DoF socket-residual limb interface dynamics, similar to previous work by LaPrè et al. (2018). The rotational and translational stiffness as well as displacement and velocity constraints were designed according to previous gait experiments (LaPrè et al., 2018) and finite element analysis (Jia et al., 2004). The translational aspect of the bushing joint has a stiffness of 20 N/mm and damping of 10 N·s/mm. Vertical displacement of the residual limb with respect to the prosthetic socket (i.e. socket pitoning) is constrained to 35 mm maximum displacement and 100 mm/s maximum displacement velocity. The rotational aspect of the joint has a stiffness of 10 N·mm/deg and damping of 5 (N·mm)·s/deg The VSF model (McGeehan et al., 2020) is rigidly attached to the socket via a pylon and pyramid adapter using weld joints. Separate generic models with right and left side amputations were developed for this study and are available in the supplementary materials.

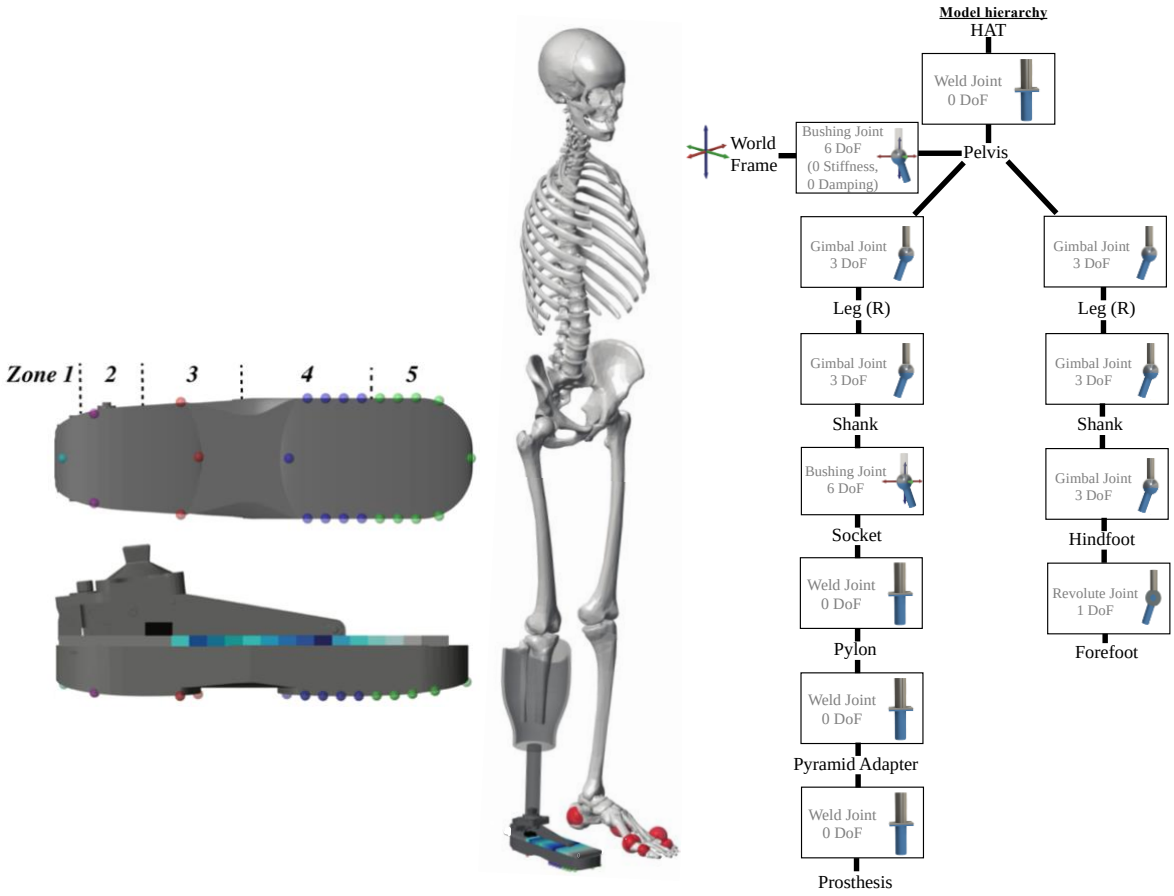

Figure 4.1: Model of the VSF (left), generic anatomic gait model a right side below-knee amputation (center), and model hierarchy (right). Sphere-to-plane contact models are depicted in red (intact side) and multi-color (VSF side). These parameters are mirrored for the model with left side amputation. The discretization of the VSF's keel is represented through the color gradient. The fulcrum (black square) is positioned at 66 mm.

Methods for modeling the mechanical stiffness and ground contact dynamics of the VSF were previously described in McGeehan et al. (2020). Briefly, the VSF model was designed using the lumped parameter approach for approximating flexible body dynamics. The keel of the VSF is discretized into 16 segments connected with alternating revolute joints and weld joints, yielding eight DoF. The most posterior segment is 66 mm in length, which matches the minimum possible fulcrum position. The rest of the keel

consists of 11.64-mm segments for a total beam length of 229 mm. The stiffness and damping values for the revolute joints were parameterized to represent the material properties of the VSF's G10/FR4 composite keel. A custom MATLAB script controls continuous fulcrum position (i.e. variable stiffness). Stiffness of the VSF model was characterized by simulating static compression tests and optimizing the load-displacement response based on that of the physical VSF across the full range of fulcrum positions.

Segment masses were estimated according to De Leva (1996). Mass distribution and inertial properties of the lower limbs and pelvis are modeled as conical frusta and an ellipsoid, respectively. The geometry of the conical frustum for each limb is defined using the proximal and distal joint radii for each segment, as derived from marker coordinates (see "Model scaling and parameterization"). The ellipsoid's radii are defined based on the distances between the right and left anterior and posterior superior iliac spines. The estimated mass of the HAT segment was added to the mass of the pelvis.

The model is designed with variant subsystems, which are Simscape coding structures that allow for multiple implementations of code where only one implementation is active during a simulation. In this design, gait simulations can be computed within a forward kinematics framework (i.e. joint kinetics and end effector positions estimated given joint kinematics as inputs) or forward dynamics framework (i.e. joint kinematics and end effector positions estimated given joint torques as inputs). Implementation of the variant subsystems is controlled via user-defined inputs.

Model scaling and parameterization

Model scaling and parameterization are completed through a pipeline of custom MATLAB scripts (Figure 4.2). The pipeline uses raw marker coordinates from optical motion capture trials of subjects walking with the VSF to programmatically generate a scaled subject-specific gait model, parameterize the model, and drive forward gait simulations. First, data from a static capture trial are used to scale and assemble the generic gait model according to subject-specific anthropometrics. Estimates for segment dimensions, mass, and inertial properties are derived from the static data (De Leva, 1996). Then, the subject-specific gait model may be used for subsequent forward kinematics or forward dynamics simulations to determine the movements or forces of the model based on inputs of joint angles or joint torques, respectively. Custom methods for signal processing and derivation of joint angles (e.g. Cardan-Euler sequences or quaternions) may be defined by the user. A variety of MATLAB-based approaches can be used to solve the model. These include both continuous and discrete options, an extensive set of ordinary differential equation (ODE) solvers, and a variety of numerical integration settings (e.g. fixed or variable time steps, step size constraints, and tolerance values). Each of these parameters may be strategically selected based on their suitability for a given simulation scenario, such as system dynamics, solution stability, computation speed, or solver robustness.

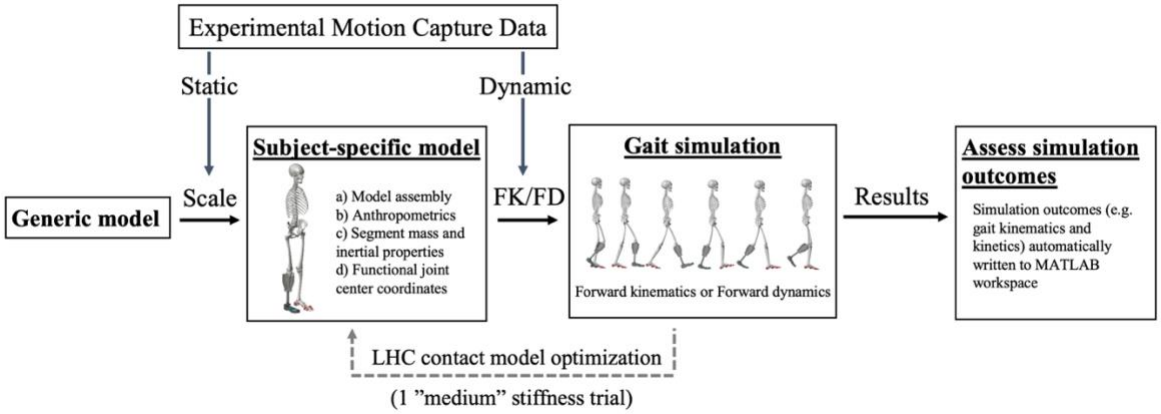

Figure 4.2: Overview of data processing and model parameterization pipeline. **FK**: Forward kinematics, **FD**: Forward dynamics.

Contact model design and parameterization

Foot-ground contact models were designed for the VSF and the intact foot. A model of VSF-ground contact consists of 24 sphere-to-plane contact models (Miller, 2020) parameterized to represent the geometry and dynamics of the VSF's foam base. On the intact side, contact spheres were placed on anatomical locations that experience high localized pressure during stance phase (Figure 4.1) (Lugade and Kaufman, 2014). Methods for the design and parameterization of the contact model were previously described in McGeehan et al. (2020). Briefly, each contact sphere estimates normal (F_n) (eq. **4.**1) and frictional (F_f) (eq. 4.2) forces associated with the collision of a viscoelastic sphere (a massless spring and damper system) and a rigid plane. For the intact foot, each contact sphere is parameterized independently according to Equations 4.1-4.2.

$$\textbf{eq. 4. 1}: F_n = \begin{cases} (k \times \delta^n) + y(b \times \dot{\delta}) & \delta > 0, \dot{\delta} > 0 \\ k \times \delta & \delta > 0, \dot{\delta} < 0 \\ 0 & \delta < 0 \end{cases}$$

$\boldsymbol{F_n}$: normal force

$\boldsymbol{k}$: contact stiffness

$\boldsymbol{\delta}$: penetration depth

$\boldsymbol{n}$: penetration exponent

$\boldsymbol{y}$: damping force scaling factor

$\boldsymbol{b}$: contact damping coefficient

$$\textbf{eq. 4. 2}: F_f = \begin{cases} F_n \times \mu_{static} & v_{poc} < v_{threshold} \\ F_n \times \mu_{kinetic} & v_{poc} > v_{threshold} \end{cases}$$

$\boldsymbol{F_f}$: frictional force

$\boldsymbol{\mu}$: coefficient of friction

$\boldsymbol{v_{poc}}$: velocity at point of contact

$\boldsymbol{v_{threshold}}$: velocity threshold

For the VSF, the overall foot contact model was divided into five zones; the sphere-to-plane models were parameterized by zone (Figure 4.1). The heel of the VSF model is comprised of three zones; this choice was motivated by the sensitivity of contact parameters when few spheres are in contact with the walking plane (e.g. the heel of the foot early in stance phase). Contact parameters for each zone were optimized the match the experimental ground reaction force data from a sample trial using procedures

described below. The foam base of the physical VSF undergoes compression throughout stance phase. To account for these effects, a modified Kelvin-Voigt nonlinear spring and damper force law (eq. 4.1) was implemented to represent contact between the VSF and walking plane.

Gait simulations

The data presented in this study were derived via the processing and simulation pipeline described above. Forward kinematics gait simulations were computed for four subjects (one female) with a unilateral BKA (Table 4.1) walking with the VSF configured to "high", "medium", and "low" stiffness settings for three trials each (Table 4.2). To be included, participants must have been at least 2 years post-amputation and able to safely complete nine over ground gait trials walking at 1.2 ± 0.1 m/s. Prior written informed consent was provided by all subjects as approved by the Health Sciences Institutional Review Board at the University of Wisconsin-Madison. All simulations were computed in Simscape Multibody using the *ode15s* solver profile with variable step sizes for numerical integration. Simulations were performed on a computer with a 4.0 GHz quad-core processor.

Table 4.1: Participant characteristics.

Subject	Sex	Age (y)	Height (cm)	Mass (kg)	Amputation side	Years post-amputation
1	Male	34	181	77.3	Right	15
2	Male	51	175	111	Right	8
3	Male	70	180	83.8	Left	14
4	Female	61	163	63.8	Right	8
Mean ± SD	–	54 ± 15	175 ± 19.9	84.0 ± 19.9	–	11 ± 3.8

Table 4.2: Summary of experimental trials.

Number of trials	VSF condition (Forefoot stiffness)	Gait condition
3	"High" stiffness (32 N/mm)	1.2 ± 0.1 m/s, over ground walking
3	"Medium" stiffness (19 N/mm)	1.2 ± 0.1 m/s, over ground walking
3	"Low" stiffness (10 N/mm)	1.2 ± 0.1 m/s, over ground walking

Motion capture (Optitrack, Natural Point, Inc. Corvallis, OR) and ground reaction force (GRF) data (Bertec Inc. Columbus, OH) collected from subjects during nine gait trials (Table 4.2), a static neutral pose, and functional joint movements (Schwartz and Rozumalski, 2005) were used to generate scaled subject-specific models and compute forward kinematics gait simulations. Marker coordinates and GRF data were sampled at 200 and 1200 Hz, respectively. Marker data were low-pass filtered (4^{th} order Butterworth, f_c: 6 Hz). Force data were down-sampled (f_s: 200 Hz) and low-pass filtered (4^{th} order Butterworth, f_c: 40 Hz). Segment and joint kinematics were estimated using Cardan Euler rotation calculations in accordance with International Society of Biomechanics recommendations (Grood and Suntay, 1983; Wu et al., 2002; Wu and Cavanagh, 1995). These data were then used to drive the corresponding joints in the model during simulations. Localized joint center coordinates were estimated for the hips, knees, and intact ankle joint using functional joint movements and methods described in Schwartz and Rozumalski (2005). The location of the pylon-pyramid adapter interface (i.e. prosthetic "ankle") was calculated based on a measured offset from markers placed on the VSF. This interface was assumed to be rigid. Motion at the socket-limb interface was considered to be passive based on the aforementioned velocity and displacement

constraints. Residual limb length was estimated as the distance from the knee joint center to the base of the prosthetic socket and scaled accordingly. The mass and inertial properties of the residual limb were estimated first by deriving estimated density of the intact limb modeled as a conical frustum with an assigned mass estimated per De Leva (1996). The derived density of the intact limb was applied to the residual limb model, which was also modeled as a conical frustum. This limb was then truncated at the respective level of amputation for each subject.

Contact model parameters were optimized on a subject-specific basis. Contact model parameterization was formulated as a least-squares optimization problem with the objective of minimizing the sum of squared errors between model-predicted and experimentally measured GRF_R. A Latin Hypercube Sampling-based optimization algorithm was used to programmatically derive the stiffness, damping, and friction terms for each sphere. For each subject, contact model-derived GRF_R prediction was optimized using data from one medium stiffness trial. The GRF_R error resulting from this trial represents the theoretical optimal performance of the comprehensive VSF-ground contact model. The transferability of the optimized parameter values was determined by simulating the two remaining medium stiffness trials and the three remaining trials each for the low and high stiffness configurations. No GRF data were available to optimize or verify contact model parameters on the intact side. As such, stiffness and damping for contact spheres on the intact side were parameterized to simplify the model of the intact side, so that the contact spheres were able to support the model's mass throughout stance phase.

Gait model evaluation

The gait model's performance was evaluated under two scenarios: static and dynamic gait conditions. Of the three trials per condition (Table 4.2), Subject 2 did not complete one medium stiffness trial, and Subject 4 did not complete one high stiffness trial. In total, forward kinematics simulations were computed for 38 trials (4 static, and 34 dynamic). For the static condition, the model was simulated with anatomically neutral joint angles for ten seconds. Model-predicted GRF_R was averaged over the course of the trial and compared to the mass of the subject. This comparison represents the accuracy of the contact parameters to estimate the ground contact force imparted by the subject with no dynamic component. For the dynamic conditions, forward kinematics gait simulations were computed for the nine gait trials per subject with high, medium, and low VSF stiffness configurations.

The Simscape solver computes the model's initial conditions by finding state values at the initial time step that exactly satisfy the model's system of equations. For all simulations in this study, the model conditions were assumed to start from steady state (i.e. zero derivative). The model was initialized in a posture taken from the experimental motion capture data at the first time step. The model's initial position in the gait environment was derived based on the initial coordinates of a virtual motion capture marker placed at the pelvis' origin frame. Then, joint kinematics, also from experimental data, were applied at each joint and the model was simulated forward in time, allowing kinematic movements and contact with the ground to evolve in time according to the model's dynamics. Continuous differential equations were integrated with respect to time in order to compute all model variables as a function of time. A forward kinematics-

based approach was selected for this study because the goal was to apply experimentally-observed joint kinematics and allow the resulting contact forces under the prosthesis to evolve accordingly.

Joint kinematics and GRF_R data derived from simulations were low-pass filtered (4^{th} order Butterworth: f_c: 6 Hz and 40 Hz, respectively). Simulation and experimental GRF_R were time locked and indexed to 0.25 s before and 0.25 s after stance phase. Including the brief period before and after stance phase provides insights regarding how the contact model behaves outside of stance phase and whether or not key gait events (e.g. heel strike and toe off) occur at similar time points in the simulated and experimental data. Resultant ground reaction force time series were re-sampled to 101 data points via cubic spline interpolation to allow for comparison between stance phases of differing lengths. Ensemble curves (mean ± SD) were generated for each condition. The cumulative impulse of GRF_R was calculated to verify the dynamic compatibility of the simulation with the known force of gravity. The time integral of GRF_R has been shown previously to be indicative of whole-body energetics (Peterson et al., 2011).

Anterior-posterior center of pressure (CoP_{AP}) position was calculated as the weighted sum of each contact sphere's predicted force multiplied by its anterior-posterior position (x) (eq. 4.3). Raw normal forces arising from each sphere during stance phase were low-pass filtered (4^{th} order Butterworth: f_c: 40 Hz) and summed. Anterior-posterior CoP position was calculated throughout the stance phase. The CoP_{AP} time series data

$$\textbf{eq. 4. 3}: \mathrm{CoP_{AP}} = \frac{\sum_{i=1}^{N} x_i F_{n_i}}{\sum F_n}$$

$\mathbf{CoP_{AP}}$: Anterior-posterior center of pressure position

$\boldsymbol{x_i}$: Anterior posterior coordinate of contact sphere

were low-pass filtered (4th order Butterworth: f_c: 6 Hz) and re-sampled to 101 data points via cubic spline interpolation to allow for comparison between stance phases of differing lengths. Joint kinematics, GRF_R, and CoP_{AP} derived from the simulations were compared to the corresponding data measured during experimental gait trials using coefficient of determination and RMSE.

Results

In the static condition, model-predicted subject mass was 2.1 ± 0.1% less than measured mass. In the dynamic conditions, simulated joint angles matched experimental joint angles well (mean RMSE: 0.14 ± 0.01 deg, mean R^2: 1.00 ± 0.00). All simulated joint angles matched experimental values with less than 0.23 deg RMSE.

Optimization of the medium stiffness trial for each subject resulted in a mean GRF_R RMSE value of 7.6 ± 1.0% body weight (BW) and a mean R^2 of 0.97 ± 0.01 across stance phase (Figure 4.3). Cumulative impulse also matched well (RMSE: 0.76 ± 0.00% BW·s, R^2: 1.00 ± 0.00). In the time domain, model-predicted stance phases were, on average, 0.03 ± 0.03 s shorter compared to experimental data.

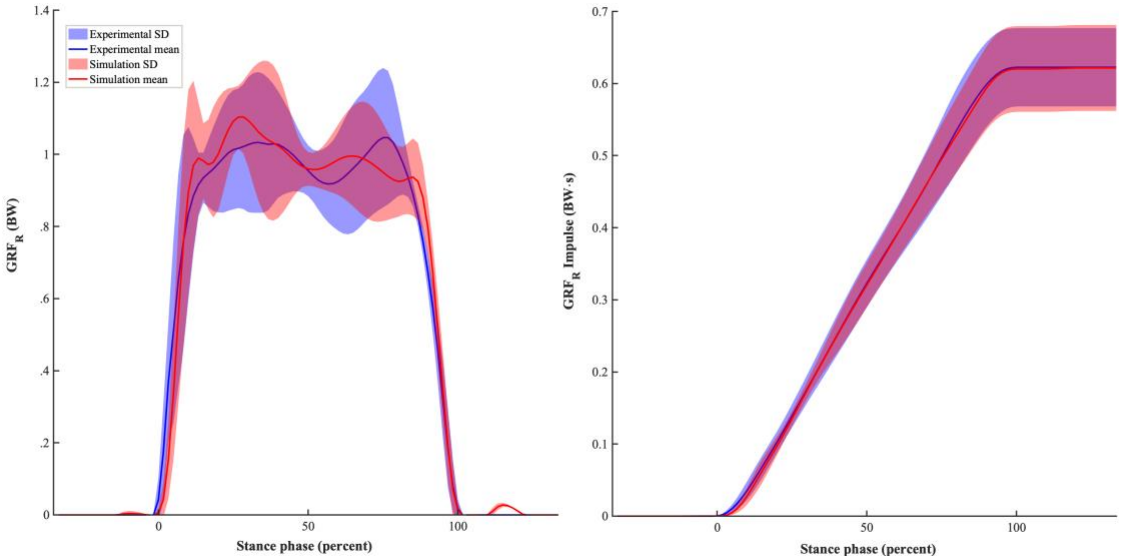

Figure 4.3: Optimized GRF_R (left) and GRF_R impulse (right) response for the medium stiffness trials. n = 4 trials.

In the unoptimized trials, experimental GRF_R and GRF_R impulse responses were similar in the time and amplitude domains across the three stiffness conditions (Figure 4.4). On average, stance phase times were 0.01 ± 0.01 s shorter in the simulations across the stiffness conditions. Time errors were least for the medium stiffness and greatest for the high stiffness simulations. Variability for GRF_R was greatest during the first 15% of stance phase for simulations and lowest for the experimental data during this time. The contact parameters optimized for the medium stiffness condition transferred well across the low and high stiffness conditions, which is evident by the similar RMSE values for GRF_R and GRF_R impulse (Table 4.3). Model-predicted GRF_R values were better in the high stiffness configuration, whereas predictions for GRF_R impulse were best in the medium and high stiffness conditions (Table 4.3).

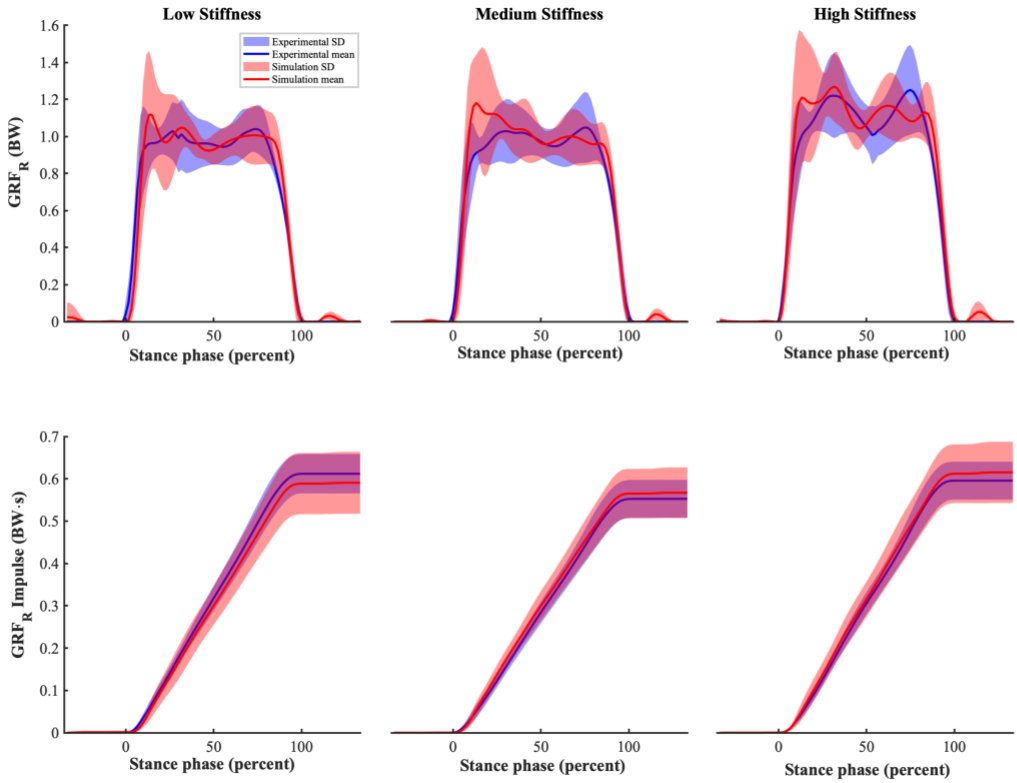

Figure 4.4: Ensemble curves (mean ± SD) for GRF_R (top) and GRF_R Impulse (bottom) for the low, medium, and high stiffness conditions (left, middle, and right). n = 34 trials.

Table 4.3: Summary of GRF_R, GRF_R impulse, and COP_{AP} comparison between simulated and experimental data.

Stiffness Configuration	GRF_R		GRF_R Impulse		COP_{AP}	
	R^2	RMSE (BW)	R^2	RMSE (BW·s)	R^2	RMSE (% FL)
Low	0.93 ± 0.04	0.12 ± 0.03	0.98 ± 0.06	0.03 ± 0.03	0.79 ± 0.10	13 ± 3.2
Medium	0.93 ± 0.09	0.11 ± 0.05	0.99 ± 0.01	0.02 ± 0.01	0.73 ± 0.16	15 ± 3.8
High	0.93 ± 0.02	0.11 ± 0.01	0.99 ± 0.01	0.01 ± 0.01	0.73 ± 0.22	14 ± 5.6

BW: Body weight, **COP_{AP}**: Anterior-posterior center of pressure, **FL**: Foot length, Data are mean ± SD

Anterior-posterior CoP trajectory during stance phase was similar between simulated and experimental data (Figure 4.5, Table 4.3). However, divergent trajectories were observed, primarily between 15–40% of stance phase. Overall, RMSE values were 14 ± 4.4 percent foot length across all conditions, with the low stiffness condition

performing the best. Simulated data exhibited a strong correlation ($R^2 > 0.70$) with experimental data for all stiffness conditions. Simulation-predicted CoP_{AP} showed similar variability compared to experimental data.

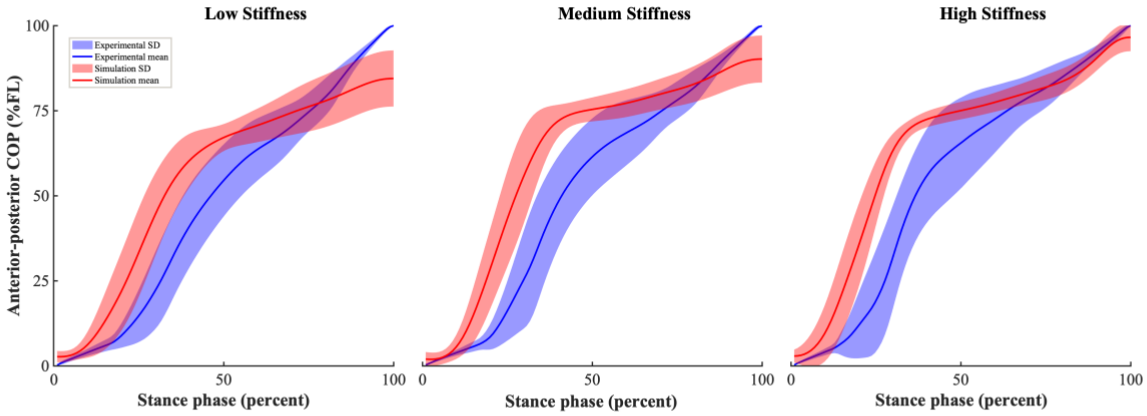

Figure 4.5: Ensemble curves for COP_{AP} position for the low, medium, and high stiffness conditions (left, middle, and right). **FL**: foot length

Discussion

The objective of this study was to develop and evaluate a forward simulation-capable gait model with lower limb loss and a semi-active VSF prosthesis. The gait model and VSF-ground contact model were evaluated under static and dynamic gait conditions. Under static conditions, model-predicted mass exhibited an average error of 2.6% with respect to the measured mass of the subjects. This value represents the performance of the contact model with no dynamic component. Under dynamic gait conditions, the model's predictions of GRF_R, GRF_R impulse, and COP_{AP} within a forward kinematics framework were evaluated. For all trials, simulated joint angles were strongly correlated with experimental angles ($R^2 > 0.999$ for all joints) with RMSE values of less than 0.23 deg for all joints. These values are logical for forward kinematics simulations, but importantly indicate that the model is numerically stable when actuated by joint

kinematics measured during gait with the VSF. Further, concomitant agreement between the model's kinematic and kinetic response is critical for forward dynamics simulations of human gait.

Optimization of contact model parameters in the medium stiffness trials achieved a mean RMSE value of 7.6 ± 1.0 percent BW for GRF_R and 0.76 ± 0.00% BW·s for GRF_R impulse. These values represent the theoretical optimal performance of the comprehensive contact model within the present simulation framework. This contact model performance is similar to the values previously reported in biomechanical contact modeling work (Brown and McPhee, 2018; Lopes et al., 2015; Van Hulle et al., 2020). However, the focus of those studies was to predict foot-ground contact dynamics during gait for individuals with intact limbs. Direct comparison of these data was limited to work in intact limb biomechanical modeling due to a lack of studies reporting validation data for prosthesis-ground contact modeling in gait biomechanics. The strong correlation and low error for GRF_R impulse indicates that the contact model is able to predict the shape and trajectory of the GRF_R waveform arising from gait kinematics. Accurate prediction of GRF_R impulse is important for capturing whole-body energetics throughout gait (Peterson et al., 2011). The concomitant agreement for both simulated kinematics and kinetics further suggests that these methods are viable for simulating whole-body dynamics during gait.

The transferability of the optimized contact model parameters from the medium stiffness condition was assessed by simulating the two remaining medium stiffness trials and the six total trials with low and high stiffness configurations per subject. Compared to the optimized trials, error for simulation-derived GRF_R predictions increased by an

average of 4% across the unoptimized trials. Mean GRF_R RMSE and R^2 were 12.3 ± 6.1% BW and 0.91 ± 0.02 respectively for the remaining medium stiffness trials. These errors were slightly greater than those for the low and high stiffness trials (Table 4.3). There was one outlier trial for the medium stiffness condition, classified as a RMSE response greater than three standard deviations from the mean. This trial was not removed from the mean values presented in Figures 3 and 5 and Table 3, since it could not be definitively discerned what the source of the increased error was. With this trial removed, the model's GRF_R response for the medium stiffness was 9.0 ± 2.0% BW RMSE and 0.96 ± 0.01 R^2. The same subject had a single high error trial in the low and high stiffness conditions. However, these trials did not meet the mathematical criteria for outlier classification at 2.50 and 2.76 standard deviations above the mean, respectively. Data from these trials show a brief but large overshoot (>1 BW) for model-predicted GRF_R at initial heel contact. Each of these trials likely contributed to the higher mean error and variability in model-predicted GRF_R early in stance phase (Figure 4.4). Given that all outlier or near outlier trials were from the same subject, these errors may be due to errors or noise in the kinematic data used to drive the model. Errors early in stance phase could be compounded by the relative sensitivity of contact model parameters when a single sphere is in contact with the walking surface.

Model-predicted stance phase times agreed well with experimental values. On average, simulated stance phases were 0.01 ± 0.01 s shorter than experimental times. Errors were similar between stiffness conditions. Accurate prediction of stance phase length is important because it contributes to the model's ability to quantify metrics such as the time integral of GRFs, which may be indicative of whole-body energetics

(Peterson et al., 2011). Presented by ascending stiffness condition, stance phase times were 0.68 ± 0.06, 0.72 ± 0.06, and 0.71 ± 0.07 s.

Simulated CoP_{AP} values were strongly correlated ($R^2 > 0.70$) with experimental data in all stiffness conditions. The RMSE values achieved using this model were similar to those reported in a previous study (Jackson et al., 2016), which used a subject-specific 38 contact point model to predict CoP_{AP} for individuals with intact limbs. Accurate mapping of CoP_{AP} throughout stance phase is vital for simulating the effects of variable prosthesis stiffness on joint forces and moments during gait. Errors in model-predicted CoP_{AP} may be reduced by increasing the density of contact spheres distributed on the plantar surface of the foot, which would improve the resolution of CoP_{AP} predictions. However, this would likely result in increased execution time for simulations due to increased model complexity and also increase complexity of the contact parameter optimization problem. The low density of contact spheres in the heel of the VSF model is a likely source of the steep inflection in the CoP_{AP} trajectory early in stance phase, which contrasts the more gradual progression depicted in the experimental data (Figure 4.5). Model-derived CoP_{AP} predictions may also be improved by incorporating kinematics of the head, arms, and trunk, which were unaccounted for in the present study.

Computation times are an important consideration in simulation-based approaches. Previous work has shown the lumped parameter approach for modeling ESR prosthesis dynamics to be more computationally efficient compared to more robust finite element models (McGeehan et al., 2020). Total execution times for the gait model were 13.7 ± 2.48, 16.8 ± 4.66, and 64.3 ± 71.2 times slower than real time for the low, medium, and high stiffness conditions. Increased execution times for the stiff conditions

are a reflection of the need for small time-steps in solving a rapidly-evolving, stiff differential equation. Computation times were also increased for participants with more mass. These times could be reduced by utilizing "Accelerator" or "Rapid Accelerator" modes in Simscape Multibody, which improve simulation times by generating a C-code executable of the model.

The present data show promise for predicting GRF_R arising from gait with a semi-active VSF prosthesis. These methods may be applied to the design and prescription of lower limb prostheses and forward dynamics simulations in robotics and biomechanics. For example, simulations could be used to evaluate the potential effects of varied prosthesis design parameters on the gait mechanics of a user. Simulations could also be computed within an optimal control framework to identify optimal device configurations and manufacture customized prostheses. Evaluating these effects within a simulation-based framework rather than tradition *in vivo* experimentation minimizes risk and time spent by the user. Further, a broad spectrum of prosthesis design parameters could be modeled and simulated without the need to manufacture multiple devices or the costs associated with doing so.

Within biomechanics, future work could formulate gait with the VSF as an optimal control problem in which stiffness is varied to minimize a biomechanical cost function such as peak or average joint moment or metabolic cost. Further optimization of the VSF-ground contact model may be necessary for simulation scenarios with error tolerances less than 11% BW (Table 4.3). Similar improvements may be required if the mean difference between simulation conditions is less than the error of the model, as was the case for the variation in GRF_R by VSF stiffness condition presented in this study.

Reducing error in model-predicted GRF_R may be accomplished through improved methods in optimizing contact model parameters. For example, the objective function could be evaluated under a variety of conditions, thereby improving the generalizability of the contact model. A deformable contact model, such as presented in Jackson, Hass, and Fregly (2016), may also be a viable means of representing foam deformation throughout stance phase and thus reducing error.

Previous work in gait simulations with biomechatronic devices has often relied on abstract representations of components such as motors, electronics, and control systems (Dembia et al., 2017; Khamar et al., 2019; Willson et al., 2020). In contrast, Simscape Multibody and Simulink offer a large library of these components, which can be readily integrated into the model for more realistic representations of biomechatronic systems. Further, control system parameters derived from simulations can be readily deployed to prototype devices. As such, this model may be advantageous for simulating gait with biomechatronic devices.

These methods assume accurate estimation of segment length, joint centers, and joint angles which were derived from marker-based motion capture data. Each of these metrics likely suffers from small errors due to marker placement, localization, and coordinate system design. Such errors would contribute to decrements in contact model performance. The components and joints of the prosthetic limb were also modeled as rigid, which may not be completely accurate to represent the physical limb. This discrepancy would manifest as small differences in kinematics and energy transfer between the components of the prosthetic limb. Similarly, the model's anatomical joints were considered to be frictionless, which is not representative of the properties of these

joints *in vivo*. Modeling joint friction and viscosity may improve accuracy for model-predicted joint kinetics during forward kinematics simulations or joint kinematics during forward dynamics simulations. Nevertheless, simulated motions were consistent with experimental data of subjects walking with the VSF and other previously reported data of spatiotemporal gait patterns among persons with lower limb loss (Su et al., 2008; Winter and Sienko, 1988). Another limitation is inherent to the reduced order design of the lumped parameter VSF keel, which constrains keel motion to the sagittal plane. While this design is computationally efficient compared to more robust finite element models, it fails to account for small torsional keel motions that would be possible under ecological gait conditions with the physical VSF. Future work could develop a lumped parameter model that allows for torsional keel movement in the frontal plane. Within the gait model, future work should incorporate biologically-inspired muscle models (e.g. Hill (Hill, 1938) or Thelen (Thelen, 2003) models) to actuate joints for forward dynamics simulations. This would improve the biomechanical and physiological validity of the model and also allow for evaluation of neuromuscular coordination during simulated gait.

Conclusions

The present study demonstrates that the ESR properties of a semi-active VSF can be modeled and integrated into a scalable gait model that incorporates the altered lower limb mass, inertia, and mechanical properties associated with use of an ESR foot and prosthetic socket. The model captured whole-body energetics associated with gait with varied prosthesis stiffnesses. Foot-ground contact models were used to estimate GRF_R with 7.6% BW mean RMSE in optimized gait trials, which translated to a mean RMSE of

11% across unoptimized trials. The contact models also predicted COP_{AP} with mean RMSE of 14% foot length. This model performance may be sufficient for gait simulations among persons with lower limb loss. Such simulations may be used to aid in the prosthesis design and prescription process in order to improve user mobility. These methods may also be helpful to identify other important prosthesis design parameters, which can be modified to optimize gait. Further contact model optimization and error reduction may be required for simulation-based comparisons of varied prosthesis stiffness, where differences in GRF_R magnitude may be nuanced.

Statement of acknowledgements: The authors would like to thank Evan Glanzer for his work in developing and testing the variable-stiffness foot and Terry Denery for his intellectual contributions in optimizing the contact model.

Funding sources: This work was funded in part by the Lokey Doctoral Science Fellowship (MAM) and NIH grant HD074424 (PGA).

Acronyms widely used in text

BKA	Below-Knee Amputation
BW	Body Weight; M*g
CoP	Center of Pressure
DoF	Degrees of Freedom
ESR	Energy Storage and Return
GRF_R	Resultant Ground Reaction Force, N; $\sqrt{GRF_X{}^2 + GRF_y{}^2 + GRF_z{}^2}$
LHS	Latin Hypercube Sampling
LLA	Lower Limb Amputation
ode15s	Ordinary Differential Euation 15 solver
SD	Standard Deviation
RMSE	Root Mean Square Error; $\sqrt{\frac{\sum_{i=1}^{N}(Experimental_i - Simulation_i)^2}{N}}$
VSF	Variable Stiffness Foot

Abbreviations

a	Overhung length, mm
b	Damping coefficient, N·s/mm
B	Support fulcrum position, mm
D	Displacement, mm
F	Force, N
k	Linear stiffness, N/mm
L	Total beam length, mm
l	Supported length, mm
n	Penetration exponent
R^2	Coefficient of determination
μ	Coefficient of friction
v	Linear velocity
y	Scaling factor
δ	Penetration depth, mm
$\dot{\delta}$	Penetration velocity, mm/s
ω	Angular velocity, rad/s

Superscripts and subscripts

CoP_{AP}	Anterior-posterior (Center of Pressure)
F_f	Frictional force, N
F_n	Normal force, N
GRF_R	Resultant ground reaction force, N
v_{poc}	Linear velocity at point of contact, mm/s
$v_{threshold}$	Linear velocity threshold, m/s
$\mu_{kinetic}$	Coefficient of kinetic friction
μ_{static}	Coefficient of static friction

Bridge

This study expands upon Chapter III in two key areas. The ground contact model and algorithm for programmatically deriving contact parameters were assessed for three additional subjects, thereby providing insight into the generalizability of the methods presented in Chapter III. Further, the VSF model was integrated into a scalable 28-degree-of-freedom gait model capable of computing forward kinematics or forward dynamics simulations. Methods for developing a generic gait model and generating subject-specific models based on optical motion capture data were presented.

Data presented in this chapter support the use of these modeling methods to compute forward simulations of gait with a semi-active VSF. Simulations are advantageous compared to traditional gait experiments because of the ability mathematically model and estimate values that cannot be measured *in vivo* (e.g. interface dynamics between the prosthetic socket and residual limb interface). In Chapter V, these methods are applied in a simulation-based analysis of the effects of prosthesis stiffness on residual limb-prosthetic socket interface dynamics (Specific Aim 4).

CHAPTER V

A SIMULATION-BASED ANALYSIS OF THE EFFECTS OF VARIABLE PROSTHESIS STIFFNESS ON RESIDUAL LIMB-SOCKET INTERFACE DYNAMICS

This work is currently in preparation for submission to the *Journal of Biomechanics.* Dr. Michael E. Hahn, Dr. Peter G. Adamczyk, and Mr. Kieran M. Nichols provided mentorship including assistance with study design, data interpretation, and editing and finalizing the final manuscript.

Introduction

Rehabilitation following a lower limb amputation (LLA) often includes prescription of a prosthesis designed to replace the functionality of the removed limb. For an individual with a below-knee amputation (BKA), a prosthesis system typically consists of a socket, which interfaces with the residual limb, a rigid pylon, and a foot-ankle prosthesis. Use of lower limb prostheses can improve mobility, health, and quality of life. However, abnormal loading of the soft tissues surrounding the truncated shank (e.g. asymmetric pressure distribution and elevated shear forces) can cause tissue deformation and ischemia during load bearing activities (Portnoy et al., 2009). These conditions can lead to cell death, macerate tissue, and give rise to ulceration and pain (Highsmith and Highsmith, 2007).

Dermatological issues are experienced by 75% of individuals using lower limb prostheses (Highsmith and Highsmith, 2007; Highsmith et al., 2016), at 65% greater

incidence compared to their counterparts with intact limbs (Highsmith et al., 2016). These conditions lead to prosthesis disuse (Meulenbelt et al., 2006) and can cause an individual with BKA to become wheelchair-bound. Recent estimates suggest that 11-22% of individuals abandon their prosthesis within one year of prescription (Balk et al., 2018). These data are supported by a second study which found that 25% of users abandoned prosthetic limbs, with 29% citing discomfort, 25% citing pain, and 12% claiming poor fit as the determining factor (*National Health Services Audit Commission Briefing: Assisting Independence*, 2002). This transition represents a substantial reduction in quality of life and increased healthcare-related financial burden.

The socket is a crucial component of mobility and quality of life for individuals with BKA due to its role as the interface between the human, prosthesis system, and ground. An improved understanding of biomechanical interaction between the residual limb and prosthetic socket during gait is necessary to attenuate rates of tissue damage and prosthesis disuse. Previous experiments evaluating residual limb-socket interface dynamics have relied on sensors integrated into the prosthetic socket (Al-Fakih et al., 2013; Courtney et al., 2016; Laszczak et al., 2016, 2015; Sanders and Daly, 1993; Schiff et al., 2014). However, previous systems have utilized bulky sensors (Al-Fakih et al., 2013; Laszczak et al., 2016, 2015), tethered cables (Ali et al., 2013; Boutwell et al., 2012; Courtney et al., 2016; Gholizadeh et al., 2014; Laszczak et al., 2016, 2015; Safari et al., 2015; Schiff et al., 2014), or required modifications to the socket (Al-Fakih et al., 2013; Schiff et al., 2014), thereby compromising the integrity of the socket interface and likely altering gait mechanics of participants.

Simulations based on computational models may be useful for evaluating the relationships between anatomical morphologies, gait mechanics, design of prosthesis systems, and residual limb loading conditions. Previous model-based research has primarily employed finite element (FE) analysis techniques to derive dynamic mathematical models of the residual limb-socket interface (Jia et al., 2004; Lee et al., 2004; Portnoy et al., 2009; Schiff et al., 2014). While FE models allow for complex characterization of the biological materials and their mechanical properties, they are computationally costly and thus may be limiting factors when integrated within complex gait models. Other studies have used abstract representations of the interface, such an idealized joint parameterized with spring and damper force laws (LaPrè et al., 2018). These methods may be appropriate for estimating generalized residual limb kinematics within the socket, but are unable to differentiate the forces and torques applied (e.g. normal pressure and shear stresses) and offer little insight regarding the relative load distribution at different anatomical locations around the limb. There remains a need for a computationally economical reduced order model of the biomechanical contact forces arising from the residual limb-socket interaction during gait.

This chapter presents the design and development of a spatial contact force model motivated by the material properties of the residual limb and prosthetic socket. The contact model was integrated into a larger computational gait model in order to simulate kinematics and kinetics at the socket interface during gait. This model could assist experimental studies by providing insight into the effects of varied prosthesis design parameters or gait conditions on residual limb-socket interface dynamics.

Methods

Model Design

A spatial contact model of the residual limb-socket interface was developed in Simscape Multibody. The geometry of the residual limb bone element was simplified as a rectangular cuboid with struts to represent the dimensions of the limb inclusive of the soft tissue (Figure 5.1). Within the residual limb model, soft tissue and bone element

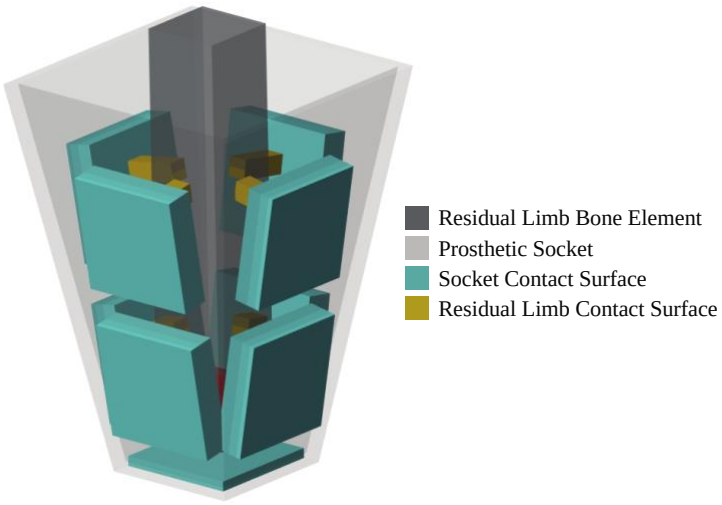

Figure 5.1: Depiction of the rotationally symmetrical residual limb and socket geometries, as well as the nine interface frames.

mechanics are not differentiated (i.e. the modeled dynamics are considered to be an aggregate of soft tissue and bone mechanics). The prosthetic socket was modeled as a rigid hollow square cone with an aperture of 100 deg. The residual limb interfaces with the socket at the same angle. The residual limb and socket have nine interface frames with attached cuboid structures to model interface dynamics. The mass of the residual limb was estimated first by deriving estimated density of the intact limb by modeling it as

a conical frustum with an assigned mass estimated per De Leva (1996). The derived density of the intact limb was applied to the residual limb model, which was then truncated at the respective level of amputation for each subject. The mass of the residual limb was distributed evenly as point masses about the nine interface frames. The residual limb has two contact interfaces (one proximal, one distal) on each of the four sides of the cuboid. The ninth interface is between the distal limb and base of the prosthetic socket. The distance between the distal residual limb and base of the socket was assumed to be 1.5 cm (Henrikson et al., 2018). This distance is representative of an air gap, which is common between the socket and liner in prosthetic socket systems (Henrikson et al., 2018). Figure 5.1 depicts a rotationally symmetrical rendering of the model.

Contact forces at the interfaces between the limb and socket in the normal plane are implemented as modified Kelvin-Voigt models with progressive spring and damper characteristics. Shear stresses between the socket and residual limb are considered analogous to the frictional forces arising from these interactions. In total, the residual limb has 4 degrees of freedom (DoF) with respect to the prosthetic socket (vertical translation and rotations about three axes).

Model Parameterization

A Kelvin-Voigt material model (spring and damper force law) was implemented to estimate residual limb-prosthetic socket interaction forces. The model estimates normal (F_n) and frictional forces (F_f) associated with the collision between a viscoelastic residual limb (spring and damper system) and rigid prosthetic socket (eq. 5.1). The present model does not include a socket-liner interface, but one could be implemented in

the future. The spring force (k) increases as a function of penetration depth (δ), whereas damping force (b) increases with penetration velocity ($\dot{\delta}$). Damping force is only applied when $\dot{\delta} > 0$. Frictional forces are calculated as the product of normal force and a user-

eq. 5.1: $$F_n = \begin{cases} (k \times \delta) + (b \times \dot{\delta}) & \delta > 0, \dot{\delta} > 0 \\ k \times \delta & \delta > 0, \dot{\delta} < 0 \\ 0 & \delta < 0 \end{cases}$$

$\boldsymbol{F_n}$: normal force

$\boldsymbol{k}$: contact stiffness

$\boldsymbol{\delta}$: penetration depth

$\boldsymbol{b}$: contact damping coefficient

defined coefficient of friction (μ) (eq. 5.2). A stick-slip friction law defines the transition between static (μ_{static}) and kinetic ($\mu_{kinetic}$) coefficients of friction based on a velocity threshold (v_{thresh}). Forces are applied along a common contact plane and conform to Newton's Third Law of Motion.

eq. 5.2: $$F_f = \begin{cases} F_n \times \mu_{static} & v_{poc} < v_{threshold} \\ F_n \times \mu_{kinetic} & v_{poc} > v_{threshold} \end{cases}$$

$\boldsymbol{F_f}$: frictional force

$\boldsymbol{\mu}$: coefficient of friction

$\boldsymbol{v_{poc}}$: velocity at point of contact

$\boldsymbol{v_{threshold}}$: velocity threshold

Values for spring stiffness in the normal plane (k_n) were formulated according to Hooke's Law (eq. 5.3), as described in Noll et al. (2017) and Zheng et al. (1999). The effective tissue moduli for individuals with a below-knee LLA (Table 5.1) were previously described in Zheng et al. (1999) and Mak et al. (1994). In both studies,

eq. 5.3: $k_n = \frac{EA}{l}$

kn: Stiffness in the normal plane

E: Young's modulus of the tissue

A: Area of the contact point

l: Width of the residual limb

Poisson's ratio was assumed to be 0.45. The stiffness values were parameterized independently for the anterior, posterior, medial, lateral, and distal contact interfaces in order to best represent the varying moduli at corresponding anatomical locations. Due to a lack of information reported in previous literature, damping coefficients (N·s/mm) were set to half the numerical value of stiffness (N/mm) in an effort to reduce high frequency oscillations at the contact interfaces.

Table 5.1: Summary of Young's Modulus values for various anatomical locations on the residual limb.

Anatomical location	Effective modulus (kPa)	Corresponding interface(s) on the model
Tibial tuberosity[1]	105	Anterior
Posterior tibia[3]	30	Posterior
Distal tibia[1]	60	Distal
Medial proximal tibia[2]	56	Medial
Lateral proximal tibia[1]	78	Lateral

[1](Zheng et al., 1999)
[2](Mak et al., 1994)
[3](Shan et al., 2019)

The static coefficient of friction (μ_{static}) between the limb and socket was assigned a value of 0.5, based on an *in vivo* study of the interaction between silicon (a commonly used material for prosthetic socket liners) and the skin of the human leg (Zhang and Mak, 1999). Coefficients of friction between 0.5 and 3.0 have been reported for various other socket liner materials (Cagle et al., 2018; Sanders et al., 1998). The dynamic coefficient of friction ($\mu_{dynamic}$) was set to 70% of the μ_{static} based on Cagle et al. (2018). A velocity threshold (μ_{vth}) of 0.005 m/s defines the transition between the two values. In the future, subject-specific values for μ_{static} and $\mu_{dynamic}$ could be implemented.

The developed model predicts normal pressure and shear stress at the contact interfaces. Based on these forces, relative kinematics between the residual limb and prosthetic socket are simulated. Model-derived estimates may be compared to the range of experimental values reported in the literature for pressure, shear stress, and residual limb kinematics (Courtney et al., 2016; Eshraghi et al., 2012; Gholizadeh et al., 2014; Jia et al., 2004; LaPrè et al., 2018; Laszczak et al., 2016; Sanders et al., 2000; Sanders and

Daly, 1993). Previously-reported peak values for normal pressure range from 40-160 kPa (Ali et al., 2013; Courtney et al., 2016; Sanders et al., 2000), and peak values for shear stress range from 3-50 kPa (Laszczak et al., 2016; Noll et al., 2017; Sanders and Daly, 1993; Schiff et al., 2014). The broad range of values in the literature may be attributed to variation in sensors used, sensor placement, socket materials, individual-specific residual limb tissue properties, and experimental gait protocols. Further, values should vary based on phase of the gait cycle and anatomical location (Courtney et al., 2016; Noll et al., 2017; Portnoy et al., 2009; Sanders and Daly, 1993). Nevertheless, values within these ranges may be used as target criteria.

The reported values for kinematics between the residual limb and prosthetic socket also vary within the literature. Values of 1.0 to 4.2 cm have been reported for relative vertical translation (i.e. residual limb pistoning) (Eshraghi et al., 2012; Gholizadeh et al., 2011; LaPrè et al., 2018; Sanders et al., 2006). These values may vary based on residual limb shape (Wirta et al., 1990) and type of socket liner used (Eshraghi et al., 2012; Gholizadeh et al., 2011; Sanders et al., 2006). Reported values for axial internal/external rotation (rotation about the residual limb's long axis) are between 0 and ±20 deg during gait (LaPrè et al., 2018). The spatiotemporal patterns and magnitude of rotation demonstrated high variability across subjects.

Gait Simulations

The spatial contact model of the residual limb-socket interface was integrated into a gait model with a BKA and a semi-active variable stiffness foot (VSF) prosthesis. This

model was previously described in Chapter IV of this dissertation. As in Chapter IV, gait simulations were computed for four individuals (Table 5.2) walking with the VSF

Table 5.2: Participant characteristics.

Subject	Sex	Age (y)	Height (cm)	Mass (kg)	Amputation side	Years post-amputation
1	Male	34	181	77.3	Right	15
2	Male	51	175	111	Right	8
3	Male	70	180	83.8	Left	14
4	Female	61	163	63.8	Right	8
Mean ± SD	–	54 ± 15	175 ± 19.9	84.0 ± 19.9	–	11 ± 3.8

configured to “high”, “medium”, and “low” stiffness settings, corresponding to forefoot stiffness values of 10, 19, and 32 N/mm. Forward kinematics simulations were computed for three trials per setting. Subject 2 did not complete one medium stiffness trial, and Subject 4 did not complete one high stiffness trial. In total, 34 simulations were computed. All simulations were computed in Simscape Multibody using the *ode23t* solver profile with variable step sizes for numerical integration. Simulations were performed on a computer with a 4.0 GHz quad-core processor.

The experimental motion capture data used to drive the model were insufficient to estimate kinematics of the residual limb with respect to the prosthetic socket. As such, data from the literature were used to constrain motion of the residual limb via a bearing joint. A progressive spring and damper force law was used to constrain motion. Limits of 0.5 cm and -3.5 cm were imposed for residual limb vertical translation (Darter et al., 2016; Eshraghi et al., 2012; Gholizadeh et al., 2011; LaPrè et al., 2018; Sanders et al., 2006). Constraints of ±10 deg, ±5 deg, and ±5 deg were imposed for axial rotation, anterior-posterior, and medial-lateral rotations (Laprè et al., 2014; LaPrè et al., 2018).

Normal forces, frictional forces, pistoning displacement, and axial rotations were estimated using the spatial contact model for the duration of stance phase. All kinematic and kinetic signals related to the limb-socket interface were low-pass filtered via a 4th order Butterworth (f_c: 6Hz). Data were indexed from heel strike to toe-off and resampled to 101 data points via cubic spline interpolation. These methods allow for comparison of stance phases of different lengths. Model-derived values were compared to those previously reported in the literature. The effects of prosthesis stiffness on these outcomes were also evaluated via repeated measures ANOVA analyses ($\alpha = 0.05$). It was hypothesized that these effects would be subject-dependent, and as such, an exemplary case study for Subject 1 is presented along with group mean data.

Results

Model Performance (Group Data)

Contact model-derived values for normal pressure and shear stress were dependent upon anatomical location (Table 5.3) and progression of stance phase (Figure 5.2). Peak average normal pressure across stance phase was 70.4 ± 4.28, 75.9 ± 4.44, and 85.0 ± 13.0 kPa for the low, medium, and high stiffness conditions, whereas peak average shear stress values were 25.0 ± 1.52, 26.6 ±1.55, and 29.9 ± 4.61 kPa for the same conditions (Table 5.5, Figure 5.2). There was no main effect of stiffness condition on normal pressure ($p = 0.28$) nor shear stress ($p = 0.31$). Similar values for average residual limb pistoning and axial rotation were observed for each of the stiffness conditions ($p > 0.05$) (Figure 5.2), though effects were subject-dependent (Table 5.3). Average peak

pistoning values were 1.46 ± 0.03, 1.52 ± 0.05, and 1.51 ± 0.07 cm for the ascending stiffness conditions.

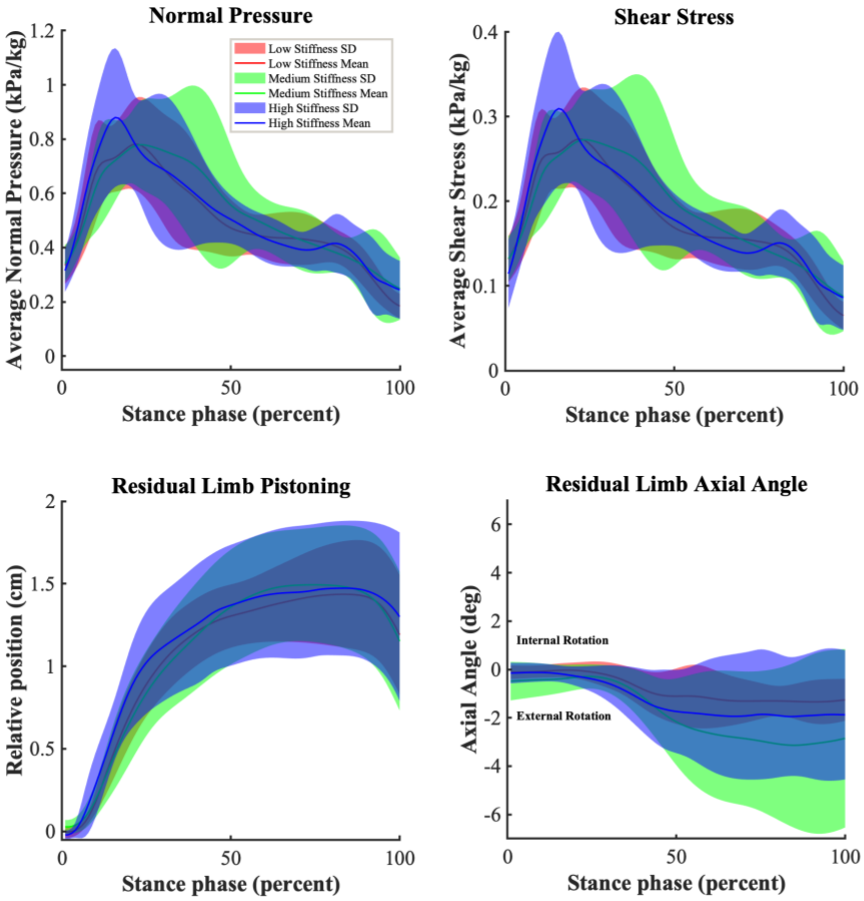

Figure 5.2: Group mean data for normal pressure, shear stress, residual limb pistoning, and residual limb internal/external rotation across stance phase for the low, medium, and high stiffness conditions. Kinetic data are normalized to subject body weight.

Spatiotemporal patterns for pressure and shear stress distribution were variable between subjects, but show similar variability across stiffness conditions (Tables 5.4 and 5.5, Figure 5.3). On average, participants displayed predominantly anterior pressure and shear distributions early in stance phase, but trended toward a more even distribution later in stance phase. Pressure trended slightly toward the lateral and proximal aspects of the

residual limb thoughout stance phase. High variability was observed among participants for the anterior-posterior and medial-lateral distributions throughout stance phase.

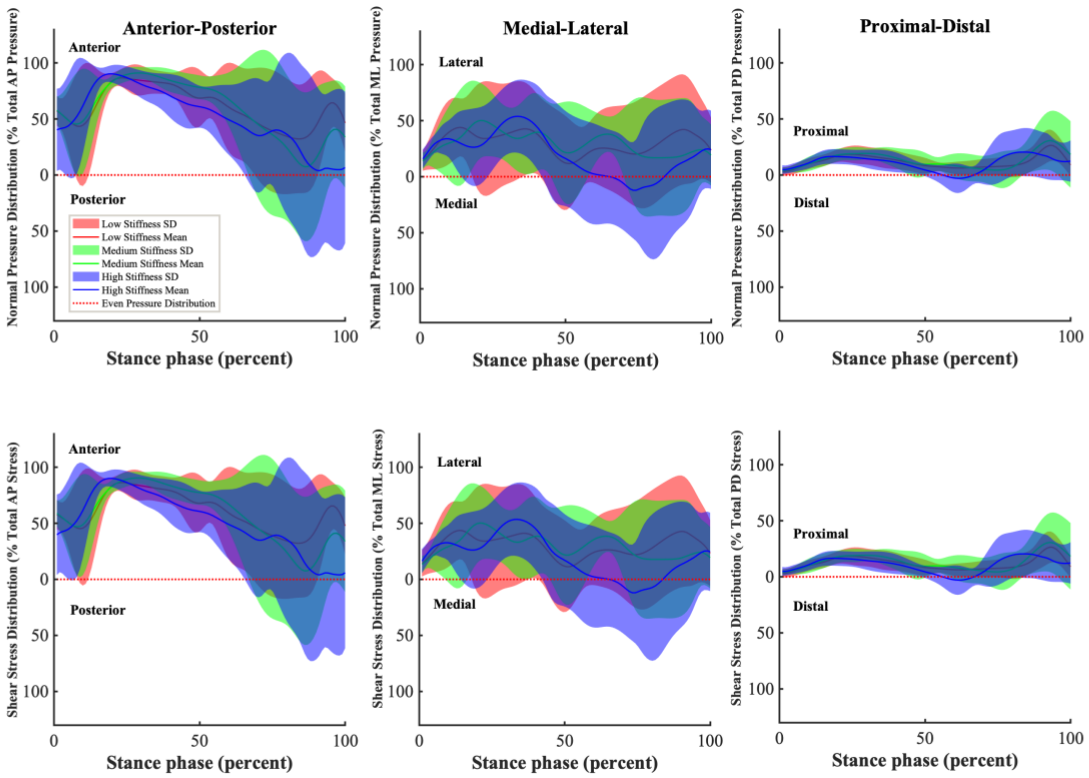

Figure 5.3: Group mean data for normal pressure (top) and shear stress (bottom) distributions in the anterior-posterior, medial-lateral, and proximal-distal directions.

Case Study (Subject 1)

Mean data for Subject 1 demonstrated less variability compared to the group data (Figure 5.4). Average pressure and shear stress values peaked at approximately 20% stance phase, whereas residual limb pistoning peaked and plateaued near 50% stance phase. Maximal pistoning displacement was approximately 1.5 cm for all conditions. A slightly increased rate of pistoning was observed between 15-40% stance phase for the high stiffness compared to the low and medium stiffness conditions (Figure 5.4). The

subject's residual limb was predominately externally rotated with respect the prosthetic socket throughout stance phase with maximal external rotation occurring near 50% stance phase (Figure 5.4). The low stiffness condition resulted in the least external rotation, though high variability was observed late in stance phase for all conditions.

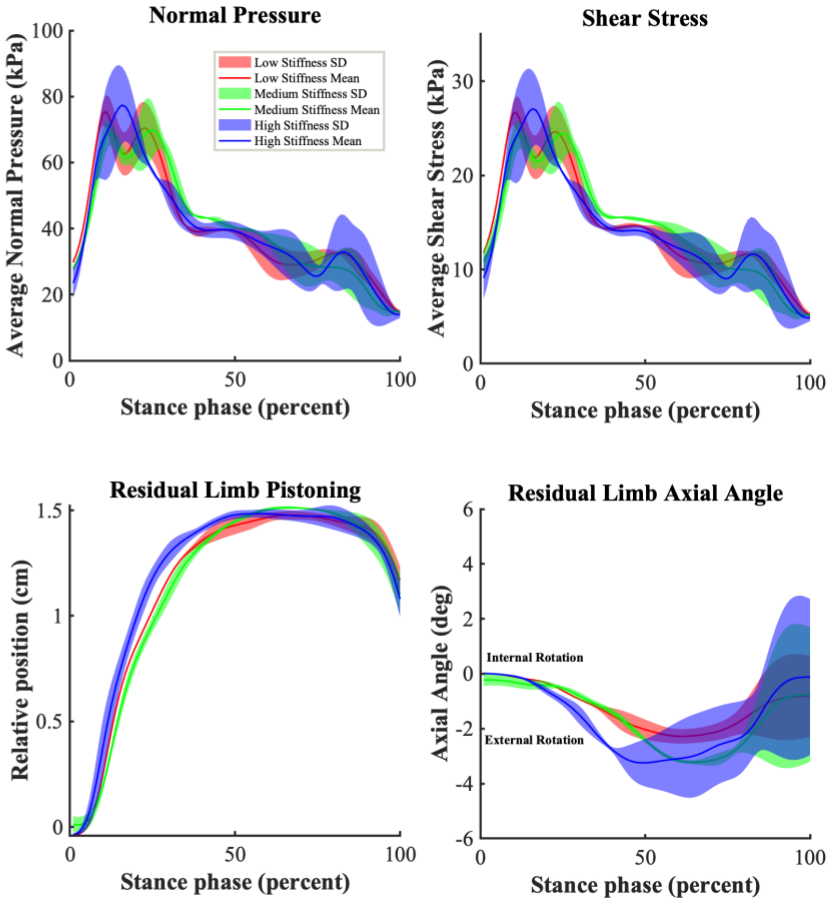

Figure 5.4: Mean data for normal pressure, shear stress, residual limb pistoning, and residual limb internal/external rotation across stance phase for the low, medium, and high stiffness conditions. Kinetic data are normalized to subject body weight.

The effects of variable prosthesis stiffness on pressure and shear stress distribution were observed primarily during 50-100% of stance phase (Figure 5.5).

However, divergent patterns in the mean data were accompanied by greater variability during this time. From 0-50% stance phase, pressure and shear stress were weighted more heavily toward the anterior aspect of the residual limb for all stiffness conditions. For the low and high stiffness conditions, mean pressure and shear stress trended toward a relatively even anterior-posterior distribution late in stance phase, whereas the medium stiffness condition resulted in a relatively posterior distribution. Pressure and shear stress distribution outcomes were similar across stiffness conditions for the medial-lateral and proximal-distal directions.

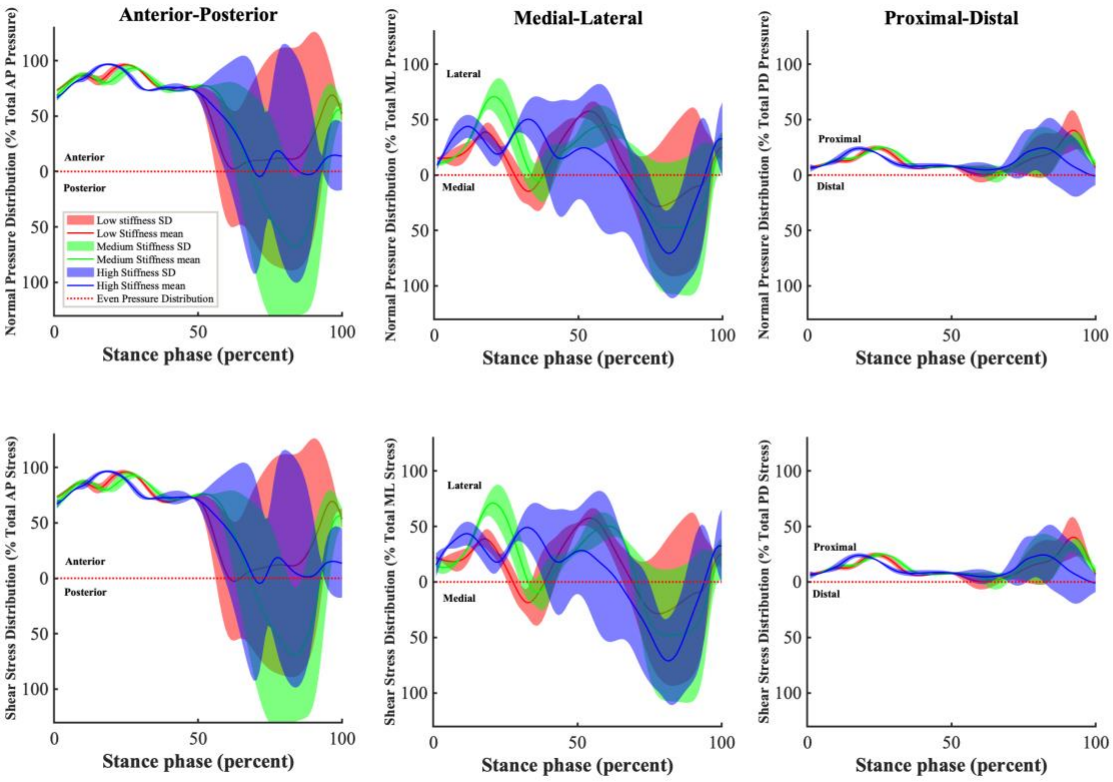

Figure 5.5: Subject 1 mean data for normal pressure (top) and shear stress (bottom) distributions in the anterior-posterior, medial-lateral, and proximal-distal directions.

Table 5.3: Average peak values for normal and shear stress (average of nine anatomical locations), and peak values for residual limb piston displacement with respect to the prosthetic socket. Data are mean ± SD.

Subject (condition)	Normal Pressure (kPa)	Shear Stress (kPa)	Piston Displacement (cm)
1 (low)	75.7 ± 3.71	26.8 ± 1.26	1.48 ± 0.02
1 (medium)	72.7 ± 6.42	25.5 ± 2.22	1.51 ± 0.01
1 (high)	81.54 ± 4.11	28.5 ± 1.44	1.50 ± 0.03
2 (low)	91.2 ± 10.93	32.0 ± 3.84	1.95 ± 0.10
2 (medium)	103 ± 6.47	36.1 ± 2.30	2.07 ± 0.15
2 (high)	119.2 ± 32.6	42.1 ± 11.7	2.09 ± 0.19
3 (low)	50.5 ± 1.08	18.6 ± 0.47	1.22 ± 0.01
3 (medium)	52.1 ± 0.61	18.2 ± 0.19	1.26 ± 0.02
3 (high)	61.0 ± 13.9	21.5 ± 4.89	1.26 ± 0.02
4 (low)	64.1 ± 1.41	22.5 ± 22.5	1.19 ± 0.00
4 (medium)	76.1 ± 4.24	36.6 ± 1.50	1.22 ± 0.03
4 (high)	78.3 ± 1.26	27.4 ± 0.42	1.19 ± 0.03
Group (low)	70.4 ± 4.28	25.0 ± 1.52	1.46 ± 0.03
Group (medium)	78.1 ± 4.44	26.6 ± 1.55	1.52 ± 0.05
Group (high)	85.0 ± 13.0	29.9 ± 4.61	1.51 ± 0.07

Table 5.4: Average peak values for normal pressure (kPa) by anatomical location, subject, and condition. A zero value for the distal contact interface implies that the distal tibia did not contact the base of the prosthetic socket (i.e. piston displacement < 1.5 cm). Data are mean ± SD.

Subject (condition)	Anterior Proximal	Anterior Distal	Posterior Proximal	Posterior Distal	Medial Proximal	Medial Distal	Lateral Proximal	Lateral Distal	Distal
1 (low)	259 ± 30.6	132 ± 6.52	41.5 ± 24.9	20.6 ± 4.86	72.9 ± 29.9	47.4 ± 1.61	84.1 ± 2.25	68.6 ± 3.28	0.08 ± 0.06
1 (medium)	238 ± 41.9	123 ± 12.0	53.4 ± 19.4	22.2 ± 4.23	78.1 ± 44.4	43.8 ± 7.41	128 ± 17.6	73.7 ± 4.35	4.91 ± 5.34
1 (high)	292 ± 14.2	141 ± 6.99	39.2 ± 15.2	20.9 ± 2.74	58.3 ± 15.9	40.0 ± 2.19	99.7 ± 10.4	73.3 ± 4.95	4.91 ± 5.34
2 (low)	199 ± 19.2	118 ± 13.9	34.5 ± 6.84	24.5 ± 0.95	56.0 ± 11.3	40.5 ± 2.72	275 ± 32.4	128 ± 11.9	89.5 ± 33.8
2 (medium)	358 ± 44.3	138 ± 12.3	29.9 ± 17.9	25.0 ± 1.03	49.9 ± 11.2	41.0 ± 3.13	283 ± 52.4	132 ± 23.3	145 ± 39.7
2 (high)	320 ± 21.4	196 ± 49.4	27.5 ± 3.37	36.6 ± 11.7	53.4 ± 15.7	71.7 ± 26.4	182 ± 31.8	131 ± 38.4	233 ± 104
3 (low)	131 ± 14.5	81.8 ± 4.62	80.1 ± 5.52	42.5 ± 3.11	76.5 ± 4.08	43.7 ± 3.01	111 ± 16.6	74.5 ± 7.04	0.00 ± 0.00
3 (medium)	151 ± 7.19	87.5 ± 2.46	57.7 ± 8.35	32.4 ± 3.90	69.4 ± 12.5	43.1 ± 5.46	90.1 ± 13.1	55.4 ± 3.07	0.00 ± 0.00
3 (high)	160 ± 3.20	87.7 ± 3.86	88.2 ± 51.4	45.7 ± 26.0	87.0 ± 13.3	54.1 ± 7.38	103 ± 23.6	75.7 ± 25.1	0.00 ± 0.00
4 (low)	188 ± 12.5	37.2 ± 5.50	17.1 ± 0.72	15.7 ± 0.72	38.1 ± 2.53	32.4 ± 2.02	138 ± 6.97	71.8 ± 2.53	0.00 ± 0.00
4 (medium)	256 ± 25.0	122 ± 9.51	26.1 ± 6.90	16.4 ± 0.57	43.3 ± 3.56	37.5 ± 0.39	145 ± 5.49	75.2 ± 1.53	0.00 ± 0.00
4 (high)	271 ± 0.24	128 ± 0.92	42.3 ± 2.83	17.8 ± 0.78	35.9 ± 4.11	30.3 ± 2.20	139 ± 7.78	73.6 ± 3.19	0.00 ± 0.00
Group (low)	194 ± 19.2	107 ± 7.65	43.3 ± 9.50	25.8 ± 2.41	60.7 ± 12.0	41.0 ± 2.34	152 ± 14.5	85.8 ± 6.19	22.4 ± 8.46
Group (medium)	251 ± 29.6	118 ± 9.05	41.8 ± 13.1	24.0 ± 2.44	60.2 ± 17.9	41.3 ± 4.10	162 ± 22.2	84.0 ± 8.05	36.9 ± 10.0
Group (high)	261 ± 9.77	138 ± 15.3	49.3 ± 18.2	30.3 ± 10.3	58.6 ± 12.3	49.0 ± 9.55	131 ± 18.4	88.5 ± 17.9	59.5 ± 27.4

Table 5.5: Average peak values for shear stress (kPa) by anatomical location, subject, and condition. A zero value for the distal contact interface implies that the distal tibia did not contact the base of the prosthetic socket (i.e. piston displacement < 1.5 cm). Data are mean ± SD.

Subject (condition)	Anterior Proximal	Anterior Distal	Posterior Proximal	Posterior Distal	Medial Proximal	Medial Distal	Lateral Proximal	Lateral Distal	Distal
1 (low)	90.5 ± 10.7	46.3 ± 2.33	15.4 ± 8.13	8.08 ± 2.10	26.9 ± 9.58	16.7 ± 0.76	29.7 ± 1.01	24.7 ± 1.14	0.03 ± 0.02
1 (medium)	83.1 ± 14.7	43.3 ± 4.17	19.0 ± 6.27	8.61 ± 1.78	27.9 ± 15.1	16.5 ± 3.47	44.7 ± 6.25	25.8 ± 1.61	0.98 ± 0.23
1 (high)	102 ± 4.98	49.5 ± 2.44	13.7 ± 5.35	7.51 ± 0.96	20.8 ± 5.05	14.1 ± 0.82	35.4 ± 3.97	26.1 ± 1.74	1.90 ± 1.99
2 (low)	69.9 ± 6.71	41.3 ± 4.89	12.1 ± 2.34	8.62 ± 0.35	19.6 ± 3.95	14.4 ± 1.23	96.5 ± 11.4	45.0 ± 4.32	35.8 ± 12.9
2 (medium)	127 ± 18.1	48.2 ± 4.30	10.5 ± 6.25	8.89 ± 0.23	17.5 ± 3.92	14.3 ± 1.10	99.3 ± 18.5	46.5 ± 8.35	51.7 ± 13.1
2 (high)	120 ± 10.2	68.9 ± 17.5	10.2 ± 1.90	12.9 ±4.18	19.4 ± 5.94	25.7 ± 9.65	64.7 ± 11.5	46.7 ± 13.9	81.9 ± 36.4
3 (low)	45.8 ± 5.10	28.6 ± 1.63	28.3 ± 1.97	15.4 ± 1.10	26.8 ± 1.43	15.3 ± 1.06	40.1 ± 5.32	27.3 ± 2.38	0.00 ± 0.00
3 (medium)	52.8 ± 2.51	30.6 ± 0.87	20.4 ± 2.91	11.6 ± 1.42	24.7 ± 4.76	15.5 ± 2.17	31.5 ± 4.58	19.5 ± 1.01	0.00 ± 0.00
3 (high)	55.9 ± 1.13	30.7 ± 1.34	31.0 ± 18.0	16.3 ± 8.99	30.4 ± 4.66	19.0 ± 2.69	36.3 ± 8.41	26.8 ± 8.95	0.00 ± 0.00
4 (low)	65.7 ± 4.37	34.0 ± 1.93	6.01 ± 0.27	5.54 ± 0.31	13.8 ± 0.69	12.2 ± 1.21	48.3 ± 2.43	25.1 ± 0.85	0.00 ± 0.00
4 (medium)	89.8 ± 8.74	42.8 ± 3.33	9.11 ± 2.42	5.73 ± 0.19	15.3 ± 1.37	13.5 ± 0.38	50.9 ± 1.93	16.3 ± 0.54	0.00 ± 0.00
4 (high)	95.0 ± 0.08	44.9 ± 0.32	15.9 ± 0.08	6.71 ± 0.73	13.7 ± 2.53	11.0 ± 0.37	48.5 ± 2.71	25.8 ± 1.16	0.00 ± 0.00
Group (low)	68.0 ± 6.72	37.6 ± 2.70	15.4 ± 3.18	9.41 ± 0.97	21.8 ± 3.91	14.7 ± 1.06	53.7 ± 5.03	30.5 ± 2.17	8.95 ± 3.23
Group (medium)	88.2 ± 11.0	41.2 ± 3.17	14.7 ± 4.46	8.70 ± 0.91	21.4 ± 6.28	14.9 ± 1.78	56.6 ± 7.82	29.5 ± 2.88	13.2 ± 3.33
Group (high)	93.3 ± 4.09	48.5 ± 5.40	17.7 ± 6.33	10.9 ± 3.72	21.1 ± 4.54	17.5 ± 3.38	46.2 ± 6.59	31.3 ± 6.43	21.0 ± 9.58

Discussion

Model Performance (Group Data)

The objective of this study was to develop a spatial contact model of the residual limb-prosthetic socket interface and evaluate its ability to estimate limb-socket interface dynamics. A secondary objective of this study was to use this model to examine the relationships between prosthetic foot stiffness and limb-socket dynamics. Model-derived values for normal pressure depict spatiotemporal patterns similar to those of a ground reaction force (GRF) curve during stance phase. The pressure and shear waveforms presented by Sanders et al. (1992) and Laszczak et al. (2016) are similar to those of the present study early in stance phase, but exhibit a brief plateau during mid-stance before values decrease. Comparatively, the present study shows similar loading rates, but a gradual decline in pressure and stress rather than a mid-stance phase plateau (i.e. the waveforms are skewed toward early stance phase) (Figure 5.2). The lack of a plateau in pressure and shear data in the present results may be due to improper constraining of residual limb motion. Using experimental kinematic data to constrain residual limb motion may help refine the trajectory of the modeled response. Alternatively, a velocity constraint could be implemented into the present model design.

Peak values for normal pressure were similar to those reported in previous sensor-based experiments (Courtney et al., 2016; Laszczak et al., 2016; Sanders et al., 2000, 1992) and finite element modeling-based analyses (Jia et al., 2004; Lee et al., 2004; Portnoy et al., 2009), which ranged from 40-160 kPa. Similarly, values for shear stress were within the 3-50 kPa range reported previously (Laszczak et al., 2016; Noll et al., 2017; Sanders and Daly, 1993; Schiff et al., 2014).

The ability of the model to predict pressure and shear stress values specific to different anatomical locations is difficult to discern based on previous experiments. Previous sensor-based experiments have typically sampled from small localized areas on the limb or present only resultant data. Nevertheless, broad comparisons can be made with data from Sanders et al. (1992), Sanders et al. (2000), and Courtney et al. (2016). Results of this study showed peak mean pressure and stress values on the medial side of approximately 60 and 21 kPa (values are the mean of the proximal and distal interfaces under all stiffness conditions). Data from Courtney et al. (2016) showed peak medial pressure to be approximately 65-70 kPa, whereas Sanders et al. (2000) present values ranging from 40-85 kPa for pressure and 7-12 kPa for shear stress. On the lateral side, results of this study showed peak mean pressure and shear stress values of approximately 117 and 41 kPa. Comparatively, Sanders et al. (2000) present values of 60-140 kPa for pressure and 18-23 kPa for shear stress. Posteriorly, the pressure and shear values of 41 and 13 kPa were lower compared to those presented by Sanders et al. (85-100 and 17-22 kPa). This discrepancy may be due to the increased stiffness of the tissue on the posterior residual limb associated with muscle contraction during gait, which is unaccounted for in this model. Muscular contraction has been shown to increase tissue modulus by 45 kPa (Zheng et al., 1999). Muscular contraction would likely have minimal effects on the frictional characteristics of the tissue. In the future, a progressive model of tissue moduli could be implemented into limb-socket contact model. The model's predicted anterior pressure and shear stress were 235 and 83 kPa, which were similar to values of 245 and 105 derived from FEA of socket interface dynamics at the patellar tendon (Lee et al.,

2004). There is a paucity of data from sensor-based experiments related to pressure or shear dynamics along the tibial plateau.

The model predicted peak residual limb displacements between 1.2 and 2.1 cm with respect to the socket. These values are within the range of 1.1-3.6 cm (mean: 2.3 ± 1.0 cm) previously reported in the literature (Gholizadeh et al., 2011; Grevsten and Erikson, 1975; LaPrè et al., 2018; Narita et al., 1997; Sanders et al., 2006; Söderberg et al., 2003; Wirta et al., 1990). It should be noted that the prosthetic socket components (e.g. liner and socket materials) and gait tasks varied between these studies. Data from the present study, among others support the idea that the amount of residual limb pistoning may be affected by liner and socket type (Sanders et al., 2000; Yiğiter et al., 2002), residual limb shape (Wirta et al., 1990), and gait conditions (Gholizadeh et al., 2011; Sanders et al., 2000). Data regarding the prosthetic socket componentry used by participants in this study were not available.

The pressure distribution profiles derived from this model were weighted toward the anterior and lateral aspects of the residual limb. These patterns may be due in part to gait kinematics of the participants. However, this may also be a result of the modulus values used to parameterize the contact interfaces. These values were 3.5 times higher for the anterior aspect of the tibia compared to posterior, and 1.4 times higher for the lateral compared to medial aspects. Increasing the number of contact points in the model may lead to a higher resolution representation of the material properties of the residual limb as they vary by anatomical location. However, this would likely increase computation time.

Computation Time

Computation time is an important consideration in simulation-based analytical approaches. Compared to previous simulations using this gait model, the addition of the residual limb-socket spatial contact model resulted in 34.5%, 28.9%, and 25.5% increases in execution times for the low, medium, and high stiffness conditions, respectively. These values correspond to increases of 20.2, 17.1, and 58.6 s. Increased execution times may be attributed increased model complexity, but also potentially to a suboptimal ratio of stiffness:damping within the limb-socket contact model. These conditions can result in small oscillations within the model's force signals, causing the solver to reduce the step sizes used for numerical integration. Optimization of the stiffness:damping ratio may improve execution times.

Case Study (Subject 1)

This study represents the first systematic evaluation of the effects of prosthetic foot stiffness on residual limb-prosthetic socket interface dynamics. Across the stiffness conditions, outcome measures for Subject 1 showed similar spatiotemporal patterns between 0-50% stance phase (Figure 5.4), which encompass progression from heel strike to foot flat (Winter, 1991). Divergent responses were observed across the stiffness conditions in the latter half of stance phase for residual limb axial angle and anterior-posterior pressure and shear stress distribution. Increased variability was also observed for all conditions during this time. The latter half of stance phase may be characterized by the progression from foot flat to toe off and involves an anterior shift in the center of pressure (CoP) (Winter, 1991). Since the stiffness behavior of the VSF's heel is

unchanged across the conditions, it is logical that the effects of variable forefoot stiffness would be primarily observed in the latter half of stance phase.

The subject presented no discernable effect of variable stiffness on peak average normal pressure, shear stress, or piston motion (Figure 5.4). Decreased external rotation was observed in the low stiffness condition, although high variability was present in the high stiffness condition. Increased external rotation may direct knee loading out of the sagittal plane and into the frontal plane, thereby compromising the ability of the knee to absorb forces and causing overloading of cartilage (Gailey et al., 2008). Increased external rotation has been also associated with high rates of medial knee osteoarthritis (Weidow et al., 2006). Elevated rates of knee osteoarthritis have been documented for both the amputated and contralateral limb for lower limb prosthesis users (Gailey et al., 2008).

There were no discernable effects of prosthesis stiffness on frontal or coronal plane pressure or shear stress distribution. This response is consistent with the mechanical principles of the VSF, which modulates forefoot stiffness primarily in the sagittal plane. From 0-50% stance phase, the subject exhibited a more anteriorly-directed distribution, which transitioned to a relatively even anterior-posterior distribution in the latter half of stance phase for the low and high stiffness conditions. In the medium stiffness condition, pressure and shear stress were more posteriorly-directed. High variability was observed across the three trials per condition, and therefore more data are necessary to discern the consistency of these patterns.

Limitations and Future Directions

The present model was parameterized using previously reported residual limb tissue mechanical properties and limb-socket kinematics for individuals with BKA. While these methods resulted in pressure and shear stress values within the range reported in the literature, the variability in the aforementioned parameters is well documented between individual subjects. Future work should strive toward individualized models by characterizing the tissue mechanical properties of subjects. Similarly, adjusting parameters based on the socket componentry used by subjects would improve the accuracy of the model. For example, coefficients of friction between 0.5-3.0 have been reported for the interaction between human skin and various socket liner materials (Cagle et al., 2018; Sanders et al., 1998). Variation within this range would have a substantial impact on model-derived shear force estimates.

Future work should also seek to quantify kinematics between the residual limb and prosthetic socket through optical motion capture or instrumenting participants with potentiometers. Using these data to constrain residual limb motion during simulations would improve accuracy on an individualized basis. Further, these data could be used to refine the ability of the current model to predict limb-socket kinematics.

The present model assumes oversimplified geometries of the residual limb and prosthetic socket. Developing more complex interface geometry could improve the fidelity of the model. For example, using a pentagonal prism shape to model the residual limb geometry would allow for differentiation of the varying moduli of the anterior, anterior lateral, anterior medial, posterior lateral, and posterior medial aspects of the residual limb and would only add two interface frames compared to the present model.

This study modeled the residual limb as composite of both the bone and soft tissue elements. However, data from x-ray (Lilja et al., 1993) and biplane fluoroscopy (Bocobo et al., 1998) studies suggest that residual limb kinematics can be differentiated into the motion of the bone and soft tissue elements. As such, it may be important to distinguish these elements and model the interface between them in future studies. Doing so could lead to improvements when simulating limb-socket dynamics.

Conclusions

Data from this study support the use of reduced order modeling techniques to estimate residual limb-prosthetic socket interfacial pressure and shear stress, as well as residual limb kinematics in a computationally economical manner. Limitations include parameterization of the contact models based on data previously reported in the literature, rather than data measured from subjects in this study. Nevertheless, residual limb-prosthetic socket interface dynamics derived from this model were within the range of values reported by previous sensor-based gait experiments. These methods may be useful to aid experimental studies by providing insights into the effects of varied prosthesis design parameters or gait conditions on residual limb-socket interface dynamics.

Data from a case study show promise for evaluating the effects of prosthesis stiffness on limb-socket dynamics. Variable prosthesis stiffness did not appear to affect residual limb pistoning, nor peak normal pressure or shear stress. The low stiffness condition resulted in decreased external rotation compared to the medium and high stiffness conditions. However, data displayed high variability and further investigation is necessary to discern the repeatability of this effect. Future work could add complexity to

the modeled interface geometry in order to better match the shape and variation in tissue material properties of the residual limb. Additionally, the model's accuracy could be improved by applying subject-specific data for residual limb tissue properties and prosthetic socket componentry when parameterizing the contact interfaces.

Acronyms widely used in text

AP	Anterior-Posterior
BKA	Below-Knee Amputation
DoF	Degrees of Freedom
LLA	Lower Limb Amputation
ML	Medial-Lateral
Ode23t	Ordinary Differential Equation 23 trapezoidal solver
PD	Proximal-Distal
SD	Standard Deviation
VSF	Variable Stiffness Foot

Abbreviations

F	Force, N
k	Linear stiffness, N/mm
μ	Coefficient of friction
v	Linear velocity
δ	Penetration depth, mm
$\dot{\delta}$	Penetration velocity, mm/s

Superscripts and subscripts

F_f	Frictional force, N
F_n	Normal force, N
v_{poc}	Linear velocity at point of contact, mm/s
$v_{\text{threshold}}$	Linear velocity threshold, m/s
μ_{kinetic}	Coefficient of kinetic friction
μ_{static}	Coefficient of static friction

CHAPTER VI

CONCLUSION

Summary of Results and Findings

This dissertation set out to elucidate the relationships between anatomical morphologies associated with below-knee amputation (BKA), gait mechanics, and prosthesis design through computational modeling and simulations. This work was motivated by the immense potential of simulations to explore these relationships and optimize prosthesis design on a user-specific basis. Yet, there was a lack of a readily-available gait model, which incorporated the anatomical morphologies associated with BKA, energy storage and return properties of a passive prosthetic foot, and interface dynamics of the residual limb-prosthetic socket interface. In pursuit of this goal, a computational model of a semi-active variable-stiffness foot (VSF) prosthesis was developed, along with a model of VSF-ground contact dynamics (Chapter III). Parameterizing the VSF-ground contact model in order to accurately predict ground reaction forces (GRF) presented a complex parameterization problem, and so an algorithm for programmatically deriving and optimizing these parameters was developed. In Chapter IV, a computational gait model with a unilateral BKA was developed and the VSF model from Chapter III was integrated. Chapter V summarized the development of a spatial contact model of the residual limb-prosthetic socket interface motivated by the biophysical properties of the residual limb and mechanical properties of the prosthetic socket. This model was integrated with the models developed in Chapters III and IV, and gait simulations were computed to evaluate the limb-socket contact model's ability to

predict normal pressure, shear stress, and residual limb-socket kinematics occurring during gait. The effects of variable prosthesis stiffness on these outcomes were also evaluated.

Chapter III resulted in a reduced order computational model of a semi-active VSF prosthesis, a model of VSF-ground contact, and an algorithm for programmatically deriving and optimizing the ground contact model parameters. Results of controlled static compression tests showed agreement between simulated and experimental data across a three-fold range of stiffness settings. Under dynamic gait conditions where there is increased variation in the load distribution and rate of loading, the model exhibited greater error compared to static compression tests, but similar predictive capacity compared to previous work in this area. These findings support the use of the methods outlined in Chapter III for modeling the energy storage and return dynamics of a VSF. The reduced order nature of this model makes it computationally economical and thus ideally suited to be integrated with a gait model. The models developed may be useful for simulating gait with a VSF and identifying important prosthesis design parameters (e.g. stiffness) for optimizing gait.

Chapter IV resulted in the development and validation of a computational gait model that incorporated the anatomical morphologies associated with BKA. The VSF and ground contact models developed in Chapter III were integrated into the gait model. This chapter expanded upon Chapter III in two key areas: The ground contact model and algorithm for programmatically deriving contact parameters were assessed for three additional subjects, thereby providing insight into the generalizability of the methods presented in Chapter III. Further, the VSF model was integrated into a scalable 28-

degree-of-freedom gait model capable of computing forward kinematics or forward dynamics simulations. The results of forward kinematics simulations showed strong correlations for lower limb joint kinematics, resultant GRF, resultant GRF impulse, and anterior-posterior center of pressure across all subjects and stiffness conditions. These results suggest that the methods and models developed in this chapter may be viable for simulating human locomotion with a semi-active VSF. These methods are useful for elucidating the relationships between anatomical morphologies associated with BKA, gait mechanics, and prosthesis design.

Chapter V detailed the design and development of a reduced order spatial contact model of the residual limb-prosthetic socket interface. Parameters for this model were motivated by the biophysical properties of the two structures. Gait simulations using this model provided insights into model performance and how variable prosthesis stiffness affects dynamics at the limb-socket interface. Model-predicted values for normal pressure, shear stress, and residual limb kinematics were similar to values reported by previous sensor-based experiments and finite element analyses. Simulations also demonstrated that the effects of variable prosthesis stiffness on these outcomes were subject-dependent, highlighting the need for quantitative methods to aid in the prosthesis design and prescription processes. Results of a case study provided some insight regarding how variable prosthesis stiffness affects limb-socket interface dynamics on a user-specific basis. However, high variability in the outcome measures indicated that more data are necessary to discern the repeatability of these trends.

In summation, the models, methods, and results presented in this dissertation provide a powerful framework for evaluating the effects of varied prosthesis design

parameters on user-specific gait mechanics. The level of accuracy achieved by the VSF and ground contact models were similar to those of previous modeling work developed for individuals with intact limbs. The residual limb-socket spatial contact model predicted normal pressure, shear stress, and limb-socket kinematics similar to those reported by previous sensor-based experiments and finite element analyses. The reduced order nature of this model design makes it ideal to integrate within a computational gait model for analyzing limb-socket dynamics during gait. These cumulative methods could be used to add quantitative elements to the prosthesis design and prescription processes, thereby helping to account for the well-documented diversity of gait mechanics, anatomical morphologies, and mobility capacity among individuals with BKA. Further, these methods could be deployed within an optimal control framework with the goal of optimizing gait through user-specific prosthesis design and prescription.

Limitations

The model-predicted outcomes presented in this dissertation agreed well with experimental data. Nevertheless, limitations exist. An inherent limitation of the lumped parameter approach to modeling the VSF's keel is constraining keel motion in the sagittal plane. While this design is computationally efficient compared to more robust finite element models, it fails to account for small torsional keel motions that would be possible under ecological gait conditions with the physical VSF. Future work could develop a lumped parameter model that allows for torsional keel motion in the frontal plane. Accounting for these motions would improve model-based predictions of frontal plane gait mechanics, which are often amplified among individuals with BKA compared to

those without. Additionally, the hysteresis response of the VSF model was not evaluated as part of model validation, as those data were not available for the physical VSF. It is possible that there is a discrepancy between the hysteresis response of the model and physical VSF, which would alter energy storage and return during gait.

The primary limitation for the gait model is the assumption of accurate estimates for segment lengths, joint centers, and joint angles, which were derived from marker-based motion capture data. Each of these metrics likely suffers from small errors due to marker placement, localization, and coordinate system design. Such errors would contribute to decrements in model accuracy. The limb segments and joints were also modeled as rigid, which may not be completely accurate to represent the biological limb. This discrepancy would manifest as small differences in kinematics and energy transfer between segments. Nevertheless, simulated motions were consistent with experimental data of subjects walking with the VSF and other previously reported data of spatiotemporal gait patterns among persons with lower limb loss.

The spatial contact model of the residual limb-prosthetic socket interface was parameterized with data previously reported in the literature. However, high variability has been documented for limb-socket dynamics based on anatomical morphologies, prosthetic socket componentry, and gait conditions. Data for residual limb anatomical morphologies (e.g. tissue composition and mechanical properties) or prosthetic socket componentry (e.g. socket design, suspension system, and liner material) were not available for subjects in this study; therefore differences in limb-socket dynamics due to variations in these parameters were not accounted for. Further, the inability to constrain limb-socket kinematics with data measured during each gait trial likely further

contributed to a more generalized, rather than subject-specific, characterization of limb-socket dynamics.

Lastly, the cuboid and hollow square cone shapes used to model geometry of the residual limb and prosthetic socket were oversimplified compared to their physical equivalents. Using discrete shapes to represent the continuous geometry of these structures likely induces inaccuracies for kinetic and kinematic predictions. Similarly, simplification of interface between these structures (i.e. nine points of contact) offers a relatively low resolution description of the overall contact dynamics occurring throughout the continuous *in situ* contact surface.

Each of the aforementioned assumptions and limitations should be considered when interpreting data derived using these models and/or methods. The level of biomechanical fidelity achieved may be sufficient for some simulation scenarios where large differences are observed between conditions, but insufficient in others where differences are more nuanced. It is recommended to use caution when using these models to evaluate sensitive simulation scenarios.

Recommendations for Future Work

This dissertation provides a foundation from which to build more complex and biologically motivated models of human gait with assistive devices. In the future, the VSF model could be improved by incorporating frontal plane torsional deformations of the elastic keel, which would improve accuracy of the modeled gait dynamics in the frontal plane. Additionally, characterizing the hysteresis response of the physical VSF

and using those data to improve the model's energy storage and return response would lead to improved prediction of gait kinetics.

Future work could explore methods for refining the VSF-ground contact model. For example, a deformable contact model such as the one presented by Jackson, Hass, and Fregly (2016) may be a viable means of representing foam deformation throughout stance phase. Reducing errors in contact-model derived predictions of VSF-ground contact dynamics could also be achieved through improved optimization methods. Future optimization algorithms could co-optimize multiple objective functions (e.g. GRF, GRF impulse, and center of pressure) and/or optimize the objective functions over multiple gait conditions, thereby improving the generalizability of the model.

The gait model relies on accuracy of optical motion capture to simulate model kinematics. Accuracy of the current kinematic pose estimation methods could be improved through an inverse kinematics approach and accompanying algorithms for residual reduction. These methods would integrate more marker data and yield improved model pose estimation at a given time step. These methods could also supplant the current offline method of deriving joint kinematics (Cardan-Euler sequences).

The gait model disregards kinematics of the head, arms, and trunk, since marker data for those segments were not available. Integrating motion of these segments into future simulations may improve the model's ability to capture whole-body dynamics. Incorporating kinematics of the trunk during gait may also improve model-derived COP_{AP} predictions. Incorporating motion of these segments may be especially relevant for representing mechanical asymmetries present in gait of individuals with LLA.

The aforementioned recommendations for future work were based largely on the limitations of this dissertation. However, there is also immense potential to build upon the current body of work and improve the model's capacity to simulate gait with assistive devices. One key addition to the gait model will be incorporating biologically-inspired muscle models, such as Hill (Hill, 1938) or Thelen (Thelen, 2003), to actuate joints for forward dynamics simulations. This should include algorithms for translating experimentally-measured EMG data into estimates of muscle forces, and ultimately joint kinetic and kinematic profiles. Incorporating muscle models will serve two key functions. Muscle models are key to computing fully predictive simulations without the need for experimental data as inputs. Further, muscle models will improve the biological relevance of simulation-derived data and provide the foundation for other useful metrics such as metabolic cost of transport, tissue loading, and neuromuscular coordination.

There is also opportunity to define more complex and realistic joint models, which would improve estimates of joint loading. For example, the knee joint could be differentiated into bone, cartilage, and meniscal components, which would be useful for interpreting the effects of various gait scenarios on short term joint loading and long term joint health. Further, finite element models of joints and other structures could be incorporated in series with the gait model via MATLAB's finite element modeling and analysis tools, which would allow even more robust characterization of joint dynamics.

One of the design goals of the physical VSF is to optimize forefoot stiffness to meet a variety of gait conditions. For example, the VSF provides greater push-off power during gait when configured to low stiffness (Glanzer and Adamczyk, 2018), which could assist individuals with LLA when walking at higher speeds. Similarly, a more compliant

forefoot may aid in ramp ascents, while a less compliant forefoot may provide improved stability when descending ramps. Simulations could be used to optimize the stiffness response to these conditions on a user-specific basis. In the future, the model should be validated under gait conditions such as variable speed, ramp ascents/descents, and stair ascents/descents.

Lastly, previous work in gait simulations with biomechatronic assistive devices has often relied on abstract representations of components such as motors, electronics, and control systems. In contrast, Simscape Multibody and Simulink offer a large library of these components, which can be readily integrated into the model for more realistic representations of biomechatronic systems. Further, control system parameters derived from simulations can be readily deployed to prototype devices. As such, this model may be advantageous for future simulations of gait with biomechatronic devices such as powered prostheses, orthoses, or exoskeletons.

REFERENCES CITED

Al-Fakih, E.A., Abu Osman, N.A., Mahmad Adikan, F.R., 2016. Techniques for interface stress measurements within prosthetic sockets of transtibial amputees: A review of the past 50 years of research. Sensors (Switzerland). https://doi.org/10.3390/s16071119

Al-Fakih, E.A., Osman, N.A.A., Eshraghi, A., Adikan, F.R.M., 2013. The capability of fiber Bragg grating sensors to measure amputees' trans-tibial stump/socket interface pressures. Sensors (Switzerland) 13, 10348–10357. https://doi.org/10.3390/s130810348

Ali, S., Abu Osman, N.A., Eshraghi, A., Gholizadeh, H., Abd Razak, N.A. Bin, Wan Abas, W.A.B. Bin, 2013. Interface pressure in transtibial socket during ascent and descent on stairs and its effect on patient satisfaction. Clin. Biomech. 28, 994–999. https://doi.org/10.1016/j.clinbiomech.2013.09.004

Balk, E.M., Gazula, A., Markozannes, G., Kimmel, H.J., Saldanha, I.J., Resnik, L.J., Trikalinos, T.A., 2018. Lower Limb Prostheses: Measurement Instruments, Comparison of Component Effects by Subgroups, and Long-Term Outcomes. https://doi.org/10.23970/AHRQEPCCER213

Bocobo, C., Castellote, J., MacKinnon, D., Gabrielle-Bergman, A., 1998. Videofluoroscopic evaluation of prosthetic fit and residual limbs following transtibial amputation. J. Rehabil. Res. Dev. 35, 6–13.

Boutwell, E., Stine, R., Hansen, A., Tucker, K., Gard, S., 2012. Effect of prosthetic gel liner thickness on gait biomechanics and pressure distribution within the transtibial socket. J. Rehabil. Res. Dev. 49, 227–240. https://doi.org/10.1682/JRRD.2010.06.0121

Brown, P., McPhee, J., 2018. A 3D ellipsoidal volumetric foot–ground contact model for forward dynamics. Multibody Syst. Dyn. 42, 447–467. https://doi.org/10.1007/s11044-017-9605-4

Cagle, J.C., Hafner, B.J., Taflin, N., Sanders, J.E., 2018. Characterization of prosthetic liner products for people with transtibial amputation. J. Prosthetics Orthot. 30, 187–199. https://doi.org/10.1097/JPO.0000000000000205

Casillas, J.M., Dulieu, V., Cohen, M., Marcer, I., Didier, J.P., 1995. Bioenergetic comparison of a new energy-storing foot and SACH foot in traumatic below-knee vascular amputations. Arch. Phys. Med. Rehabil. 76, 39–44.

Courtney, A., Orendurff, M.S., Buis, A., 2016. Effect of alignment perturbations in a trans-tibial prosthesis user: A pilot study. J. Rehabil. Med. 48, 396–401. https://doi.org/10.2340/16501977-2075

Darter, B.J., Sinitski, K., Wilken, J.M., 2016. Axial bone-socket displacement for persons with a traumatic transtibial amputation: The effect of elevated vacuum suspension at progressive body-weight loads. Prosthet. Orthot. Int. 40, 552–557. https://doi.org/10.1177/0309364615605372

De Leva, P., 1996. Adjustments to zatsiorsky-seluyanov's segment inertia parameters. J. Biomech. 29, 1223–1230. https://doi.org/10.1016/0021-9290(95)00178-6

Dembia, C.L., Silder, A., Uchida, T.K., Hicks, J.L., Delp, S.L., 2017. Simulating ideal assistive devices to reduce the metabolic cost of walking with heavy loads. PLoS One 12. https://doi.org/10.1371/journal.pone.0180320

Eshraghi, A., Osman, N.A.A., Gholizadeh, H., Karimi, M., Ali, S., 2012. Pistoning assessment in lower limb prosthetic sockets. Prosthet. Orthot. Int. 36, 15–24. https://doi.org/10.1177/0309364611431625

Farris, D.J., Sawicki, G.S., 2012. The mechanics and energetics of human walking and running: a joint level perspective. J. R. Soc. Interface 9, 110–18. https://doi.org/10.1098/rsif.2011.0182

Fey, N.P., Klute, G.K., Neptune, R.R., 2013. Altering prosthetic foot stiffness influences foot and muscle function during below-knee amputee walking: A modeling and simulation analysis. J. Biomech. 46, 637–644. https://doi.org/10.1016/j.jbiomech.2012.11.051

Fey, N.P., Klute, G.K., Neptune, R.R., 2012. Optimization of Prosthetic Foot Stiffness to Reduce Metabolic Cost and Intact Knee Loading During Below-Knee Amputee Walking: A Theoretical Study. J. Biomech. Eng. 134, 111005-1–10. https://doi.org/10.1115/1.4007824

Fey, N.P., Klute, G.K., Neptune, R.R., 2011. The influence of energy storage and return foot stiffness on walking mechanics and muscle activity in below-knee amputees. Clin. Biomech. 26, 1025–1032. https://doi.org/10.1016/j.clinbiomech.2011.06.007

Gailey, R., Allen, K., Castles, J., Kucharik, J., Roeder, M., 2008. Review of secondary physical conditions associated with lower-limb amputation and long-term prosthesis use. JRRD 45, 15–30. https://doi.org/10.1682/JRRD.2006.11.0147

Gholizadeh, H., Azuan, N., Osman, A., Eshraghi, A., Anuar, N., Razak, A., 2014. Clinical implication of interface pressure for a new prosthetic suspension system. Biomed. Eng. Online 13. https://doi.org/10.1186/1475-925X-13-89

Gholizadeh, H., Osman, N.A.A., Lúvíksdóttir, Á.G., Eshraghi, A., Kamyab, M., Wan Abas, W.A.B., 2011. A new approach for the pistoning measurement in transtibial prosthesis. Prosthet. Orthot. Int. 35, 360–364. https://doi.org/10.1177/0309364611423130

Glanzer, E.M., Adamczyk, P.G., 2018. Design and Validation of a Semi-Active Variable Stiffness Foot Prosthesis. IEEE Trans. Neural Syst. Rehabil. Eng. 26, 2351–2359. https://doi.org/10.1109/TNSRE.2018.2877962

Grevsten, S., Erikson, U., 1975. A roentgenological study of the stump-socket contact and skeletal displacement in the PTB-suction prosthesis. Ups. J. Med. Sci. 80, 49–57. https://doi.org/10.3109/03009737509178991

Grood, E.S., Suntay, W.J., 1983. A joint coordinate system for the clinical description of three-dimensional motions: application to the knee. J. Biomech. Eng. 105, 136–44. https://doi.org/10.1115/1.3138397

Henrikson, K.M., Weathersby, E.J., Larsen, B.G., Cagle, J.C., McLean, J.B., Sanders, J.E., 2018. An inductive sensing system to measure in-socket residual limb displacements for people using lower-limb prostheses. Sensors 18. https://doi.org/10.3390/s18113840

Highsmith, J.T., Highsmith, M.J., 2007. Common skin pathology in LE prosthesis users. J. Am. Acad. Physician Assist. 20, 33–36. https://doi.org/10.1097/01720610-200711000-00018

Highsmith, M.J., Kahle, J.T., Klenow, T.D., Andrews, C.R., Lewis, K.L., Bradley, R.C., Ward, J.M., Orriola, J.J., Highsmith, J.T., 2016. Interventions to manage residual limb ulceration due to prosthetic use in individuals with lower extremity amputaiton: A systematic review of the literature 18, 115–123. https://doi.org/10.21300/18.2-3.2016.115

Hill, A., 1938. The heat of shortening and the dynamic constants of muscle. Proc. R. Soc. London. Ser. B - Biol. Sci. 126, 136–195. https://doi.org/10.1098/rspb.1938.0050

Hofstad, C.J., van der Linde, H., van Limbeek, J., Postema, K., 2004. Prescription of prosthetic ankle-foot mechanisms after lower limb amputation. Cochrane Database Syst. Rev. https://doi.org/10.1002/14651858.cd003978.pub2

Jackson, J.N., Hass, C.J., Fregly, B.J., 2016. Development of a Subject-Specific Foot-Ground Contact Model for Walking. J. Biomech. Eng. 138, 091002-1–12. https://doi.org/10.1115/1.4034060

Jia, X., Zhang, M., Lee, W.C.C., 2004. Load transfer mechanics between trans-tibial prosthetic socket and residual limb - Dynamic effects. J. Biomech. 37, 1371–77. https://doi.org/10.1016/j.jbiomech.2003.12.024

Jin, L., Roland, M., Hahn, M.E., Adamczyk, P.G., 2016. The Effect of High-and Low-Damping Prosthetic Foot Structures on Knee Loading in the Uninvolved Limb Across Different Walking Speeds. J. Appl. Biomech. 32, 233–240. https://doi.org/10.1123/jab.2015-0143

Johansson, R., Magnusson, M., Akesson, M., 1988. Identification of human postural dynamics. IEEE Trans. Biomed. Eng. 35, 858–869. https://doi.org/10.1109/10.7293

Khamar, M., Edrisi, M., Zahiri, M., 2019. Human-exoskeleton control simulation, kinetic and kinematic modeling and parameters extraction. MethodsX 6, 1838–1846. https://doi.org/10.1016/j.mex.2019.08.014

Kikuchi, R., Misaka, T., Obayashi, S., 2016. International journal of computational fluid dynamics real-time prediction of unsteady flow based on POD reduced-order model and particle filter. Int. J. Comut. Fluid Dyn. 30, 285–306. https://doi.org/10.1080/10618562.2016.1198782

LaPrè, A.K., Price, M.A., Wedge, R.D., Umberger, B.R., Sup, F.C., 2018. Approach for gait analysis in persons with limb loss including residuum and prosthesis socket dynamics. Int. j. numer. method. biomed. eng. 34, e2936. https://doi.org/10.1002/cnm.2936

Laprè, A.K., Umberger, B.R., Sup, F., 2014. Simulation of a powered ankle prosthesis with dynamic joint alignment, in: 2014 36th Annual International Conference of the IEEE Engineering in Medicine and Biology Society, EMBC 2014. https://doi.org/10.1109/EMBC.2014.6943914

Laszczak, P., Jiang, L., Bader, D.L., Moser, D., Zahedi, S., 2015. Development and validation of a 3D-printed interfacial stress sensor for prosthetic applications. Med. Eng. Phys. 37, 132–137. https://doi.org/10.1016/j.medengphy.2014.10.002

Laszczak, P., Mcgrath, M., Tang, J., Gao, J., Jiang, L., Bader, D.L., Moser, D., Zahedi, S., 2016. A pressure and shear sensor system for stress measurement at lower limb residuum/socket interface. Med. Eng. Phys. 38, 695–700. https://doi.org/10.1016/j.medengphy.2016.04.007

Lee, W.C.C., Zhang, M., Jia, X., Cheung, J.T.M., 2004. Finite element modeling of the contact interface between trans-tibial residual limb and prosthetic socket. Med. Eng. Phys. 26, 655–662. https://doi.org/10.1016/j.medengphy.2004.04.010

Legro, M.W., Reiber, G.D., Smith, D.G., Del Aguila, M., Larsen, J., Boone, D., 1998. Prosthesis evaluation questionnaire for persons with lower limb amputations: Assessing prosthesis-related quality of life. Arch. Phys. Med. Rehabil. 79, 931–938. https://doi.org/10.1016/S0003-9993(98)90090-9

Lilja, M., Johansson, T., Öberg, T., 1993. Movement of the tibial end in a PTB prosthesis socket: A sagittal X-ray study of the PTB prosthesis. Prosthet. Orthot. Int. 17, 21–26. https://doi.org/10.3109/03093649309164351

Lin, C.-C., Chang, C.-H., Wu, C.-L., Chung, K.-C., Liao, I.-C., 2004. Effects of liner stiffness for trans-tibial prosthesis: a finite element contact model. Med. Eng. Phys. 26, 1–9. https://doi.org/10.1016/S1350-4533(03)00127-9

Linde, H. Van Der, Hofstad, C.J., Geurts, A.C.H., 2004. A systematic literature review of the effect of different prosthetic components on human functioning with a lower - limb prosthesis. J. Rehabil. Res. Dev. 41, 555–570.

Lopes, D.S., Neptune, R.R., Ambrósio, J.A., Silva, M.T., 2015. A superellipsoid-plane model for simulating foot-ground contact during human gait. Comput. Methods Biomech. Biomed. Engin. 1–10. https://doi.org/10.1080/10255842.2015.1081181

Lugade, V., Kaufman, K., 2014. Center of pressure trajectory during gait: A comparison of four foot positions. Gait Posture 40, 719–722. https://doi.org/10.1016/j.gaitpost.2014.07.001

Major, M.J., Twiste, M., Kenney, L.P.J., Howard, D., 2014. The effects of prosthetic ankle stiffness on ankle and knee kinematics, prosthetic limb loading, and net metabolic cost of trans-tibial amputee gait. JCLB 29, 98–104. https://doi.org/10.1016/j.clinbiomech.2013.10.012

Mak, A.F.T., George, ;, Liu, H.W., Lee, ; S Y, 1994. Biomechanical assessment of below-knee residual limb tissue. J. Rehabil. Res. Dev. 31, 188–198.

McGeehan, M., Adamczyk, P., Nichols, K., Hahn, M., 2020. A reduced order computational model of a semi-active variable-stiffness foot prosthesis. https://doi.org/10.31224/osf.io/zhs53

Mckechnie, P.S., John, A., 2014. Anxiety and depression following traumatic limb amputation: a systematic review. Injury 45, 1859–66. https://doi.org/10.1016/j.injury.2014.09.015

Menard, M.R., Mcbride, M.E., Sanderson, D.J., Murray, D.D., 1992. Comparative Biomechanical Analysis of Energy-Storing Prosthetic Feet. Arch Phys Med Rehabil 73.

Meulenbelt, H.E.J., Dijkstra, P.U., Jonkman, M.F., Geertzen, J.H.B., 2006. Skin problems in lower limb amputees: A systematic review. Disabil. Rehabil. https://doi.org/10.1080/09638280500277032

Miller, S., 2020. Simscape Multibody Contact Forces Library.

Mitsuhashi, N., Fujieda, K., Tamura, T., Kawamoto, S., Takagi, T., Okubo, K., 2009. BodyParts3D: 3D structure database for anatomical concepts. Nucleic Acids Res. 37, D782–D785. https://doi.org/10.1093/nar/gkn613

Narita, H., Yokogushi, K., Shii, S., Kakizawa, M., Nosaka, T., 1997. Suspension effect and dynamic evaluation of the total surface bearing (TSB) trans-tibial prosthesis: A comparison with the patellar tendon bearing (PTB) trans-tibial prosthesis. Prosthet. Orthot. Int. 21, 175–178. https://doi.org/10.3109/03093649709164551

National Health Services Audit Commission Briefing: Assisting Independence, 2002.

Noll, V., Eschner, N., Schumacher, C., Beckerle, P., Rinderknecht, S., 2017. A physically-motivated model describing the dynamic interactions between residual limb and socket in lower limb prostheses. Curr. Dir. Biomed. Eng. 3, 15–18. https://doi.org/10.1515/cdbme-2017-0004

Peterson, C.L., Kautz, S.A., Neptune, R.R., 2011. Braking and propulsive impulses increase with speed during accelerated and decelerated walking. Gait Posture 33, 562–567. https://doi.org/10.1016/j.gaitpost.2011.01.010

Peterson, T.J., 2012. The Effect of Prosthetic Foot Component Stiffness on Initiation and Termination of Transtibial Amputee Gait. University of Washington.

Porsa, S., Lin, Y.-C., Pandy, M.G., 2015. Direct Methods for Predicting Movement Biomechanics Based Upon Optimal Control Theory with Implementation in OpenSim. Ann. Biomed. Eng. 44, 2542–2557. https://doi.org/10.1007/s10439-015-1538-6

Portnoy, S., Siev-Ner, I., Shabshin, N., Kristal, A., Yizhar, Z., Gefen, A., 2009. Patient-specific analyses of deep tissue loads post transtibial amputation in residual limbs of multiple prosthetic users. J. Biomech. 42, 2686–2693. https://doi.org/10.1016/j.jbiomech.2009.08.019

Postema, K., Hermens, H.J., De Vries, J., Koopman, H.F.J.M., Eisma, W.H., 1997. Energy storage and release of prosthetic feet Part 1: biomechanical analysis related to user benefits. Prosthet. Orthot. Int. 21, 17–27.

Rajagopal, A., Dembia, C.L., DeMers, M.S., Delp, D.D., Hicks, J.L., Delp, S.L., 2016. Full-Body Musculoskeletal Model for Muscle-Driven Simulation of Human Gait. IEEE Trans. Biomed. Eng. 63, 2068–79. https://doi.org/10.1109/TBME.2016.2586891

Robbins, C.B., Vreeman, D.J., Sothmann, M.S., Wilson, S.L., Oldridge, N.B., 2009. A Review of the Long-Term Health Outcomes Associated With War-Related Amputation. Mil. Med. 174, 588–592. https://doi.org/10.7205/milmed-d-00-0608

Russel Esposito, E., Miller, R.H., 2018. Maintenance of muscle strength retains a normal metabolic cost in simulated walking after transtibial limb loss. PLoS One 13, 1–19. https://doi.org/10.1371/journal.pone.0191310

Safari, M.R., Tafti, N., Aminian, G., 2015. Socket Interface Pressure and Amputee Reported Outcomes for Comfortable and Uncomfortable Conditions of Patellar Tendon Bearing Socket: A Pilot Study. Assist. Technol. 27, 24–31. https://doi.org/10.1080/10400435.2014.949016

Sagawa, Y., Turcot, K., Phane Armand, S., Thevenon, A., Vuillerme, N., Watelain, E., 2011. Biomechanics and physiological parameters during gait in lower-limb amputees: A systematic review. Gait Posture 33, 511–526. https://doi.org/10.1016/j.gaitpost.2011.02.003

Sanders, J.E., Daly, C.H., 1993. Measurement of Stresses in Three Orthogonal Directions at the Residual Limb-Prosthetic Socket Interface. IEEE Trans. Rehabil. Eng. 1, 79–85. https://doi.org/10.1109/86.242421

Sanders, J.E., Daly, C.H., Burgess, E.M., 1992. Interface shear stresses during ambulation with a below-knee prosthetic limb. J. Rehabil. Res. Dev. 29, 1–8. https://doi.org/10.1682/jrrd.1992.10.0001

Sanders, J.E., Greve, J.M., Mitchell, S.B., Zachariah, S.G., 1998. Material properties of commonly-used interface materials and their static coefficients of friction with skin and socks. J. Rehabil. Res. Dev. 35, 161–176.

Sanders, J.E., Karchin, A., Fergason, J.R., Sorenson, E.A., 2006. A noncontact sensor for measurement of distal residual-limb position during walking. J. Rehabil. Res. Dev. 43, 509–516. https://doi.org/10.1682/JRRD.2004.11.0143

Sanders, J.E., Zachariah, S.G., Baker, A.B., Greve, J.M., Clinton, C., 2000. Effects of changes in cadence, prosthetic componentry, and time on interface pressures and shear stresses of three trans-tibial amputees. Clin. Biomech. 15, 684–694.

Sanderson, D.J., Martin, P.E., 1997. Lower extremity kinematic and kinetic adaptations in unilateral below-knee amputees during walking. Gait Posture 6, 126–136. https://doi.org/10.1016/S0966-6362(97)01112-0

Schaarschmidt, M., Lipfert, S.W., Meier-Gratz, C., Scholle, H.C., Seyfarth, A., 2012. Functional gait asymmetry of unilateral transfemoral amputees. Hum. Mov. Sci. 31, 907–917. https://doi.org/10.1016/j.humov.2011.09.004

Schiff, A., Havey, R., Carandang, G., Wickman, A., Angelico, J., Patwardhan, A., Pinzur, M., 2014. Quantification of Shear Stresses Within a Transtibial Prosthetic Socket. Foot ankle Int. 35, 779–782. https://doi.org/10.1177/1071100714535201

Schwartz, M.H., Rozumalski, A., 2005. A new method for estimating joint parameters from motion data. J. Biomech. 38, 107–116. https://doi.org/10.1016/j.jbiomech.2004.03.009

Seth, A., Sherman, M., Reinbolt, J.A., Delp, S.L., 2011. OpenSim: a musculoskeletal modeling and simulation framework for in silico investigations and exchange. Procedia IUTAM 2, 212–232. https://doi.org/10.1016/j.piutam.2011.04.021

Shan, X., Otsuka, S., Yakura, T., Naito, M., Nakano, T., Kawakami, Y., 2019. Morphological and mechanical properties of the human triceps surae aponeuroses taken from elderly cadavers: Implications for muscle-tendon interactions. PLoS One 14. https://doi.org/10.1371/journal.pone.0211485

Simscape Multibody Documentation [WWW Document], 2020. URL https://www.mathworks.com/help/physmod/sm/ (accessed 10.10.20).

Söderberg, B., Ryd, L., Persson, B.M., 2003. Roentgen Stereophotogrammetric Analysis of Motion between the Bone and the Socket in a Transtibial Amputation Prosthesis: A Case Study. J. Prosthetics Orthot. 15, 95–99. https://doi.org/10.1097/00008526-200307000-00008

Strbac, M., Popović, D.B., 2012. Software tool for the prosthetic foot modeling and stiffness optimization. Comput. Math. Methods Med. 2012, 1–8. https://doi.org/10.1155/2012/421796

Su, P.-F., Gard, S.A., Lipschutz, R.D., Kuiken, T.A., 2008. Differences in Gait Characteristics Between Persons With Bilateral Transtibial Amputations, Due to Peripheral Vascular Disease and Trauma, and Able-Bodied Ambulators. Arch Phys Med Rehabil 89, 1386–1394. https://doi.org/10.1016/j.apmr.2007.10.050

Thakallapelli, A., Ghosh, S., Kamalasadan, S., 2016. Real-time frequency based reduced order modeling of large power grid, in: IEEE Power and Energy Society General Meeting. IEEE Computer Society. https://doi.org/10.1109/PESGM.2016.7741877

Thelen, D.G., 2003. Adjustment of muscle mechanics model parameters to simulate dynamic contractions in older adults. J. Biomech. Eng. 125, 70–77. https://doi.org/10.1115/1.1531112

Tryggvason, H., Starker, F., Lecomte, C., Jonsdottir, F., 2020. Use of Dynamic FEA for Design Modification and Energy Analysis of a Variable Stiffness Prosthetic Foot. Appl. Sci. 10, 650. https://doi.org/10.3390/app10020650

Van Hulle, R., Schwartz, C., Denoël, V., Croisier, J.-L., Forthomme, B., Brüls, O., 2020. A foot/ground contact model for biomechanical inverse dynamics analysis. J. Biomech. 100. https://doi.org/10.1016/j.jbiomech.2019.109412

van Schaik, L., Geertzen, J.H., Dijkstra, P.U., Dekker, R., 2019. Metabolic costs of activities of daily living in subjects with lower limb amputation: a systematic review and meta-analysis. Article submitted for publication. PLoS One 14, e0213256.

Ventura, J.D., Klute, G.K., Neptune, R.R., 2011. The effects of prosthetic ankle dorsiflexion and energy return on below-knee amputee leg loading. Clin. Biomech. 26, 298–303. https://doi.org/10.1016/j.clinbiomech.2010.10.003

Versluys, R., Desomer, A., Lenaerts, G., Beyl, P., Van Damme, M., Vanderborght, B., Vanderniepen, I., Van Der Perre, G., Lefeber, D., 2008. From conventional prosthetic feet to bionic feet: A review study. Proc. 2nd Bienn. IEEE/RAS-EMBS Int. Conf. Biomed. Robot. Biomechatronics, BioRob 2008 49–54. https://doi.org/10.1109/BIOROB.2008.4762839

Webber, C.M., Kaufman, K., 2017. Instantaneous stiffness and hysteresis of dynamic elastic response prosthetic feet. Prosthet. Orthot. Int. 41, 463–8. https://doi.org/10.1177/0309364616683980

Weidow, J., Tranberg, R., Saari, T., Kärrholm, J., 2006. Hip and Knee Joint Rotations Differ between Patients with Medial and Lateral Knee Osteoarthritis: Gait Analysis of 30 Patients and 15 Controls. J Orthop Res 24, 1890–1899. https://doi.org/10.1002/jor.20194

Willson, A.M., Richburg, C.A., Czerniecki, J., Steele, K.M., Aubin, P.M., 2020. Design and Development of a Quasi-Passive Transtibial Biarticular Prosthesis to Replicate Gastrocnemius Function in Walking. J. Med. Device. 14, 025001. https://doi.org/10.1115/1.4045879

Winter, D.A., 1991. The Biomechanics and Motor Control of Human Gait.

Winter, D.A., 1983. Energy generation and absorption at the ankle and knee during fast, natural, and slow cadences. Clin. Orthop. Relat. Res. 175, 147–154. https://doi.org/10.1097/00003086-198305000-00021

Winter, D.A., Sienko, S.E., 1988. Biomechanics of below-knee amputee gait. J. Biomech. 21, 361–367. https://doi.org/10.1016/0021-9290(88)90142-X

Wirta, R.W., Golbranson, F.L., Mason, R., Calvo, K., 1990. Analysis of below-knee suspension systems : Effect on gait. J. Rehabil. Res. Dev. 27, 385–396. https://doi.org/10.1682/JRRD.1990.10.0385

Womac, N.D., Neptune, R.R., Klute, G.K., 2019. Stiffness and energy storage characteristics of energy storage and return prosthetic feet. Prosthet. Orthot. Int. https://doi.org/10.1177/0309364618823127

Wu, G., Cavanagh, P.R., 1995. ISB Recommendations For the Standardized Reporting In Kinematic Data. J. Biomech. 28, 1257–1261.

Wu, G., Siegler, S., Allard, P., Kirtley, C., Leardini, A., Rosenbaum, D., Whittle, M., D'Lima, D.D., Cristofolini, L., Witte, H., Schmid, O., Stokes, I., 2002. ISB recommendation on definitions of joint coordinate system of various joints for the reporting of human joint motion - Part I: Ankle, hip, and spine. J. Biomech. https://doi.org/10.1016/S0021-9290(01)00222-6

Yiğiter, K., Şener, G., Bayar, K., 2002. Comparison of the effects of patellar tendon bearing and total surface bearing sockets on prosthetic fitting and rehabilitation. Prosthet. Orthot. Int. 26, 206–212. https://doi.org/10.1080/03093640208726649

Zelik, K.E., Collins, S.H., Adamczyk, P.G., Segal, A.D., Klute, G.K., Morgenroth, D.C., Hahn, M.E., Orendurff, M.S., Czerniecki, J.M., Kuo, A.D., 2011. Systematic variation of prosthetic foot spring affects center-of-mass mechanics and metabolic cost during walking. IEEE Trans. Neural Syst. Rehabil. Eng. 19, 411–419. https://doi.org/10.1109/TNSRE.2011.2159018

Zheng, Y., Mak, A.F.T., Lue, B., 1999. Objective assessment of limb tissue elasticity: Development of a manual indentation procedure. J. Rehabil. Res. Dev. 36, 71–85.

Ziegler-Graham, K., MacKenzie, E.J., Ephraim, P.L., Travison, T.G., Brookmeyer, R., Ziegler-Graham, A.K., 2008. Estimating the Prevalence of Limb Loss in the United States: 2005 to 2050. Arch Phys Med Rehabil 89, 422–429. https://doi.org/10.1016/j.apmr.2007.11.005